# An experimental study of slag foaming

S.A.C. Stadler

Thesis submitted in partial fulfilment of the requirements for the degree of Master of Science (Extractive Metallurgy) at the University of Stellenbosch

Department of Chemical Engineering

Supervisors:

Prof. C. Aldrich & Mr. J.J. Eksteen

Stellenbosch

December 2002

# Declaration

I, the undersigned, hereby declare that the work contained in this thesis is my own original work, except where specifically acknowledged in the text. The present thesis has not previously in its entirety or in part been submitted at any university for a degree.

# Synopsis

Slag foaming occurs in several pyrometallurgical processes. These processes include steelmaking in basic oxygen steelmaking furnaces and electric arc furnaces (EAF) as well as various non-ferrous operations like sulphide smelting/converting and base metal slag cleaning. Although slag foaming in steelmaking processes has been extensively researched, little attention has been given to slag foaming in non-ferrous operations. Slag foaming phenomena are complex because often the system consists of three or more phases.

The objectives of this study is to review the published work on slag foaming, to obtain through physical modelling an understanding of the principles governing foaming and to investigate slag foaming phenomena through pyrometallurgical experiments.

To obtain these objectives, experiments were carried out with aqueous mixtures at different column sizes, different pore sizes for gas injection and varying liquid depths, and also for high temperature metallurgical slags with varying composition and at different temperatures. Through gas injection, foaming conditions were simulated and the equilibrium foam height was measured for different gas velocities.

The following conclusions were drawn:

1. For physical modelling of slag foaming in 3-phase systems the average foam index increases with increasing amounts of solids present in the system. The effect of additional solids in the system is independent of the system geometry.
2. The following conclusions were reached by determining coefficients for an empirical dimensional model fitted to aqueous mixtures: Higher liquid density leads to lower foam index values. The influence of the liquid viscosity is dependent on the system investigated and may have a positive or negative result on foaming. The

empirical model should only be applied to the property range and geometric set-up for which it was derived, as coefficients may vary greatly for different systems.

3. Influence of solid precipitates on slag foaming can be summarised by noting that small amounts of magnetite stabilise slag foaming, while precipitates of wollastonite and anorthite decreased foaming. The influence of solid precipitates is thought to be related to the density, morphology and degree of surface activity of the solid precipitates.
4. The foam index decreases with increasing basicity due to the lowering of the slag viscosity. This continues until the precipitation of solids starts and the foam index once again increases.
5. For increasing "FeO" concentration the foam index will decrease due to lower viscosity, but higher surface tension depression may lead to increased foam index values at high "FeO" concentrations.
6. Higher foam index values were obtained for slags with lower densities. The empirical relationship observed is $\Sigma \propto \rho^{-\frac{2}{3}}$.
7. Higher foam index values were obtained for slags with higher viscosity. The empirical relationship observed is $\Sigma \propto \mu$.
8. Higher foam index values were obtained for slags with lower surface tensions. The empirical relationship observed is $\Sigma \propto \sigma^{-1}$.
9. Models derived for the foaming of basic steelmaking slags does not satisfactorily describe the foaming behaviour of acidic slags.
10. The physical properties of the slag influence the foam stabilisation mechanism.

# Opsomming

Slak skuiming kom in verskeie pirometallurgiese prosesse voor. Hierdie prosesse sluit die maak van staal in basiese staalmaakoonde en elektriese boogoonde in, sowel as verskeie nie-yster prosesse soos sulfied smelting/omsetting en die skoonmaak van basis metaal slakke. Alhoewel slak skuiming in staalmaak slakke reeds intensief nagevors is, is min aandag gegee aan slak skuiming in nie-yster prosesse. Slak skuiming verskynsels is kompleks, want dikwels betaan die sisteem uit drie of meer fases.

Die doelwitte van hierdie studie is om werk wat reeds oor slakskuiming gepubliseer is te hersien, om deur fisiese modellering 'n begrip van die prinsiepe waarop skuiming berus te bekom en om slak skuiming verskynsels na te vors deur pirometallurgiese eksperimente te beplan en uit te voer.

Ten einde hierdie doelwitte te bereik, is eksperimente uitgevoer met water mengsels in verskillende kolom grootte s, verskillende porie grootte s vir gas inspuiting en by verskillende vloeistof hoogtes, en ook vir hoë temperatuur metallurgiese slakke met variërende samestelling en by verskillende temperature. Skuimingskondisies is deur gas inspuiting gesimuleer en die ewewig skuimhoogte is gemeet by verskillende gas snelhede.

Die volgende gevolgtrekkings is bereik:

1. Tydens fisiese (koue) modellering van slak skuiming in 3-fase sisteme styg die gemiddelde skuim indeks met toenemende hoeveelhede vastestof in die sisteem. Die uitwerking van addisionele vastestof in die sisteem is onafhanklik van die sisteem geometrie.
2. Die volgende gevolgtrekkings is gemaak deur die koëffisiente vir 'n empiriese dimensionale model te pas op waterige mengsels. Hoër vloeistof digtheid lei na laer skuim indeks waardes. Die invloed van die vloeistof viskositeit is afhanklik van die sisteem ondersoek en mag 'n positiewe of 'n negatiewe resultaat op skuiming hê. Die empiriese model moet slegs toegepas word op die eienskap omvang en

geometriese opstelling waarvoor dit bepaal is, omdat koëffisiënte grootliks kan varieer vir verskillende sisteme.

3. Die invloed van vastestof partikels op slak skuiming kan opgesom word deur die waarneming dat klein hoeveelhede magnetiet slakskuiming stabiliseer terwyl neerslag van wollastoniet en anhortiet skuiming verminder. Die invloed van vastestof neerslag hou vermoedelik verband met die digtheid, vorm en graad van oppervlak aktiviteit van die vastestof partikels.
4. Die skuim indeks verminder met toenemende basisiteit as gevolg van die afname in die slak viskositeit. Dit geld tot die neerslag van vastestof begin en die skuim indeks weereens toeneem.
5. Vir toenemende 'FeO' konsentrasie sal die skuim indeks afneem as gevolg van laer viskositeit, maar hoër oppervlakspanning onderdrukking kan lei na hoër skuim indeks waardes by hoër 'FeO' konsentrasies.
6. Hoër skuim indeks waardes is verkry vir slakke met laer digthede. Die empiriese verhouding is bepaal as $\Sigma \propto \rho^{-\frac{2}{3}}$.
7. Hoër skuim indeks waardes is verkry vir slakke met hoër viskositeit. Die empiriese verhouding is bepaal as $\Sigma \propto \mu$.
8. Hoër skuim indeks waardes is verkry vir slakke met laer oppervlakspannings. Die empiriese verhouding is bepaal as $\Sigma \propto \sigma^{-1}$.
9. Modelle afgelei vir die skuiming van basiese staalmaak slakke beskryf nie die skuimings gedrag van suur slakke bevredigend nie.
10. Die fisiese eienskappe van die slak beïnvloed die skuim stabiliseerings meganisme.

# Acknowledgements

My supervisors, Chris Aldrich and Jacques Eksteen, for broadening my horizons and teaching me that something seemingly meaningless can contain valuable gems if you look at it from a different angle;

the workshop staff, Anton, Howard, Christiaan and Oom Jannie for always lending a helping hand and giving practical advise that has the backing of experience behind it;

my assistants in carrying out the high temperature experiments, J.B. Aggenbach, Stéan Barrie and Simon Frank;

Mintek, for providing financial support without which this work would not have been possible;

my parents who taught me perseverance and always support me in my choices in life
you gave me the courage to dream;

my brother and sisters, your encouragement carried me through some tough times;

the many friends that stood by me in good times and bad, knowing that laughter is always the best medicine ;

my Creator and Heavenly Father, to whom all the credit is due, but none of the criticism.

# Table of Contents

## Table of figures

## List of tables

# 1 Introduction

## 1.1 Motivation for the study

Slag foaming is a phenomenon that occurs in several pyrometallurgical processes. These processes include steelmaking in basic oxygen steelmaking furnaces and electric arc furnaces (EAF), as well as various non-ferrous operations like sulphide smelting or converting and base metal slag cleaning.

In slag-based, smelting-reduction processes, the foaming and overflow of slag from a vessel owing to either gas injection or reaction-driven gas generation, is considered a major limitation to productivity. Severe foaming of the slag causes this overflow phenomenon. In plasma arc smelting it also causes the cathode to respond wildly to maintain constant arc resistance, leading to operating instabilities. In lance-based applications, slag foaming would also require dynamic lance movement to maintain a constant lance-to-bath distance. In steelmaking applications, the maintenance of stable foam is important to prevent unwanted heat loss and refractory damage arising from arc flares from 3-phase arcs. The severity of foaming is strongly dependent on the slag chemistry, operating conditions and the rate of gas addition and/or formation. Slag foaming phenomena are complex because often the system consists of three or more phases.

In published studies of slag foaming, the foam index ($\Sigma$) (Bikerman, 1973; B. Ozturk, 1995; R. Jiang, 1991; Y. Zhang, 1995; Zhang, 1992; Gaskell, 2000) was used as a measure of the foaminess of the slag. When the volume, V, of the foam formed at steady state is proportional to the gas flow rate, Q, the foaming index is defined as the constant of proportionality.

$$V = \Sigma \bullet Q \qquad \textbf{Eq. 1-1}$$

If the cross sectional area of the reactor is constant, then the foam index, Σ, can be expressed in terms of the foam height (h) and the superficial gas velocity (v):

$$\Sigma = \frac{h}{v} \qquad \textbf{Eq. 1-2}$$

The foaming index becomes equal to the residence time of the gas in the foam layer if the actual gas velocity at the temperature of the system is chosen (usually the thermal expansion of the gas is neglected).

Sometimes the foam life or foam decay rate is also used as a measure of foaming stability. Foam life refers to the rate of decay of the foam after the addition of gas to the system ceases. The foam index will be used in this study to characterise foamability as the increase and maximum foam height is of greater importance than the foam decay time in metallurgical reactors.

## *1.2 Background*

In many metallurgical processes, foamed slags are used to create large surface areas for multiphase reactions to take place, leading to improved kinetics, heat transfer and energy efficiency. However, there is still a lack of understanding of what controls the foamability of slags. Surface tension and viscosity (Bikerman 1973; Hara 1986; Ito 1989; Hara 1990; Zamalloa 1992; Utigard 1993; Ogawa 1993; Ghag 1998; Ghag 1998; Gaskell 2000), bacisity (Ito 1989; Zamalloa 1992; Utigard 1993), solid particles (Ito 1989; Utigard 1993; Zhang 1995) and bubble size (Ito 1989; Zhang 1995) have all been proposed as key factors in controlling the foaminess of the slag.

### 1.2.1 The role of liquid/melt physical properties in foaming

The physical properties of the liquid phase are expected to influence its foaming behaviour. Surface tension influences bubble size and froth stability. The viscosity of the liquid determines the ease of gas movement through the liquid and therefore the gas retention. It also influences the drainage of fluid from liquid lamella. The density of the liquid is important in liquid drainage from the foam and also relates to froth stability. According to Ren (1994) the foaming behaviour of slags is strongly dependant on their chemical composition. The alkali contents in the steelmaking blast furnace and also in reactors of other reduction processes, enriched by the circulation process, may not only reduce the softening and the melting point of the burden materials, but also the viscosity and surface tension of the slags. They also affect the reduction process undergone by the iron oxides and therefore the gas evolution rate. However, foaming is not only reliant on gas formation, but also on the gas retention capacity of specimens that is linked to the existence of a liquid phase physical properties.

### 1.2.2 Basicity

In pyrometallurgy basicity is a popular way of describing slag chemistry. The most familiar definition of basicity, $\kappa$, is

$$\kappa = \frac{M_{CaO}}{M_{SiO_2}} \quad \text{or} \quad \kappa = \frac{X_{CaO}}{X_{SiO_2}} \qquad \textbf{Eq. 1-3}$$

Slags high in CaO are more likely to be an ionic solution, while slags high in silica would mostly consist of polymer-like chains or a network structure. The molecular structure of the liquid molecules is important when considering the mechanisms of foam formation and stability. FeO is long recognised as a network modifier in slag chemistry and should also be investigated.

### 1.2.3 Bubble size

Pak (1996) found that BOF (basic oxygen furnace) slag in contact with hot metal showed a generation of very fine sized bubbles at the slag-metal interface, and formed stable foam. This indicates the influence of bubble size on foaming behaviour. Bubbles formed by gas injection are larger than those formed in a chemical reaction and foams generated by gas injection are less stable than foams resulting from chemical reaction. However, measurement of the bubble size distribution is very difficult to do for foaming slags. In this thesis the study of bubble size is confined to physical modelling at room temperature.

### 1.2.4 Solid precipitates

Few studies have considered the effect of solid precipitates on slag foaming (Gudenau 1992; Worczok 1994). The effect of solids on slag foaming is usually discussed in terms of the addition of fine coal, which is sometimes used to suppress slag foams. However, if properties such as the viscosity of the slag phase and the surface tension of the slag play as important a role as is evident from the literature (Worczok 1994; Ren 1994; Ozturk 1995; Zhang 1995), then precipitates formed in the furnace should be recognised as influencing both these properties and therefore influencing the foam behaviour. Large particles may rupture the bubble films and therefore cause a decrease in foam height. Small particles may be wetting or non-wetting and therefore affect the rheological properties of the liquid lamellae. The precipitation of wettable solids leads to enhanced foaming (Utigard 1993; Morales 1995; Pak 1996).

## *1.3 Specific objectives of this study*

The objective of this study was to review the published work on slag foaming, to obtain through physical modelling (the use of water mixtures to simulate slag) an understanding of the principles governing foaming and to investigate slag foaming phenomena by planning and executing pyrometallurgical experiments.

The specific objectives of the present study were as follows:

i. The first objective was to gain a thorough background on the factors influencing the formation, stability and decay of foams through a survey of the literature. This was critical to interpreting the results gained from experiments.

ii. Physical modelling was used as the first step towards characterising slag foaming behaviour. Physical modelling is routinely used to characterise pyrometallurgical operations where the fluid flow is to be characterised. Physical modelling includes investigating at the influence of physical properties, solid precipitates and bubble size on foaming at room temperature.

iii. The third objective was to conduct slag foaming experiments resulting in useful information comparable with published slag foaming data, but also extending existing information on slag foaming. The experiments will focus on the effects of slag composition (slag basicity and FeO concentration), physical properties and solid precipitates on slag foaming.

# 2 Literature review

## 2.1 Objectives

This chapter gives an overview of important foaming phenomena, reports on studies identifying the factors influencing slag foaming and also a review of work published on models of slag foaming.

The study of foaming phenomena was aimed at identifying the underlying physical principles of foaming. Four mechanisms of foam stability were identified, namely, the Gibbs' elasticity effect, the Marangoni effect, the surface viscosity and the electrical double layer repulsion. The Gibbs' and Marangoni effects are due to the surface tension properties of the liquid/melt, the surface viscosity is dependent on the viscous properties of the liquid, and the electrical double layer effect is due to the degree of ionisation of the liquid. One of the objectives of the literature review was therefore to become familiar with these mechanisms in order to recognise their influence when studying the data gathered from experiments.

The most commonly used measures of " foaminess" were qualified so that studies using different measures to analyse foaming could be compared. Studies on slag foaming in metallurgical processes were reviewed and interpreted in terms of the principles of foaming identified. Finally some of the models proposed for slag foaming were reviewed, evaluated and compared in terms of relevance and applicability.

## *2.2 Theory*

Foaming is a complicated phenomenon and a study of the fundamentals of foaming is essential to understanding the underlying principles of foam formation and foam breakdown. In this section (Section 2.2) foams are defined, classification of foams is reviewed and the mechanisms that have been proposed for foam formation and breakdown are discussed.

### 2.2.1 Definition of a foam

Foams are colloidal systems. In the classification based on the state of aggregation of the two phases, foams commonly belong to the first groups. These groups are (Bikerman 1973):

1. Gases dispersed in liquids (foams, gas emulsions)
2. Liquids dispersed in gases (mists, fogs, liquid aerosols)
3. Gases dispersed in solids (solid foams)
4. Solids dispersed in gasses (fumes, smokes, solid aerosols)
5. Liquids dispersed in liquids (emulsions)
6. Liquids dispersed in solids (some gels)
7. Solids dispersed in liquids (suspensions, sols)
8. Solids dispersed in solids

Foams consist therefore of an agglomeration of gas bubbles separated from each other by thin liquid films. There are many and varied factors determining foam formation, growth, aging and collapse. This is reflected in that foams could have different morphologies, gas bubble cells with a wide size range and, hence, very different degrees of stability (Zhang 1992).

### 2.2.2 Classification of foams

#### *2.2.2.1 Gas hold-up or wetness*

One of the more scientific ways of describing foam, is using the gas hold-up, 1-$\varphi$, and the wetness, $\varphi$, of the foam.

$$\frac{\text{Volume liquid in foam}}{\text{Volume of foam}} = \varphi \qquad \textbf{Eq. 2-1}$$

$$\frac{\text{Volume gas in foam}}{\text{Volume of foam}} = 1 - \varphi = \varepsilon \qquad \textbf{Eq. 2-2}$$

It is customary to speak of foams when $\varphi$ is smaller than 0.1 and of gas emulsions when $\varphi$ exceeds 0.9 (Bikerman, 1973). This classification not only distinguishes the morphologies of the foams but also categorises their stability and mechanisms of growth and aging.

#### *2.2.2.2 "Kugelschaum" or wet foam*

Dispersions of a gas in a liquid, in which the thickness of the interstitial liquid layers is at least comparable with the bubble diameter, are commonly designated as gas emulsions. This is also called "Kugelschaum" literally meaning sphere foam in German. Dispersions of gas in a liquid, in which liquid films much thinner than the bubble diameter separate the gas bubbles, are called "Polyederschaum". As the liquid films between the spherical bubbles of kugelschaum contain more liquid than that of polyederschaum, there is outflow of liquid from the films, or drainage, caused by gravity and the buoyancy of the bubbles. During this process all the bubbles expand and the total liquid surface area expands as well. The pressure of the gas inside different size bubbles differs according to equation 2-3.

$$P = P_h + \frac{2\sigma}{\mathrm{r}} \qquad \textbf{(Bikerman, 1973)} \qquad \textbf{Eq. 2-3}$$

where P is the gas/vapour pressure in the bubble, $P_h$ is the pressure of the liquid phase surrounding the bubble, r is the radius of the bubble and $\sigma$ is the surface tension of the foaming liquid

The pressure of gas in smaller bubbles is therefore higher than the pressure of gas in larger bubbles. Gas diffusion takes place from smaller bubbles to larger bubbles, which makes the larger bubbles grow at expense of the smaller ones.

Zhang (1992) sited unpublished data where slag foams were observed using an X-ray video technique. When argon gas was injected into liquid slag a column of polyhedron shaped bubbles were observed. When foams were generated by reaction between FeO containing slag and graphite, foams dominated by spherical bubbles of much smaller size were observed.

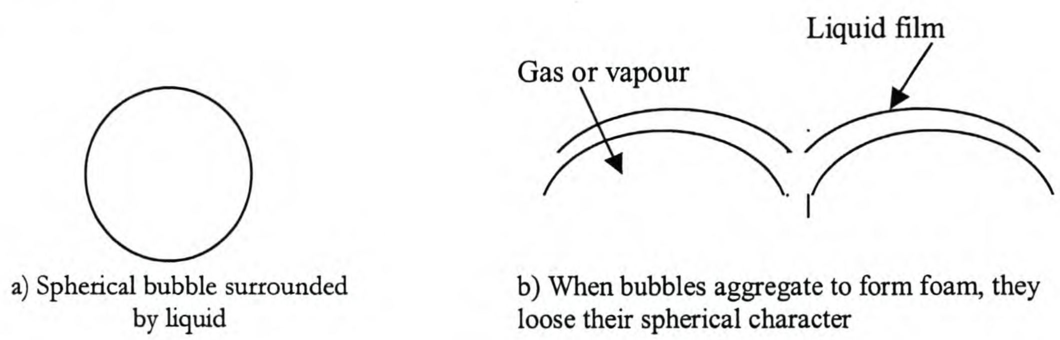


**Figure 2-1 Kugelschaum consist of mostly spherical bubbles, while polyederschaum bubbles has lost their spherical character**

#### *2.2.2.3 "Polyederschaum" or dry foam*

In polyederschaum the liquid films separating gas bubbles are much thinner than in kugelschaum. The fact that the liquid films are almost planar indicates that the pressures in adjacent bubbles are nearly equal. There is therefore no significant gas diffusion between bubbles. The drainage of liquid due to gravitation for these films can usually be discarded and the shape of the films is determined by capillary forces alone (Bikerman 1973). These capillary forces are induced by the Plateau border, which is the line along which three liquid films meet, and the Gibbs angle, which is the point where four Plateau lines meet. The reason for the stability of polyederschaum is the loss of fluidity of the liquid films/lamellae. The loss of fluidity of the lamellae stops the bubble films from rupturing.

This effect can be explained as the result of the combination of several postulated mechanisms. Theories relating to these mechanisms will be briefly outlined in sub-section 2.2.3.

#### *2.2.2.4 Foam classification according to the flow regime of the bubbles*

The behaviour of a foamy mixture changes when the gas flux is increased. At lower gas velocities the foam is in the bubbly regime and can be compared to beer or soap foam. Two distinct layers are visible, a mostly liquid layer and a foamy layer on top. As the gas flux increase, the foam behaviour becomes turbulent and churning and the two layers disappear into one uniformly mixed layer.

**Table 2-1. Comparison of foam behaviour in different flow regimes. (Gou 1996)**

| Characteristic | Bubbly Regime | Churning Regime |
| --- | --- | --- |
| **Appearance** | Like beer or soap foam | Turbulent, churning |
| **Uniformity** | Two distinguishable layers | One uniformly mixed layer |
| **Gas velocity** | 0.01 – 0.10 m/s | >1 m/s |
| **Void fraction** | 0.8 – 0.9 | Varies with velocity |
| **Foam height** | Independent of total liquid volume (if liquid is more than critical volume) | Dependent on total liquid volume. |
| **Stability** | Takes time to collapse | Collapses immediately |

According to Worczok (1994) the superficial gas velocities in a basic oxygen furnace are as high as 6m/s. This is well within the churning regime as defined in table 2-1. Foaming in the churning regime is also anticipated for reductive smelting operations, such as carbothermic reduction in plasma arc furnaces (Worczok 1994), where significant amounts of CO-gas are generated. Other operations such as zinc fuming in plasma arc furnaces have even greater gas generation per unit volume of slag. Experiments were conducted with superficial gas velocities ranging from 0.1m/s to 8m/s for water mixtures and from 0.01m/s to 0.04m/s for slags (Stadler, 2002). It is therefore expected that a transition from the bubbly regime to the churning regime would be observed for the aqueous foaming experiments, while the slag foam experiments should only show the characteristics of the bubbly regime.

### 2.2.3 Mechanisms of foam stability

There are three fundamental processes occurring in almost all foams: 1) bubble size redistribution, 2) film thinning and 3) film breakage. It is therefore important to understand the mechanisms stabilising films and preventing film breakage.

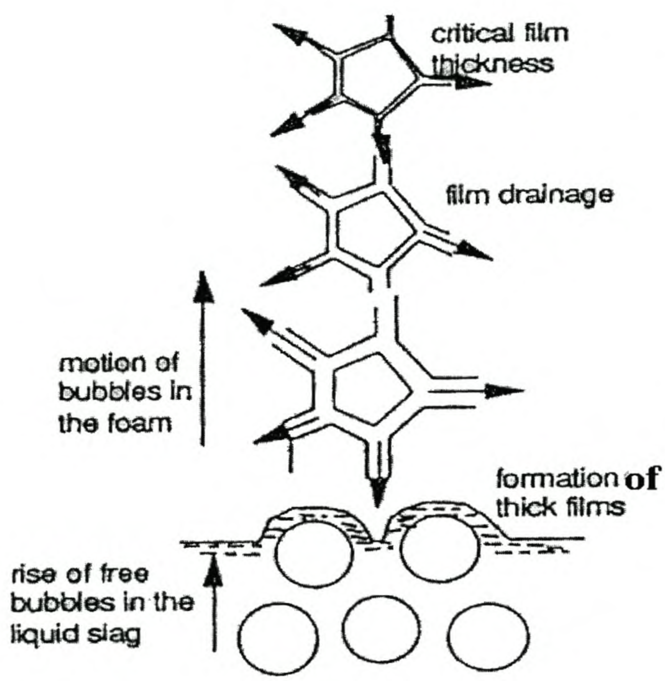


**Figure 2-2 Sketch showing the effect of film drainage on the thickness of bubble films (Zamalloa 1992)**

#### *2.2.3.1 Film elasticity –The Gibbs' elasticity effect*

For this mechanism it is assumed that a liquid film has an elasticity that counters any thinning of the film. This elasticity relies on surface tension gradients existing in the liquid film. Pure liquids lack elasticity because their surface tensions are independent of extension. Gibbs' theory states that the surface tension of a thin film in a solution increases when that film is stretched. This is due to the fact that the solute is positively adsorbed on the surface, any increase in surface area would therefore lead to a decrease of the solute concentration within the film and hence a rise of the equilibrium surface tension. This effect is only significant for very thin films, when the amount of solute adsorbed on the surface is comparable to that contained in the film. It is more important for strongly adsorbed solutes than for weakly adsorbed solutes and for low concentrations of the solute rather than for high concentrations. For liquid lamellae Gibbs' elasticity is defined by

$$E = \frac{2d\sigma}{\mathrm{d(lnA)}} \qquad \textbf{Eq. 2-4}$$

where $d\sigma$ is the change in equilibrium surface tension

and A is the surface area of the lamellae

The factor of 2 arises from the fact that the solute adsorbs on both sides of the lamellae.

#### *2.2.3.2 Marangoni effect*

The equilibrium surface tension of a pure liquid as well as a liquid solution will not be established immediately upon creation of the surface. For pure liquid to reach equilibrium, the molecules take a finite time to rearrange themselves to a preferred orientation at the newly formed surface with an increase in their intermolecular distance. In solutions of surface-active solutes the rate at which equilibrium is reached is much slower than pure liquid, as it depends on the rate of diffusion of solute molecules to the surface. Dynamic surface tensions are therefore defined as any non-equilibrium values of surface tension that arise when the surface of a liquid solution is extended or contracted.

When local areas of film are expanded, new areas of surface are created where the instantaneous surface tension is large. The higher surface tension in these new areas of surface exerts a drag on the adjoining areas at equilibrium state with lower tension, causing the surface to flow toward the region of greater tension. The viscous drag of the moving surface may carry an appreciable amount of the underlying liquid and thus create the effect of restoring the thickness of the film. This flow in response to a surface tension gradient is called the Marangoni effect. A dynamic property of a liquid film, Marangoni elasticity, could be defined as the result of this effect. It should be reiterated that the Gibbs' elasticity is measured from the equilibrium surface tension. When Marangoni effect operates, very thin and aged lamellae are less strong than younger and thicker lamellae and so are more readily broken. For lamellae made from solutions in which the surface tension gradient is small, Marangoni effect should be less effective.

#### *2.2.3.3 Surface viscosity*

The viscosity of a monolayer is measured in two dimensions and is analogous to the ordinary viscosity. The coefficient of surface viscosity ($\mu_s$) is the internal frictional force, which is induced along a unit length on a surface by a gradient of surface flow between two parallel lines. Surface viscosity of aqueous solutions can be markedly influenced by the adsorption of surface-active solute, particularly if the solute has high molecular weight. The increase in surface viscosity could also result from the formation of interfacial complexes. The consequence of the enhancement of the viscosity of the liquid surface is increasing its ability to resist surface fluid flow.

#### *2.2.3.4 Electrical double layer repulsion*

The adsorption of ionic surface-active solutes into the surface layer is evident in aqueous solutions. It establishes an electric charge at the surface, which must be balanced by a counter-ion diffuse double layer extending to the bulk liquid. If two such surfaces come together "back-to-back", as in a thinning liquid film, the two double layers repel one another and a repulsive potential result. This repulsion prevents further thinning on the film. It is obvious that this mechanism is only significant when the film thickness is very small; otherwise the repulsive potential is negligible due to the large distance between two double layers. Essentially, it does not function in non-ionising solvents.

Having discussed the character of foams, quantitive measures of analysing foams can now be addressed.

## *2.3 Measurement of foam stability*

The stability of foam has to be quantified to compare the foamability of different liquids and further relate the foamability to the physical properties of the liquid. Chemical engineers have designed a number of standard tests. These tests differ in the parameters being used and in the way the foam is generated. Gas bubbling is a convenient method, but mechanical beating and shaking has also been used. Foam stability is evaluated in two different ways, involving different parameters being measured. In the static method, foam is generated to a certain volume and then the times for the decay of the foam in terms of its volume, height or surface area are measured. These parameters are called foam lives. In the dynamic method, a foam is formed by introducing gas bubbles into the liquid phase at a fixed rate, and the volume or the height of the foam column at equilibrium is measured and a parameter called the foam index is defined as the volume or the height of the foam column at unit gas flow rate or unit gas superficial velocity. Recently Ellis (2001) showed that foam stability can be studied using digital image processing.

### 2.3.1 Foam life – A static measurement

We can define the average lifetime of the liquid and gas phases for static foam, $L_l$ and $L_g$ as

$$L_l = \frac{1}{V_{l0}} \int_0^{V_{l0}} t\, dV_l \qquad \textbf{Eq. 2-5}$$

$$L_g = \frac{1}{V_{g0}} \int_0^{V_{g0}} t\, dV_g \qquad \textbf{Eq. 2-6}$$

where $V_l$ and $V_g$ are the volumes of the liquid and gas phases in the foam at time t, $V_{l0}$ and $V_{g0}$ being their initial values at t=0 respectively.

It could be explained that $L_l$ is the average time that a unit volume of liquid can remain suspended as foam. The significance of $L_g$ is similarly the average time that a unit volume of the gas remains in the foam. In every foam there exists the drainage and film rupture processes. If drainage is a more pronounced factor than film rupture, the liquid is removed from the foam at a faster rate than the gas is liberated. Consequently, $L_g$ is greater than $L_l$. It is also possible to define an average foam life ($L_f$),

$$L_f = \frac{1}{V_{f0}} \int_0^{V_{f0}} t \, dV_f \qquad \textbf{Eq. 2-7}$$

and,

$$V_{f0}L_f = (V_{g0} + V_{l0})L_f = V_{g0}L_g + V_{l0}L_l \qquad \textbf{Eq. 2-8}$$

where $V_f$ is the volume of the foam at time t, $V_{f0}$ being its value at t=0.

For a container of uniform cross-sectional area, equation 2-8 reduces to

$$L_f = \frac{1}{h_0} \int_0^{h_0} t \, dh \qquad \textbf{Eq. 2-9}$$

where h is the foam height, $h_0$ being its value at t=0.

In a special case, the rate of drainage of liquid from the foam obeys an empirical equation,

$$V_l = V_{l0} e^{-kt} \qquad \textbf{Eq. 2-10}$$

or in terms of drainage,

$$\frac{dV_l}{dt} = -kV_l \qquad \textbf{Eq. 2-11}$$

which means that the rate of drainage is of the first order. The parameter $L_l$ can then be found to be the relaxation time of the decay of liquid volume in the foam, since

$$L_l = \frac{1}{V_{l0}} \int_0^{V_{l0}} t \, dV_l = k \int_0^{\infty} t e^{-kt} dt = \frac{1}{k} \qquad \textbf{Eq. 2-12}$$

This situation has been found in both aqueous foams and metallurgical slag foams (Zhang 1992). Foams of the second and third order of drainage were also discussed by Bikerman (1973).

A disadvantage of this foam life parameter in terms of the volume decay is that $L_g$ may depend on the initial foam height. Therefore comparisons between different liquids should be made at the same volumes of initial gas volume in the foam when $L_g$ or $L_f$ is used.

Foam life can also be characterised in terms of the decay of the total liquid surface area in the foam,

$$L_s = \frac{1}{A_0}\int_0^\infty A\,dt \qquad \textbf{Eq. 2-13}$$

where A is the liquid surface area of the foam at t, $A_0$ being its value when t=0.

### 2.3.2 Foam Index – A Dynamic measurement

The dynamic measurement of foamability was first proposed by Bikerman (1973), in which equilibrium between formation and collapse of the foam is established by generation of gas bubbles of definite size at a constant rate. The unit of "foaminess" is defined as

$$\Sigma = \frac{V_f t}{V_g} = \frac{V_f}{Q_g} \qquad \textbf{Eq. 2-14}$$

where $V_f$ is the volume of the foam at steady state, $V_g$ the volume of gas being injected through the liquid in a period of time t, $Q_g$ is the gas flow rate. The parameter $\Sigma$ has the unit of time and can be roughly interpreted as the average travelling time of a gas in the foamed liquid. Bikerman found that $\Sigma$ is independent of the amount of liquid (when that amount is more than the critical amount) and the cross-sectional area of the cylindrical container for a gas velocities that are not great enough for the blast to rupture the lamellae.

In the study of slag foam, Ito (1989) modified Bikerman's definition of the dynamic measurement of the foam stability and referred to it as the foam index,

$$\Sigma = \frac{\Delta h}{\Delta v} = \frac{\Delta H_f}{\Delta v_g} = \frac{H_f}{v_g} \qquad \textbf{Eq. 2-15}$$

where h is the height of the foam layer at steady state, $H_f$ is called foam height meaning the difference of the level of foamed liquid to the level at rest, v is the linear gas velocity in the foam and $v_g$ the superficial gas velocity which is obtained by,

$$v_g = \frac{Q_g}{A_s} \qquad \textbf{Eq. 2-16}$$

and $A_s$ is the cross-sectional area of the container.

### *2.3.2.1 Relating the foam index to foam life for ideal slags.*

For an ideal system, for which the void fraction of the foam is constant, the foam index, $\Sigma$, can be related to the foam life, $\tau$.(Ito 1989) The formation of the foam, assuming a constant void fraction, $\alpha$, is given by

$$\frac{dh}{dt} = \alpha \frac{dL}{dt} = \frac{\alpha}{A} \frac{dV^{foam}}{dt} = \frac{Q_g}{A} \qquad \textbf{Eq. 2-17}$$

where $V^{foam}$ is a volume of foam.

The rate equation for the change in foam height can be written as

$$\frac{dh}{dt} = K_1 Q_g - K_2 h \qquad \textbf{Eq. 2-18}$$

where $K_1$ and $K_2$ are the formation and the rupture constants of foam respectively.

Since $\alpha$ is constant, when we combine equation 2-17 and 2-18 we find that

$$K_1 = \frac{1}{A}. \qquad \textbf{Eq. 2-19}$$

At steady state the change in foam height is zero and equation 2-18 simplifies to equation 2-20.

$$K_1 Q_g = K_2 h \qquad \textbf{Eq. 2-20}$$

If the gas is stopped (i.e. $Q_g=0$), equation 2-18 reduces to equation 2-21.

$$\frac{dh}{dt} = -K_2 h \qquad \textbf{Eq. 2-21}$$

Integrating equation 2-21 from t = 0 to t = t and from h = $h^0$ to h = h gives the foam height as a function of time.

$$K_2 t = -\ln\left(\frac{h}{h^0}\right) \qquad \textbf{Eq. 2-22}$$

The rupture of foam is expressed as the drainage of the liquid in the foam. The rate equation of drainage is given by equation 2-23, assuming a first-order drainage rate.

$$\frac{dv}{dt} = k(V^0 - v) \qquad \textbf{Eq. 2-23}$$

where $V^0$ is the initial liquid volume in foam and v is the drained liquid volume. Integrating equation 2-23 from t= 0 gives equation 2-24.

$$kt = -\ln\left(\frac{V^0 - v}{V^0}\right) \qquad \textbf{Eq. 2-24}$$

Remembering that the void fraction is constant throughout the foam, equation 2-24 can be written as follows:

$$kt = -\ln\left(\frac{h}{h^0}\right) \qquad \textbf{Eq. 2-25}$$

The average foam life ($\tau$) is obtained in equation 2-26.

$$\begin{aligned}\tau &= \frac{1}{V^0}\int_0^{v^0} t\, dv \\ &= k\int_0^{\infty} t e^{-kt}\, dt = \frac{1}{k}\end{aligned} \qquad \textbf{Eq. 2-26}$$

From equations 2-22 and 2-25 it is clear that the rupture constant $K_2$ and the drainage constant k are the same and are correlated to the foam life by equation 2-26.

From equations 2-19, 2-20 and 2-26, the following relationship is obtained:

$$\frac{\tau}{A} = \frac{h}{Q_g} \qquad \textbf{Eq. 2-27}$$

The foaming index can now be related to the foam life by using equations 2-15, 2-16 and 2-27.

$$\tau = \frac{\Delta h}{\Delta(Q_g / A)} = \Sigma \qquad \textbf{Eq. 2-28}$$

Therefore, for an "ideal slag", the foam index $\Sigma$ is equal to the average foam life. It can therefore be assumed that in general slag foams with a long foam life would also have higher foam index values than slag foams showing instant foam decay.

Having defined the measures of foaminess in slags, studies published on slag foaming can now be looked at and interpreted accordingly.

## 2.4 Slag foaming in metallurgical processes

Research undertaken on slag foaming has shown that many authors agree on the types of stability mechanisms likely to be important in slag foams, such as surface tension, film elasticity, viscosity, solid particles and gas composition. However, their interpretation as to the relative importance of such mechanisms on slag foaming is often very different.

In this section (Section 2.4) slag foaming is discussed in terms of slag composition, the influence of surface active additives, the influence of solid particles, the bubble size in the foam and the influence of gas type and pressure.

### 2.4.1 Influence of slag composition on slag foaming

The influence of slag composition on slag foaming can be related to the physical properties of the slag. The basicity of slags is a measure of the structure and ionisation of the slag. Fully liquid slags of low basicity are expected to be more viscous than highly basic slags and the foams of these slags are likely to be stabilised by the surface viscosity mechanism. Slags of higher basicity are however more ionic of nature and the slag foam would then be stabilised by electrical double layer repulsion.

#### *2.4.1.1 Basicity*

Reactions such as the desulphurisation and dephosphorisation of steel are dependant upon the activity of the free oxygen ($a_{o^{2-}}$) in the melt. However it is known that these refining reactions are improved with the use of more basic slags. Since it is difficult to measure the activity of CaO, CaS etc. for multi-component slags, many attempts have been made to relate the desulphurisation and dephosphorisation to the basicity of the slag. The simplest index of the basicity is the "V ratio" i.e. ($\%CaO/\%SiO_2$) and this has been used considerably by steelmakers but this does not take into account MgO, $Al_2O_3$, FeO, etc.

which are frequently present in steelmaking slags. Consequently, several other indices of basicity have been used, as are outlined in table 2-2.

Duffy and Ingram (Mills, 1995) noticed that the shifts in frequency of the absorption band associated with the 6s – 6p transaction observed in the ultraviolet region of the spectrum can be related to the basicity of a glass or slag. The frequency shift can be seen as a measure of the electron donor power and is usually expressed in terms of the optical basicity, $\Lambda$.

$$\Lambda = \frac{\text{Electron doner power of slag}}{\text{Electron doner power of CaO}} \qquad \textbf{Eq. 2-29}$$

Values for the optical basicity can also be calculated from Pauling electronegativities. The values for slags can then be derived by equation 2-30

$$\Lambda = \frac{\sum x_1 n_1 \Lambda_{th1} + x_2 n_2 \Lambda_{th2} + x_3 n_3 \Lambda_{th3} + \ldots}{\sum x_1 n_1 + x_2 n_2 + x_3 n_3 + \ldots} \qquad \textbf{Eq. 2-30}$$

where x is the mole fraction of the component and $n_i$ is the number of oxygen atoms in the molecule.

**Table 2-2. Typical examples of various indices expressing basicity (Mills, 1995)**

| Index | Table equation number |
|---|---|
| $\frac{\%(CaO)}{\%(SiO_2)}$ | 2-2.1 |
| $\frac{x(CaO) + x(MgO)}{x(SiO_2)}$ | 2-2.2 |
| $\frac{\%(CaO)}{\%(SiO_2) + \%(Al_2O_3)}$ | 2-2.3 |
| $\frac{\%(CaO)}{\%(SiO_2) + \%(P_2O_5)}$ | 2-2.4 |
| $\frac{x(MeO) - 3x(P_2O_5)}{x(SiO_2)}$ | 2-2.5 |
| $\frac{\%(CaO) + 1.4\%MgO}{\%(SiO_2) + 0.84\%(P_2O_5)}$ | 2-2.6 |
| $\frac{x(MeO)}{x(SiO_2 + 2x(P_2O_5) + \frac{1}{2}x(Al_2O_3) + \frac{1}{2}x(Fe_2O_3)}$ | 2-2.7 |
| $\frac{x(CaO) - 4x(P_2O_5)}{x(SiO_2)}$ | 2-2.8 |
| $\%(CaO) - 1.86\%(SiO_2) - 1.19\%(P_2O_5)$ | 2-2.9 |
| $x(MeO) – 2x(SiO_2) - 4x(P_2O_5) - 2x(Al_2O_3) – x(Fe_2O_3)$ | 2-2.10 |
| $x(CaO) + \quad (MgO)/x(SiO_2) + x(Al_2O_3)$ | 2-2.11 |
| $x(CaO) + 0.5(MgO)/x(SiO_2) + 0.33x(Al_2O_3)$ | 2-2.12 |

Mills (1995) cited several studies that showed a direct relationship between the optical basicity and the logarithm of activity coefficients of $P_2O_5$, FeO, CaO and $Na_2O$ in slags.

The optical basicity can also be link to the structure and physical properties of slags. The optical basicity provides a global measure of the concentration of bridging ($O^0$), nonbridging ($O^{1-}$) and free oxygen ($O^{2-}$) in silicate and alumino-silicate melts and thus provides a measure of the depolymerisation of the melt.

The viscosity of molten slags is related to the structure of the melt. The viscosity of slags can be calculated from

$$\ln \mu = \frac{1}{(0.15 - 0.44\Lambda)} - \frac{1.77 + 2.88\Lambda_{corr}^{-1}}{T} \qquad \textbf{Eq. 2-31}$$

where μ is the calculated viscosity, T is the thermodynamic temperature (K), $\Lambda_{corr}$ is the optical basicity corrected for the concentration of "network-breaking" metal oxides required to charge balance any $Al_2O_3$ present.(Mills, 1995)

#### *2.4.1.2 Influence of slag basicity on slag foaming*

As slag foaming has been extensively studied in by the steelmaking industry, a fair amount of data on the influence of slag basicity on slag foaming is available. Ito (1989) defined slag basicity as equation 2-2.3 in table 2-2. Ito (1989) indicated the foam index and foam life of slags with higher basicity were lower than the foam index and foam life obtained for lower slag basicity (range 0.4-1.0). Their results are given in figure 2-3. These results also proved that for the systems studied the approximation of the foam life as equal to the foaming index (Section 2.3.2.1) is reasonable.

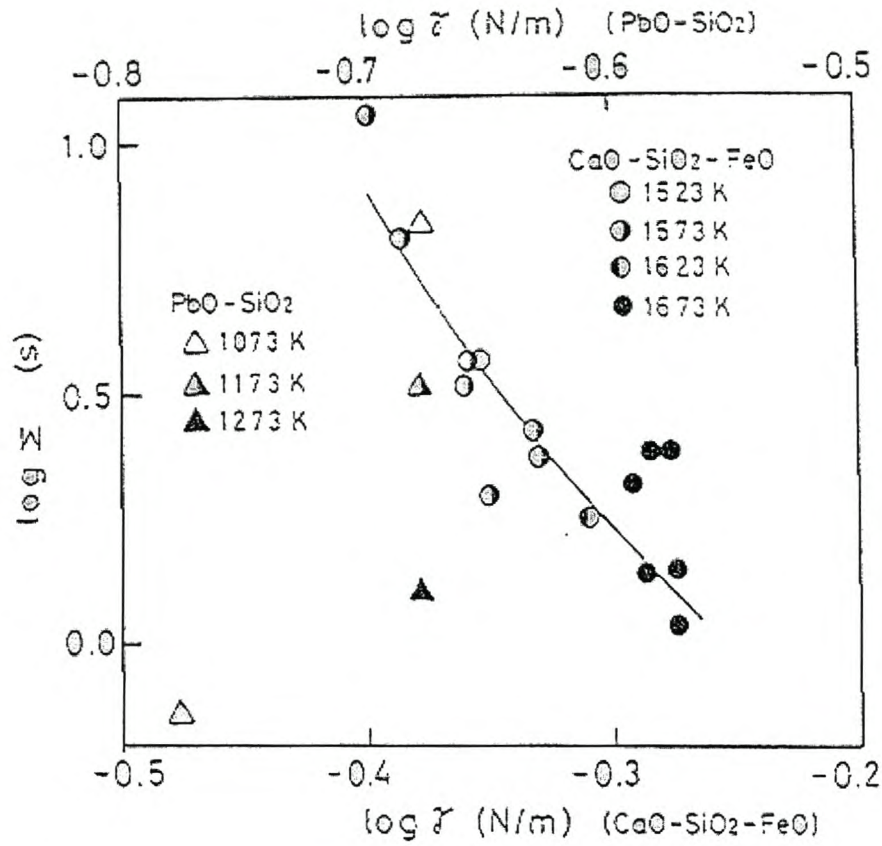


**Figure 2-3. The change of foaming index Σ and foam life τ with basicity ($CaO/SiO_2$) of the $CaO$-$SiO_2$-$FeO$ slag (Ito 1989)**

Ito (1989) explained the decrease of the foam index with an increase of the slag basicity as due to the changes in viscosity and surface tension of the slags. The surface tension increases and the viscosity decrease with increasing CaO. The conclusion was therefore reached that low surface tension and high viscosity stabilised the slag foam.

Figure 2-4 shows the foaming index again as a function of slag basicity. The foam index decreases with increasing basicity up to a value of 1.2 at 1573K and 1.22 at 1673K, which are the liquidus compositions. However, the foam index increased with increasing basicity when the basicity was in excess of the liquidus composition. This phenomenon was explained by the fact that solid particles such as $2CaO.SiO_2$ precipitate at higher CaO contents, and the particles significantly increase foam stability. The effects of solid particles on slag foaming will be discussed in detail in section 2.4.3.

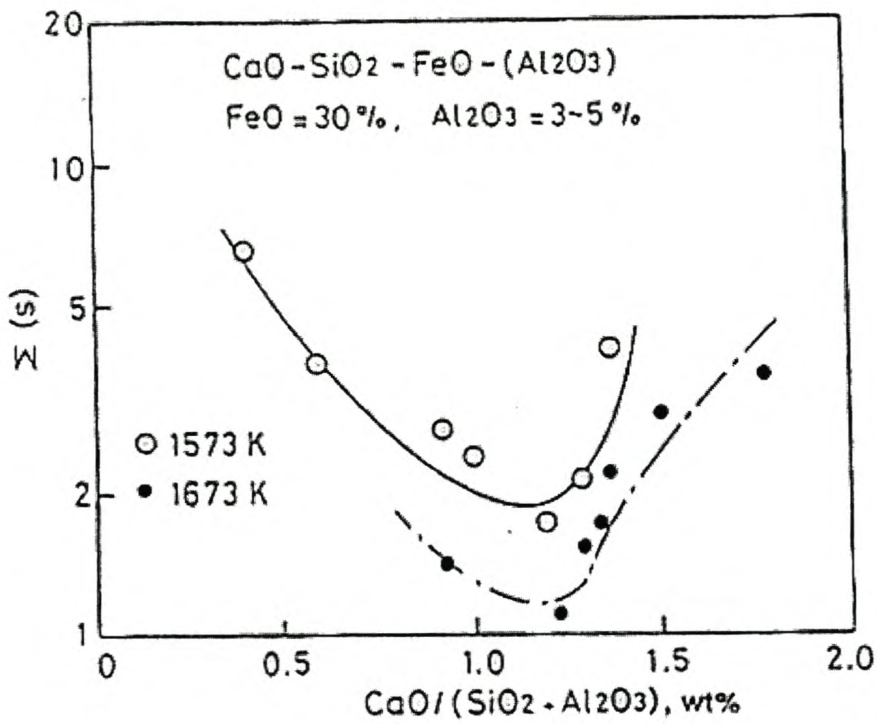


**Figure 2-4. The relationship between the foaming index and the basicity of $CaO$-$SiO_2$-$FeO$ slags (Ito 1989)**

Utigard (1993) defined slag basicity according to equation 2-2.1 in table 2-2. When they compared the foam decay rate for different slags at differing temperatures, Utigard (1993) found that the foam decay from 8 to 4 cm was consistently faster for slags of higher basicity (figure 2.5). This was in agreement with the foam index values obtained (figure 2.6). The slag basicity values ranged from 0.4 to 1.0 and good agreement with data published by Ito (1989) were achieved. For basicity values ranging from 1.0 to 3.0 they saw the same result. An increase in basicity led to a decrease in the foaming index.

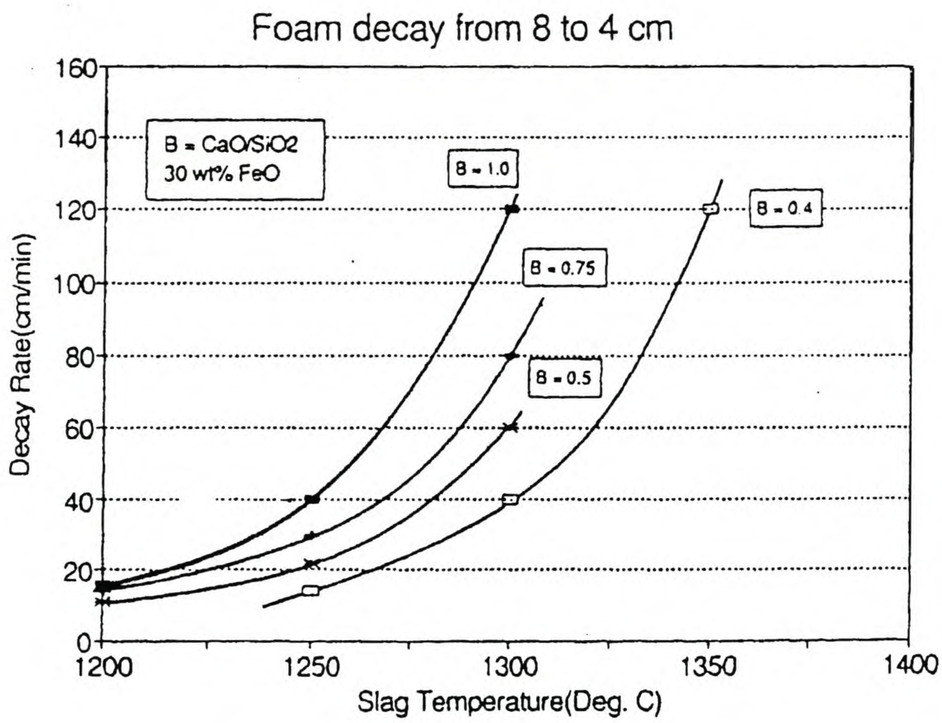


**Figure 2-5. Foam decay rate as a function of temperature (Utigard 1993)**

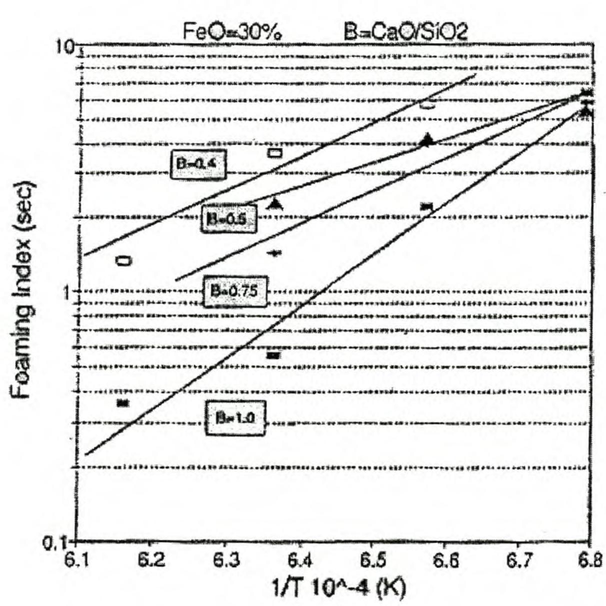


**Figure 2-6. Foaming index at various CaO/SiO$_2$ ratios plotted versus the inverse of absolute temperature ( Utigard 1993)**

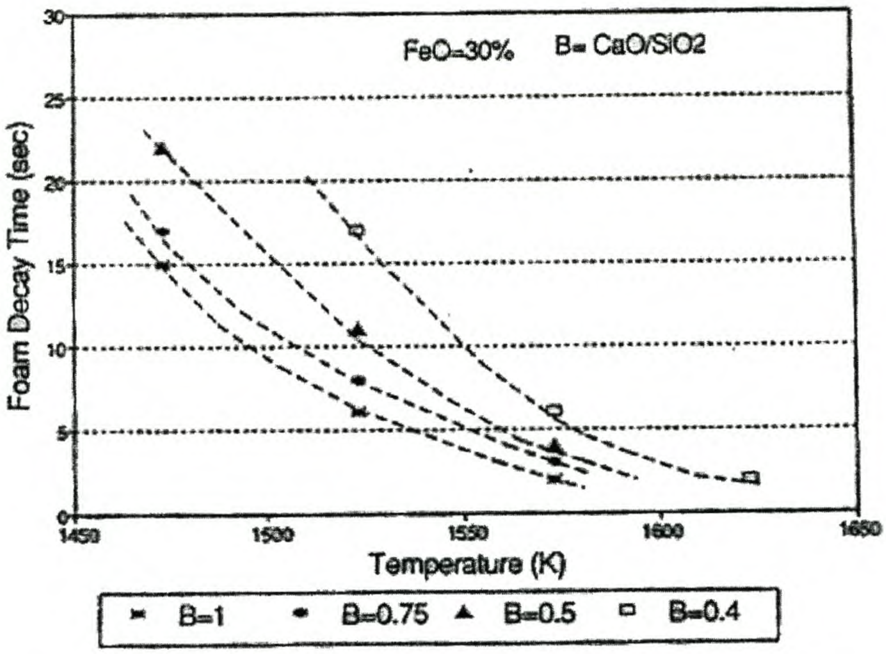


**Figure 2-7. Foam stability versus $CaO/SiO_2$ ratio and temperature (Zamalloa 1992)**

Zamalloa (1992) studied the effect of slag basicity in terms of foam decay time and found that decreasing the $CaO/SiO_2$ ratio from 1 to 0.4 increased the foam stability. Zamalloa (1992) proposed that the increase in stability could be attributed to the silica adsorption at the gas/slag interface. Silica adsorbed on the bubble surface lowers the surface tension only slightly, limiting any effect of the Marangoni flow phenomenon. However, the adsorbed mono-molecular film of silica results in an increase of the surface shear viscosity, leading to enhanced slag foam stability and decreased drainage rate of the liquid films.

Utigard (1993) defined the slag basicity as

$$\frac{\%FeO + \%CaO}{\%SiO_2} \qquad \textbf{Eq. 2-32}$$

Utigard (1993) also found that the foam index decreased with increasing basicity values (1.0 – 4.0). Utigard (1993) found that in general the foam life increases with increasing viscosity. However, at constant viscosity the foam life increases with increasing $CaO/SiO_2$ ratio (Figure 2-8). This would support the conclusion that the effect of basicity on slag foaming is not entirely due to changes in the bulk viscosity of the slag but may also be due to an increase in the surface shear viscosity and/or the precipitation of solids.

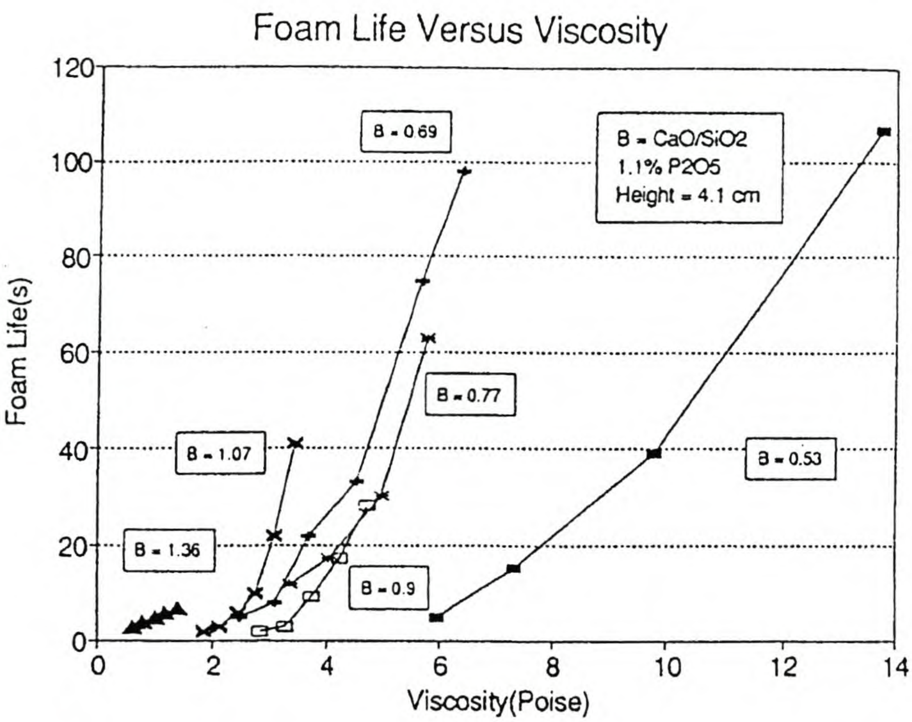


**Figure 2-8. Foam life as a function of viscosity and $CaO/SiO_2$ ratio for a slag containing 1.1% $P_2O_5$ (Utigard 1993)**

The effect of different concentrations of FeO and MgO on slag foaming are also discussed as to their influence on the physical properties of the slag. The non-linear relationships are an indication of different foam stabilising mechanisms working interdependently.

### *2.4.1.3 Effect of FeO content on slag foaming*

Ito (1989) calculated the expected foaming behaviour of an electric arc furnace as a function of the FeO content using operating conditions ($CaO/SiO_2$ =3.0 and T=1873K). The foaming was expected to significantly increase with decreasing FeO content because of the lower viscosity of the slag and the greater amount of second-phase particles. The gas flow rate was determined by the reaction between FeO and coke injected into the slag. Figure 2-

9 shows the results obtained. At first the decrease in viscosity has a smaller effect than the greater gas generation by FeO reduction. Maximum foam heights were obtained at approximately 25%FeO. For FeO values higher than 25% the decreasing viscosity limits the foam height obtained in spite of an increase in the gas flow rate.

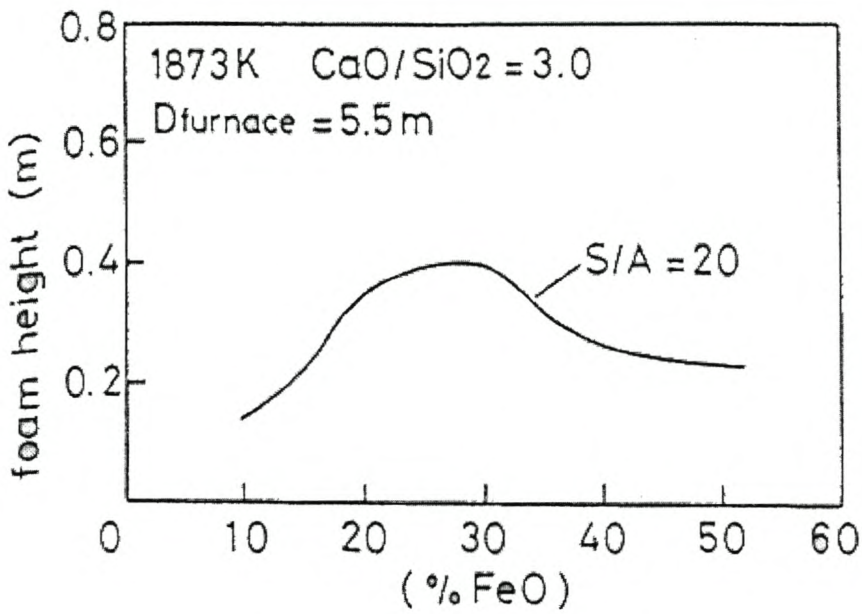


**Figure 2-9. The anticipated foaming height of slag for an EAF operation plotted as a function of FeO concentration assuming that the reduction of FeO by carbon determines the gas velocity in the furnace (Ito 1989)**

Jiang (1991) reported experimental results showing the influence of FeO concentrations (0-20%) on slag foaming. Their results are given in figure 2-10. It can be seen that the foaming index decreases with increasing FeO for FeO>2%.

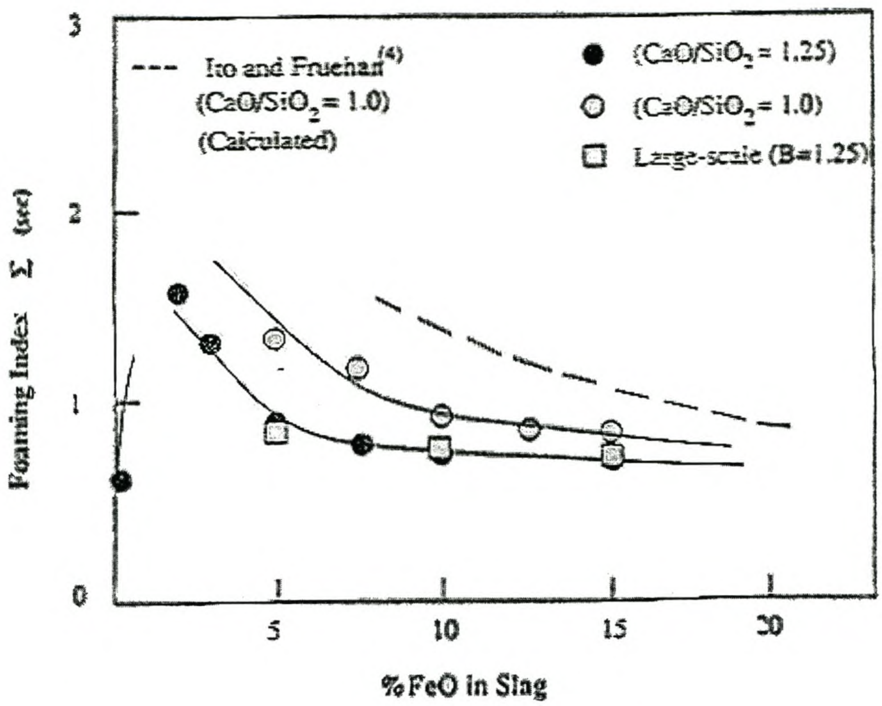


**Figure 2-10. The foaming index for CaO-$SiO_2$-FeO slags at 1773K (Jiang 1991)**

It was observed that the foaming index reached a maximum value at about 2% FeO in the slag. The conclusion was reached that the CaO-$SiO_2$ slags do not foam when no FeO is present in the slag, because it is too viscous to foam significantly.

The tendency for slags to show decreased foaming at higher FeO concentrations was affirmed by Utigard (1993). Once again it was concluded that the lowering of the slag viscosity was the reason for the decline in the foaming index.

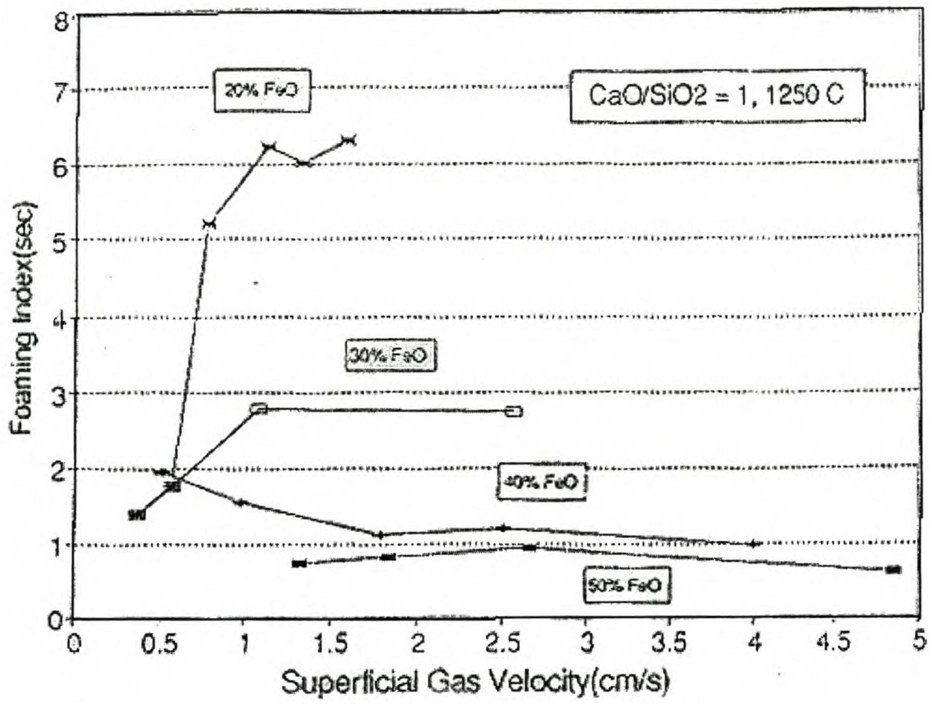


**Figure 2-11. Foaming index as a function of gas velocity for slags with various FeO content (Utigard 1993)**

### *2.4.1.4 Influence of MgO on slag foaming.*

Ren (1994) studied the effect of MgO content on slag foaming. The effect is described in terms of the maximum volume increase of the slag. It was shown that the influence of MgO on slag foaming depended on the basicity of the slag. The behaviour of this system is suspected to be a product of the influence of MgO on the $FeO_n$–CaO-$SiO_2$-MgO phase diagram. It seems that for very acidic slags (%CaO/%$SiO_2$= 0.1; 1450 C) without MgO the system is mostly heterogeneous with only a small amount of liquid and therefore little foaming. For very acidic slags with 10% MgO the system is heterogeneous with a high amount of liquid and foaming is not limited by the amount of liquid available. For slags with an basicity of 1.4 at a temperature of 1350 C and no MgO addition, the slag is heterogeneous with a high amount of liquid, but as the MgO content increase, the melt quickly changes to heterogeneous with no liquid.

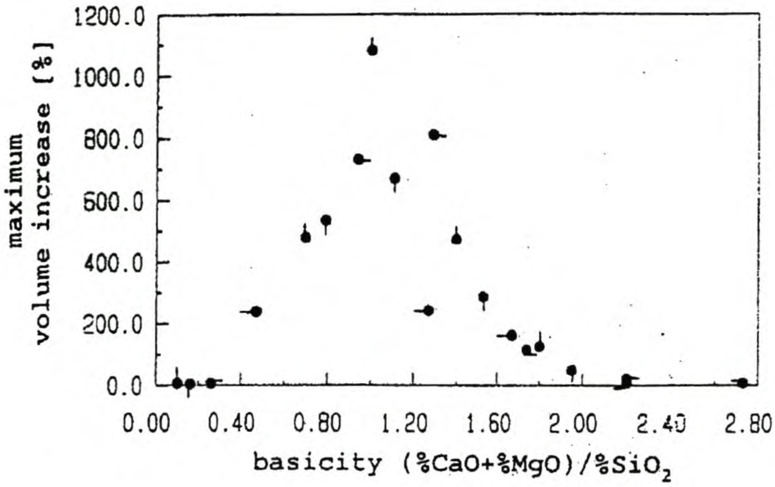


**Figure 2-12. Change in the maximum volume increase as a function of the (%CaO + %MgO)/%$SiO_2$ ratio of the specimens at 1350 C with 60%$Fe_2O_3$ and MgO content of =0%, =2%, =5%, =10% (Ren 1994)**

It appears that the influence of the basicity and the FeO and MgO concentrations in the slag on slag foaming is largely dependent on the liquid viscosity. However, small amounts of surface active compounds are not likely to influence the bulk viscosity of the liquid/melt.

### 2.4.2 Influence of surface active additives on slag foaming

Ren (1994) found that the alkali oxides, $K_2O$ and $Na_2O$, increase the foaming capacity of slags in small amounts, but as the addition increase, so the growth in foam volume decreases. Difference of foaming behaviour was again noted for acidic and basic slags.

Utigard (1993) studied the effect of $P_2O_5$ additions on slag foaming. As can be seen from figure 2-13, the more $P_2O_5$ in the slag, the higher the foaming index achieved. As the small amounts of $P_2O_5$ are unlikely to influence the bulk properties of the liquid melt, it is clear that it has to be the surface active properties of the melt that influenced the foaming behaviour.

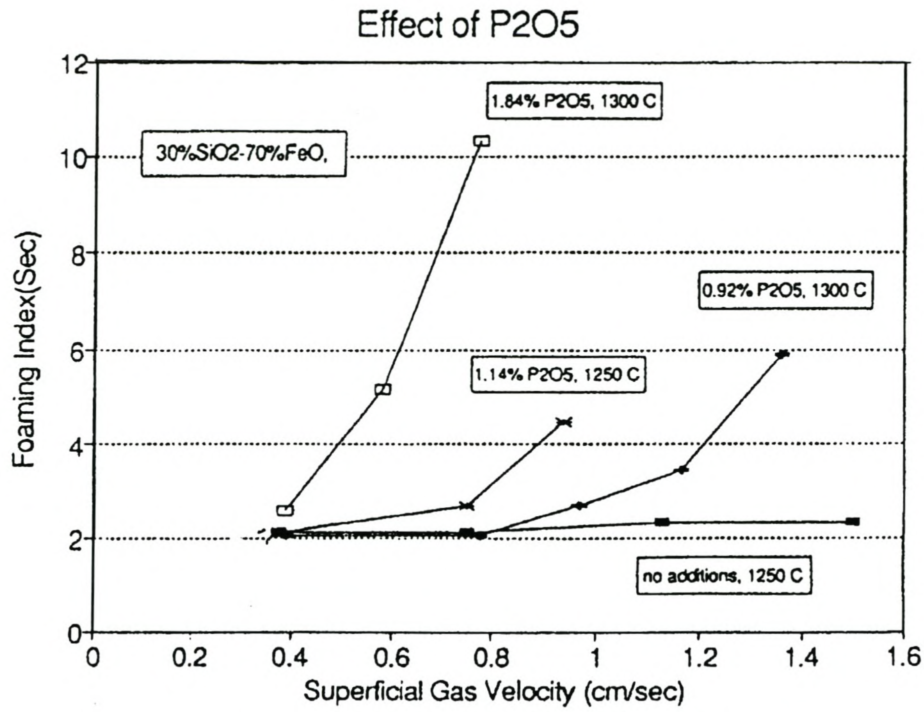


**Figure 2-13. Foaming index as a function of gas velocity and $P_2O_5$ content (Utigard 1993)**

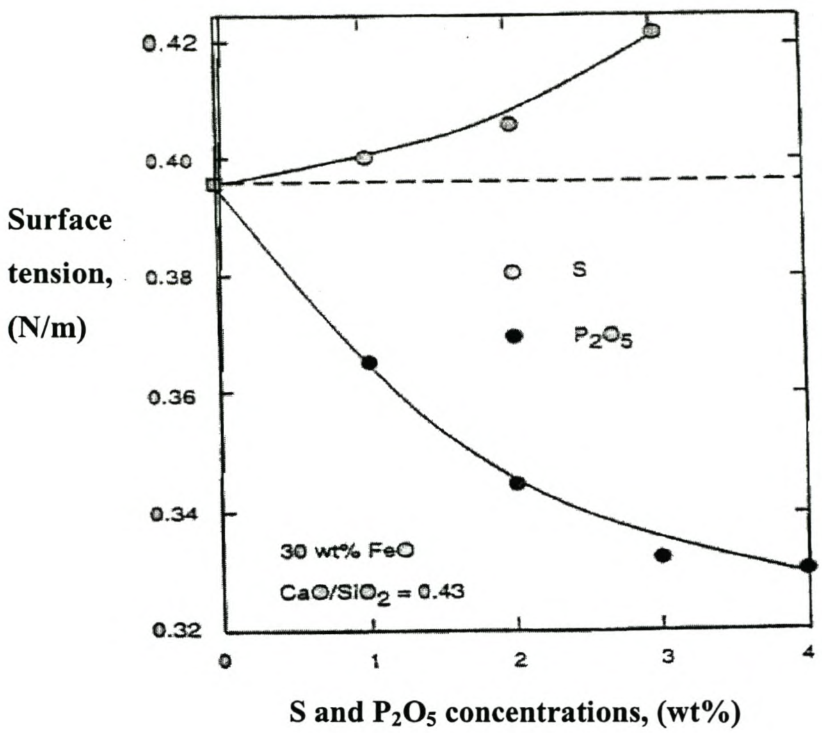


**Figure 2-14. The influence of S and $P_2O_5$ on the surface tension of 30wt pct FeO, $CaO/SiO_2$=0.43 melt at 1673K (Gaskell 2000)**

Ito (1989) found that a 2 wt % addition of $P_2O_5$ at 1673K causes the foam index to increase by a factor of 1.3 and that the addition of 2 wt % S causes the foam life to decrease by 20%. This is consistent with the observation that S increases surface tension and $P_2O_5$ decreases it. It also demonstrates the dependence of foam life on surface tension.

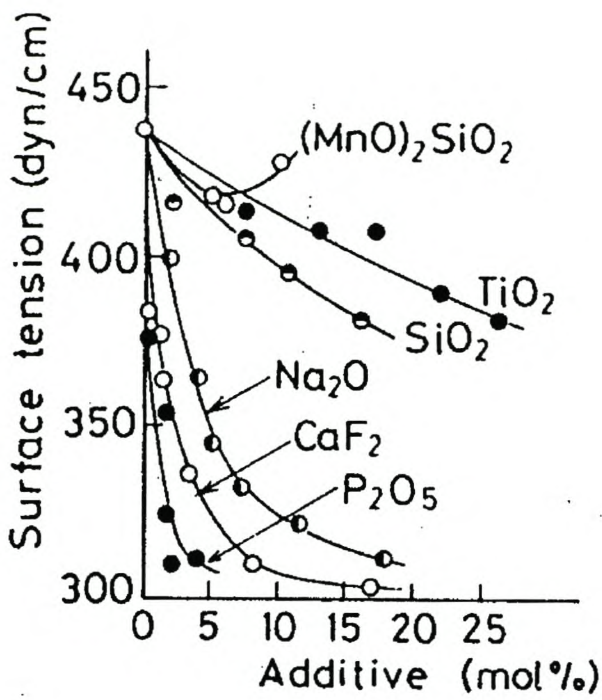


**Figure 2-15. Effect of some additives on surface tension of iron silicate melts (Hara 1986)**

Foam is a dynamic and a non-equilibrium system, and hence the thinning of bubble lamellae results in the break-up of bubbles. Accordingly the retardation of the drainage of liquid increases the foam stability. It is intuitively expected that the retardation is caused by increase of the surface viscosity of melts, but that is not always the case (Hara 1990). It is also suggested that the foam stability for iron oxide-rich melts strongly depends on the surface tension, because the surface tension driven flow (the Marangoni effect) caused by the local difference of surface active components such as $CaF_2$, $Na_2O$, and $P_2O_5$, on the lamellar surface promotes the stability of the foam.

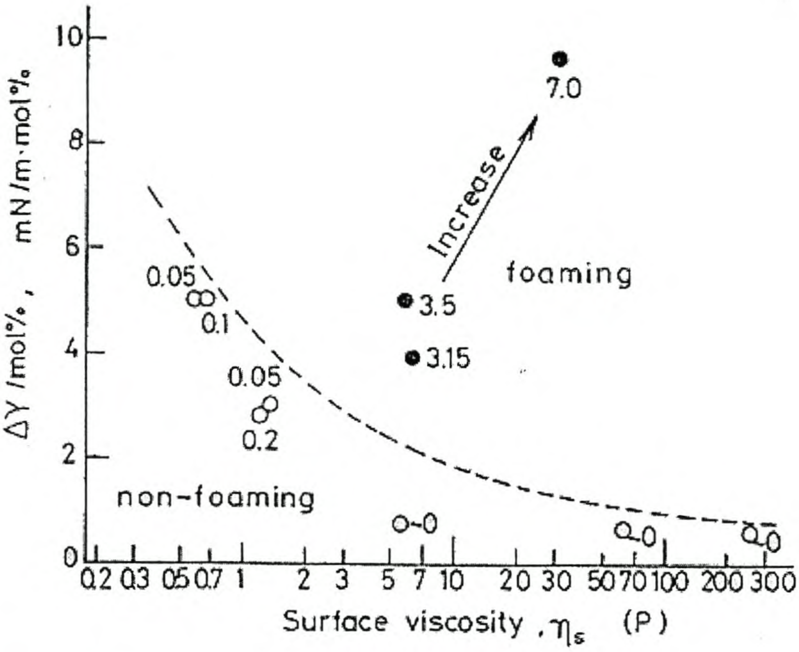


**Figure 2-16. Effect of surface viscosity $\eta_s$ and surface tension depression with melt composition $\Delta\gamma$/mol% on foaminess (numerical values in the figure correspond to the foam height (cm) at Ar gas flow rate of $5cm^3$/min) (Hara 1990)**

Furthermore, it is not the surface tension itself that has the effect on foam height, but rather the depression of the surface tension per unit concentration change of surface active component. This can be seen in figure 2-16. It therefore follows that higher surface viscosity of the melt is necessary, but not enough to stabilise foam. A high surface tension depression is also necessary for a stable foam.

The stabilising effect of solid precipitates on slag foaming has already been mentioned in section 2.4.1.2. The addition of carbonaceous particles, however has been found to decrease the foam height. These phenomena are discussed in section 2.4.3.

## 2.4.3 Influence of solid particles on slag foaming

### *2.4.3.1 Carbonaceous particles*

The addition of coke has been known to suppress slag foaming in steelmaking processes. Zhang (1995) investigated the antifoam effect of carbonaceous particles and the possible mechanisms that could lead to bubble rupture. The comparison of the effect of coke spheres and coke discs on the foam index led to the conclusion that the foam index was reduced as a function of the surface area of the slag covered by the particles, rather than of the weight, volume or total surface area of the particles. When the coverage ratio ($A_{particles}/A_{crucible}$) reached about 15-20% of the slag surface, foaming was almost totally suppressed. Through X-ray examinations Zhang (1995) confirmed the slag foam depression achieved with coke and coal char particles. It was also found that an iron ore pellet and an alumina rod did not cause bubble rupture. This may be due to the fact that the iron ore pellet and the alumina rod are wettable by the slag, while coke particles and coal char particles are not. The interaction of a single ascending bubble with a coke sphere is illustrated in figure 2-17.

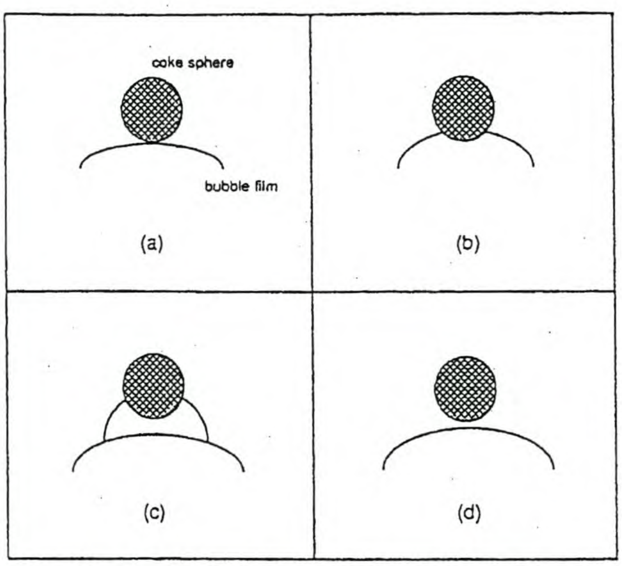


**Figure 2-17. Interaction of a coke particle with an ascending gas bubble (Zhang 1995)**

In the first frame, a bubble was formed above the liquid slag surface, and the liquid slag film came into contact with the spherical coke particle. Then, in the second frame, the liquid slag film was "bridged" by the particle. Subsequently, the bubble bridging the particle ascended further and a new bubble also formed underneath at the slag surface. In the last frame of the image, the bubble that was bridging the particle ruptured. This observation indicates that the rupture of the bubble film must be due to the thinning of the film at the solid-gas-liquid three-phase boundary.

The first mechanism of film rupture proposed states that when a non-wetting solid particle contacts a liquid bubble, there would be a difference between the instantaneous contact angle and the equilibrium contact angle. This driving force would cause the bubble film to move rapidly toward the particle and stretch the film thin enough to rupture. This mechanism seems in good agreement with the X-ray observations. The instantaneous contact angle was observed as about 60 deg while the equilibrium contact angle was determined as about 110 deg.

The second mechanism proposed is the de-wetting of the liquid from the liquid/solid interface when the bubble is bridged by the coke sphere and is caused by the contact angle for both surfaces of the liquid film being greater than 90 deg with the particle at almost the same point.

#### *2.4.3.2 Solid precipitates*

Ito (1989) measured the effect of the presence of second phase particles by adding $2CaO{\cdot}SiO_2$ or CaO particles (diameter 30 to 100 μm) to the slag. Figure 2-18 shows the relationship between the volumetric particle concentration and foaming where $\Sigma^0$ is the foaming index without second phase particles for that particular slag.

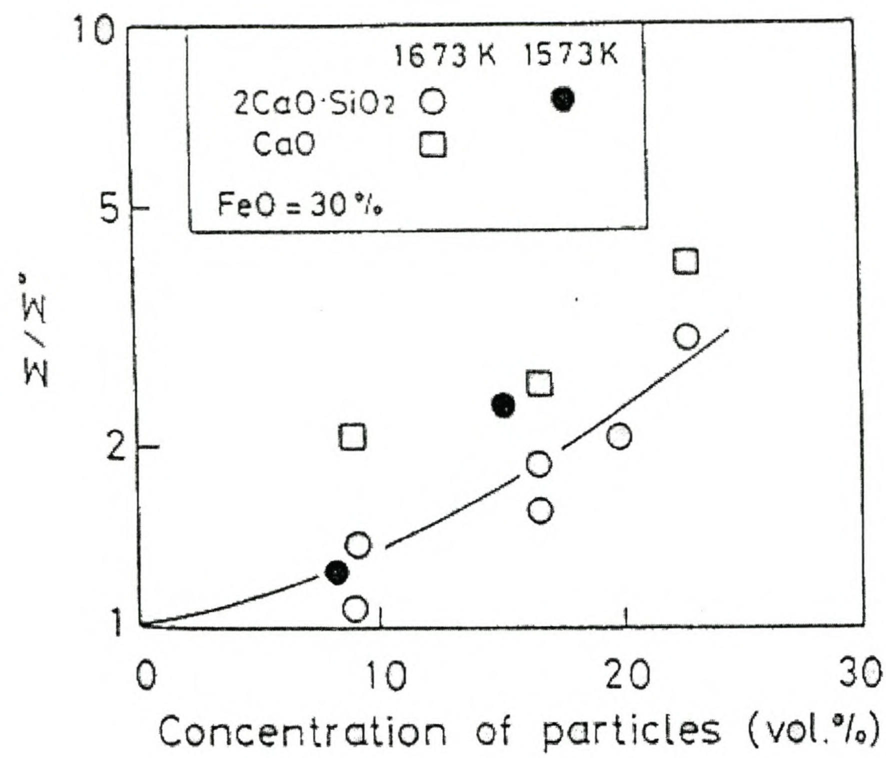


**Figure 2-18. The effect of second-phase particles such as CaO and $2CaO \cdot SiO_2$ on the foaming index (Ito 1989)**

The stabilising effect of particles on slag foaming is believed to be caused by the increase in the slag viscosity. For small solid particles (diameter <100μm) modified Einstein equations can be used to determine the new viscosity of the slag.

$$\mu = \mu_f (1 + 5.5\varepsilon) \qquad \textbf{Eq. 2-33}$$

$$\mu = \mu_f (1 - \varepsilon)^{-2.5} \qquad \textbf{Eq. 2-34}$$

where $\mu_f$ is a viscosity of the liquid slag

$\mu$ is the viscosity of the mixture

and $\varepsilon$ is the volumetric fraction of solid particles.

These equations are only accurate for the low volumetric fractions of solid particles.

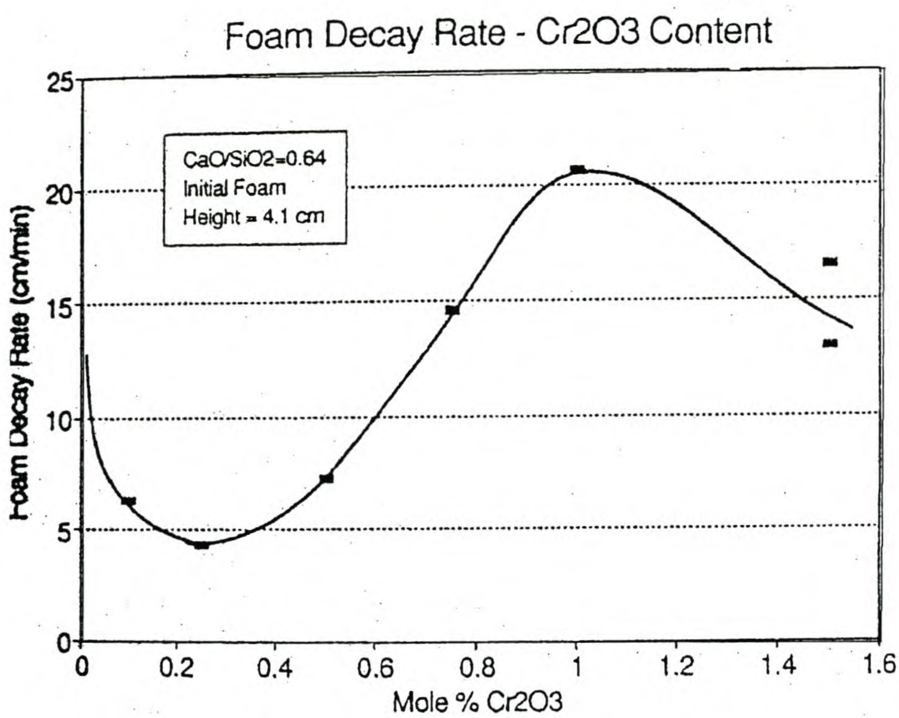


**Figure 2-19. Foam decay rate versus $Cr_2O_3$ content (Utigard 1993)**

Figure 2-19 shows that the foam decay rate for slags containing $Cr_2O_3$ reaches a minimum value at approximately 0.25mol%. This would correspond with the maximum foamability of the slag. The foamability of the slag then decreases until it approaches saturation at 0.8 to 1.2mol% $Cr_2O_3$. The foamability then increases with increasing super-saturation.

### 2.4.4 Influence of bubble size distribution on slag foaming

It has already been discussed that foams can be divided into two groups namely kugelschaum and polyederschaum. The major difference between these two foam types is the mean bubble size for the different foams. Kugelschaum consists of small spherical bubbles, while polyederschaum is usually composed of large bubble cells of polyhedron shape. Consequently, the stability of the foam of a liquid depends not only on its intrinsic physical properties but also on the bubble size.

Figure 2-20 shows the measured bubble diameter as a function of the gas flow rate (Injection nozzle diameter 2.1mm). The mean bubble diameter for bubbles formed by gas injection seems to be independent of the gas flow rate. The addition of 1 wt % $P_2O_5$ decreased the bubble diameter, because $P_2O_5$ decreases the surface tension of the slag.

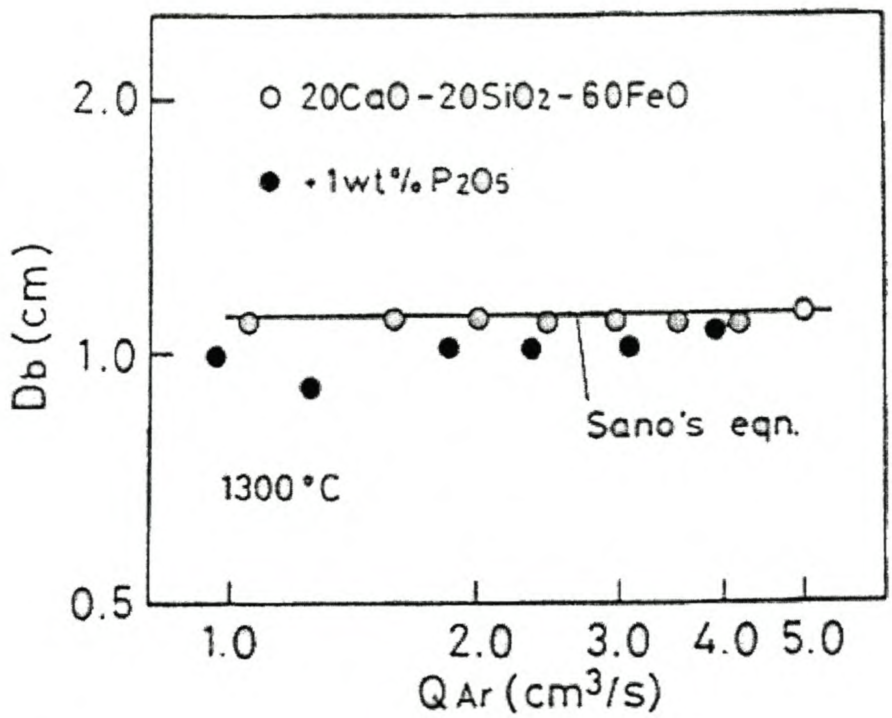


**Figure 2-20 The relation between the mean bubble diameter and gas flow rate at 1573K (Ito 1989)**

Zhang (1995) studied different bubble size distributions generated by bubbling argon through a multi-orifice nozzle through slag and also by generating foam by method of slag/metal interfacial reaction. For data generated by gas injection, the foam height increased by about 70% when the multi-orifice nozzle was used as apposed to the foam height measured for a single-orifice nozzle. Figure 2-21 shows the measured bubble size for slag foams generated by gas injection and it is clear that a smaller mean bubble size leads to higher foam heights and foaming indices. The bubbles observed were of polyhedron shape.

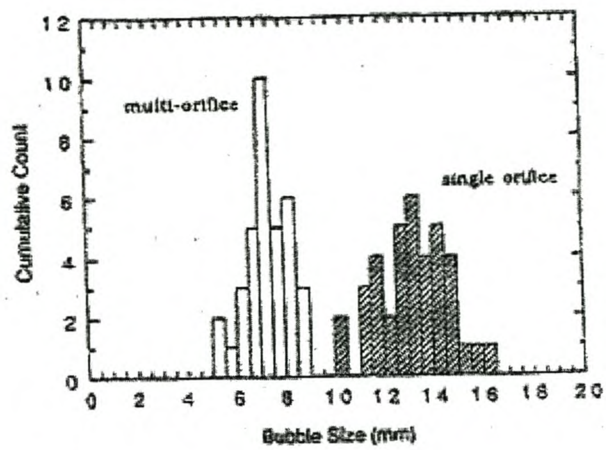


**Figure 2-21 Measured bubble size in the slag foams generated by gas injection (Zhang 1995)**

For foam generated by the slag/metal interfacial reaction, the mean bubble diameter was much smaller (0.7mm). The foam had a kugelschaum character and very high values for the foam index was observed (56 seconds). The conclusion was therefore reached that the foam index decreases for increasing mean bubble diameter.

Using dimensionless analysis, Zhang (1995) found the following relationship between the foam index, the liquid physical properties and the mean bubble size:

$$\Sigma = 115\frac{\mu^{1.2}}{\sigma^{0.2}\rho D_b^{0.9}} \qquad \textbf{Eq. 2-35}$$

where $D_b$ is the average bubble diameter.

The derivation of this equation will be discussed in detail in section 2.6 where it will be compared with other models of slag foaming.

### 2.4.5 Influence of gas type and pressure on slag foaming

The effect of gas properties on slag foaming is not very well researched and most of the data published is by Zhang (1995) and Hara (1986). Hara (1986) found that Ar + 3%$H_2$ gas mixtures showed an increase in foam height achieved for the same gas flow rate. See figure 2-22

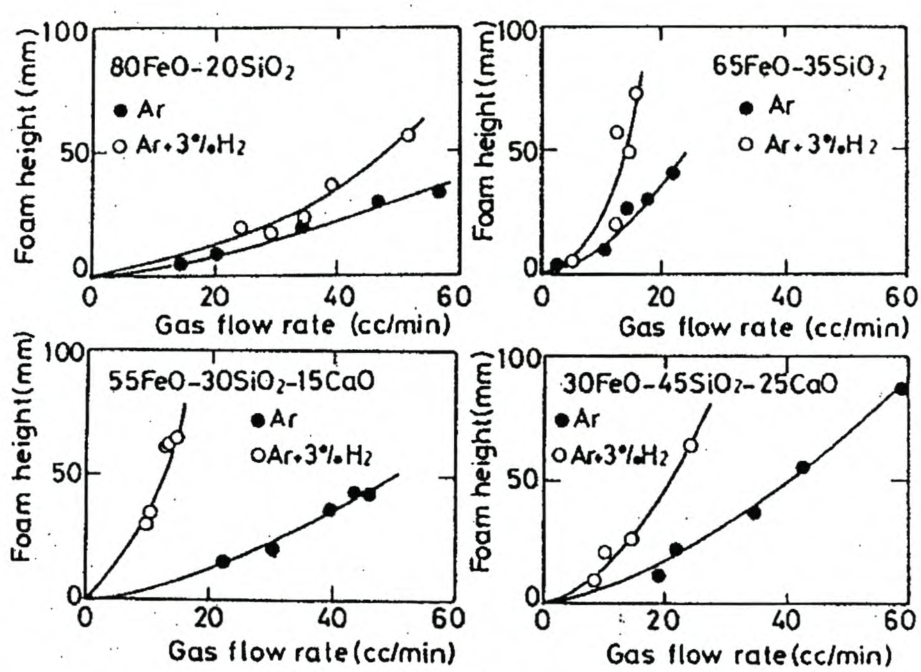


**Figure 2-22. Effect of $H_2$ addition to Ar gas on foam stability (Hara 1986)**

Zhang (1995) however, found that the foam height achieved for the same gas flow rate increased with helium, hydrogen and then argon gas as shown in figure 2-23.

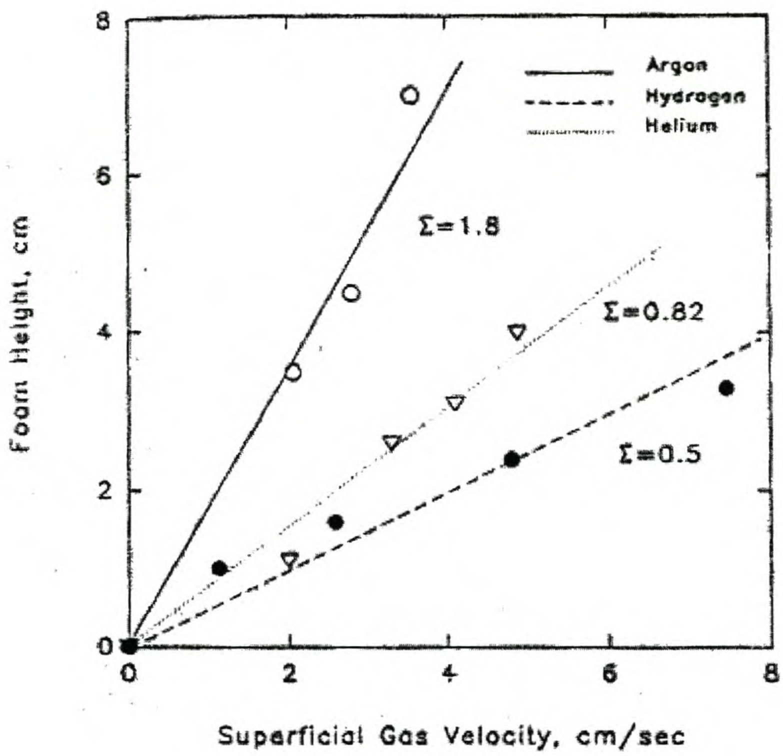


**Figure 2-23. Foam index measured with hydrogen and helium bubbling at 1773K (Zhang 1995)**

X-ray observation of the foams showed no difference in appearance of the size of bubble cells in the foam no matter what type of gas was used. It was therefore concluded that the change in the foam index for different gas type must be the result of the gas physical properties. The importance of the gas physical properties is not clear and more research is needed to conclusively state the importance of gas density, viscosity and molecular weight. It is however possible that gas with smaller molecules has a higher rate of diffusion through bubble lamella and therefore reaches equilibrium quicker than gasses with bigger molecules (see section 2.2.2.2.). For gas with a slow diffusion rate, it will take longer for small bubbles to diffuse into big bubbles and more stable foam will result.

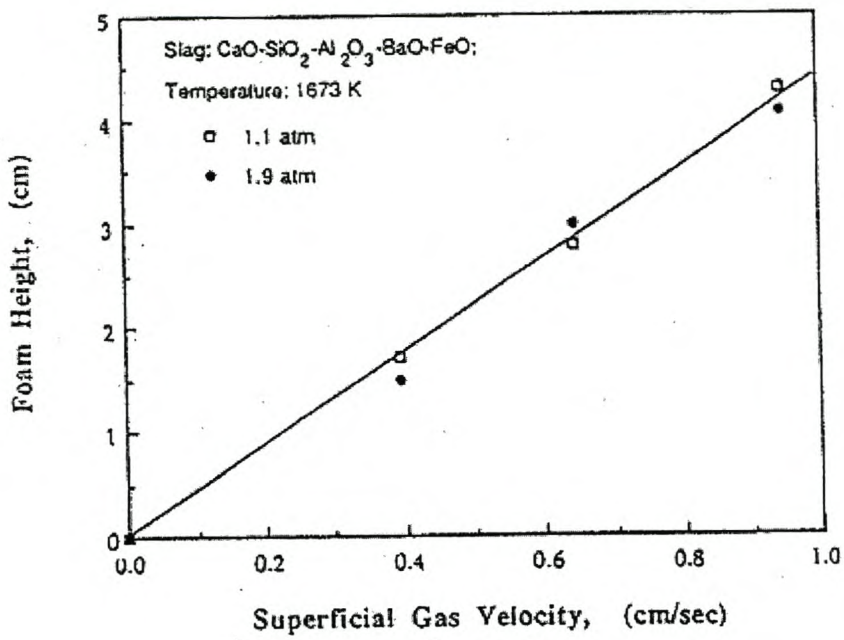


**Figure 2-24. Effect of gas pressure on slag foaming at 1450 C (Zhang 1995)**

The effect of gas phase pressure on the foam height is seen in figure 2-24. It is clear that the increase in pressure did not affect the foaming behaviour of the system investigated. As the gas phase pressure was increased, the gas density was nearly doubled. This seems to support the conclusion that the foam index is not very sensitive to the gas density and molecular mass. The molecule size and form may be what distinguishes different foaming behaviour. The practical significance of this is that when the foam index is constant, the foam volume will remain the same if the volumetric gas flow rate remains constant under different pressures. However, if the mass flow rate of the gas is constant through the liquid slag, an increase in pressure will reduce the gas volume and thus decrease the foam volume.

## 2.5 Slag foam models

The aim of this section is to review models proposed to describe slag foaming behaviour and to evaluate these models critically.

### 2.5.1 Dimensional analysis and foaming in iron and steelmaking processes (Ito, 1989)

Dimensional analysis is not a specific model based on the mechanisms of foaming, but rather a technique that is useful in determining empirical relationships illustrating the influence of different variables on a system. Ito (1989) developed a model for slag foaming that is based on dimensional analysis. They choose the foaming index ($\Sigma$ [s]), density ($\rho$ [$kg \cdot m^{-3}$]), surface tension ($\sigma$ [$N \cdot m^{-1}$]) and viscosity ($\mu$ [$Pa \cdot s$]) as variables for their analysis and included gravity (g [$m \cdot s^{-2}$]) in order to balance dimensions.

$$f(\Sigma, \sigma, \mu, \rho, g) = C \qquad \textbf{Eq. 2-36}$$

In equation 2-36 there are five variables and three fundamental dimensions; therefore according to the Buckingham's $\pi$ theorem two dimensionless groups are to be obtained.

The following two dimensionless numbers were obtained:

$$N_1 = \frac{\sigma^{3/4} \rho^{1/4}}{\mu g^{1/4}} \qquad \textbf{Eq. 2-37}$$

$$N_2 = \frac{\Sigma \rho^{1/4} g^{3/4}}{\sigma^{1/4}} \qquad \textbf{Eq. 2-38}$$

The relation between log $N_1$ and log $N_2$ were obtained as a straight line. The slope of the line was estimated to be approximately equal to $-1$. The resulting empirical equation was derived for a $CaO$-$SiO_2$-$FeO$-($Al_2O_3$) system:

$$\Sigma = 5.7 \times 10^2 \frac{\mu}{\sqrt{\sigma \rho}} \qquad \textbf{Eq. 2-39}$$

Jiang (1991) also used dimensional analysis to form an empirical model for slag foaming. Two different dimensionless numbers were however chosen:

$$\Pi_1 = \frac{\Sigma g \mu}{\sigma} \qquad \textbf{Eq. 2-40}$$

$$\Pi_2 = \frac{\rho \sigma^3}{\mu^4 g} \quad \textbf{(Morton number)} \qquad \textbf{Eq. 2-41}$$

The dimensionless number given in equation 2-41 is also called the Morton number, which describes the balance between gravitational, viscous, and surface tension forces.

Once again the logarithms of the dimensionless numbers were compared and the following relationship was found:

$$\log(\Pi_2) = -2\log(\Pi_1) + 5.11 \qquad \textbf{Eq. 2-42}$$

This equation can be rewritten into

$$\Sigma = 115 \frac{\mu}{\sqrt{\rho\sigma}} \qquad \textbf{Eq. 2-43}$$

When comparing equation 2-43 with equation 2-39 it is seen that this analysis gives the same dependence for the foam index on the slag properties, namely $\Sigma \propto \frac{\mu}{\sqrt{\rho\sigma}}$, but different coefficients were obtained. The difference in the coefficients is believed to be due to the difference in the slag properties used for each analysis. Slightly different models were used to determine slag properties. Dimensional analysis should give the same results even if the dimensionless groups are different. When Jiang did the analysis using equation 2-37 and 2-38 as dimensionless numbers, the final correlation was described by:

$$\Sigma = 108 \frac{\mu}{\sqrt{\rho\sigma}} \qquad \textbf{Eq. 2-44}$$

Within the accuracy of the determination equations 2-43 and 2-44 are identical. It must be noted that the slag properties used in these analyses were extrapolated with respect to temperature and composition and that molar volumes and surface tensions of slag solutions were calculated as linear functions of composition using the molar volumes and surface tensions of the pure components. The viscosities were obtained from Urbain's model, which is of the form:

$$\mu = A \cdot T \cdot \exp(B / T) \qquad \textbf{Eq. 2-45}$$

where A and B are viscosity parameters and T is the temperature (K)

A more detailed discussion of Urbain's model can be found in Mills (1995).

Gaskell (2000) repeated Jiang's (1991) analysis using measured data for the surface tension, viscosity and density values of the different slags. They obtained a slightly different correlation

$$\Sigma = 100 \frac{\mu^{0.54}}{\rho^{0.39} \sigma^{0.15}} \qquad \textbf{Eq. 2-46}$$

The variation, with composition, of the foaming index measured by Ito (1989) and that given by equation 2-46 are shown in figure 2-25.

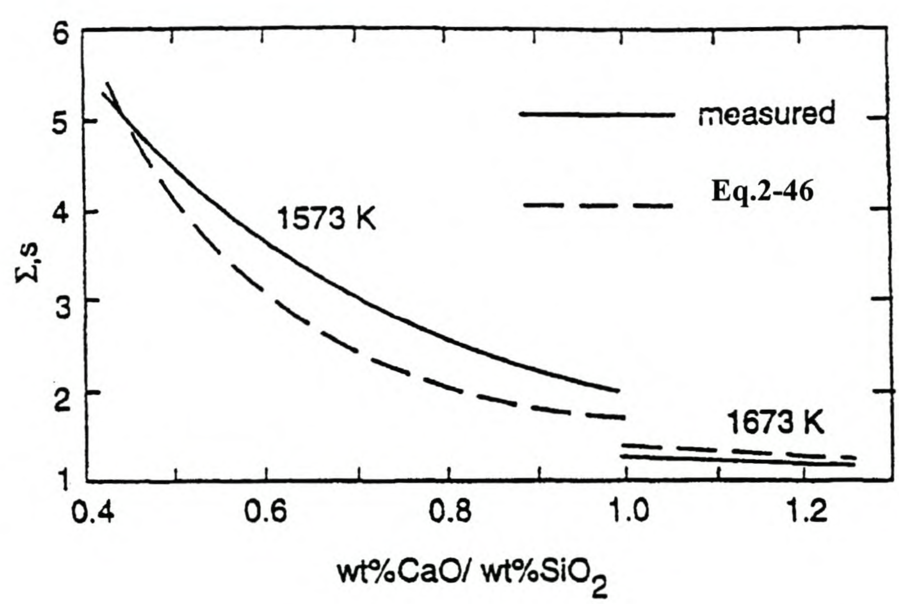


**Figure 2-25. The variations, with composition, of the measured foaming indexes and the values calculated from equation 2-46 (Gaskell 2000)**

#### *2.5.1.1 Evaluation of the model*

This model is empirical in nature and should therefore never be used to extrapolate results. The model assumes that the foam index is independent of the superficial gas velocity. This assumption is only true for low gas flow rates. The effect of the initial liquid depth is also ignored. The model does not take into account the average bubble size in the foam, and can therefore only be used for foams generated by gas injection if the parameters were determined for slags foamed by gas injection.

The model is however very easy to use, as physical properties can be estimated by correlations and no further data are required.

### 2.5.2 Dimensional analysis looking at bubble size influence on slag foaming (Zhang, 1995)

An empirical model looking at the effect of bubble size on slag foaming was derived by Zhang (1995). The model is similar to the models proposed by Ito (1989) and Jiang (1991) in that it is derived from dimensionless analysis. The variables selected as influencing the foam index are shown in equation 2-47.

$$f(\Sigma, \sigma, \mu, D_b, \rho, g) = C \qquad \textbf{Eq. 2-47}$$

The variables are the same as in equation 2-36, but with the addition of $D_b$, the average bubble diameter [m].

In equation 2-49 there are six variables and three fundamental dimensions; therefore according to the Buckingham's $\pi$ theorem three dimensionless groups are to be obtained.

The following three dimensionless numbers were obtained:

$$\Pi_1 = \frac{\Sigma g \mu}{\sigma} \quad \textbf{(Denoted as } \mathbf{N_\Sigma} \textbf{ for convenience)} \qquad \textbf{Eq. 2-48}$$

$$\Pi_2 = \frac{\rho\sigma^3}{\mu^4 g} \quad \textbf{(Morton number)} \qquad \textbf{Eq. 2-49}$$

$$\Pi_3 = \frac{\rho^2 D_b^3 g}{\mu^2} \quad \textbf{(Archimedes number)} \qquad \textbf{Eq. 2-50}$$

The Archimedes number describes the ratio of the buoyancy force to the viscous force. The following equation can therefore be written:

$$N_\Sigma = C \cdot Mo^\alpha Ar^\beta \qquad \textbf{Eq. 2-51}$$

The dimensionless numbers were calculated from the measured foam index, the average bubble diameter, and the slag physical properties. By taking the logarithm of both sides of equation 2-51 and carrying out a multiple component linear regression analysis, coefficients α, β, and C were obtained. The final result of the dimensional analysis is described by the following equation:

$$N_\Sigma = 900 \cdot Mo^{0.39} Ar^{-0.28} \qquad \textbf{Eq. 2-52}$$

Considering the experimental error, the coefficients can be taken as 0.4 and –0.3. The gravitational acceleration is 9.8m/s$^2$ and so the foam index is given by

$$\Sigma = 115 \frac{\mu^{1.2}}{\sigma^{0.2} \rho D_b^{0.9}} \qquad \textbf{Eq. 2-53}$$

In the preceding dimensional analysis the bubble diameter was taken as an independent variable. In reality the bubble diameter is also dependent on the physical properties of the fluid/melt (e.g. surface tension. See figure 2.20, p 2.35) and other conditions related to the formation of the bubble, such as the orifice diameter if the bubble is generated through gas injection or the slag/metal contact angle if the bubbles is formed by slag/metal reactions. It is therefore expected that the coefficients relating the liquid properties to the foam index change when the effect of bubble size is introduced (compare equation 2-43 with equation 2-53).

#### *2.5.2.1 Evaluation of the model*

This model is similar to the previous model in many aspects. It is empirical in nature and also ignores the effect of initial liquid depth and assumes that the foam index is independent of the superficial gas velocity. It does however take into account the influence of the average bubble size in the foam.

The inclusion of the average bubble diameter into the model makes the applications of the model more difficult, as the bubble size distribution of metallurgical foams are difficult to determine without expensive equipment.

### 2.5.3 Physical model of slag foaming (Ogawa, 1993)

In contrast with the previous models, the foaming model proposed by Ogawa (1993) is based on a more fundamental approach. The model deals with foams generated by gas formation at the slag/metal interface due to chemical reactions.

Using X-ray fluorescence observations, slag foaming phenomena are divided into three stages:

1. Formation of CO bubbles at the slag/metal interface and their detachment,
2. Rise if the bubbles in the slag layer and their accumulation under the free surface (formation of foam), and
3. Coalescence of bubbles in the foam and the rupture of bubbles films at the top surface of the slag, which tends to destroy the foam.

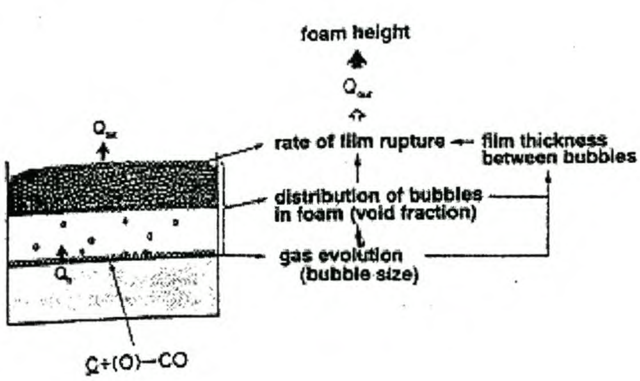


**Figure 2-26. A physical model of foaming (Ogawa 1993)**

The foam height is decided by the difference between the rate of gas generation, $Q_{in}$, and the rate of gas escape from the slag, $Q_{out}$. The rate of change in the foam height is expressed as equation

$$\frac{dH}{dt} = \frac{Q_{in} - Q_{out}}{A} \qquad \textbf{Eq. 2-54}$$

where H is the foam height and A is the cross-sectional area of the vessel.

The gas evolution rate can be determined from experiments or through reaction rate models. The model therefore concentrates on the factors influencing the gas escape rate, which determines the foam life. The gas escape rate is determined by the rupture rate of bubble films at the top surface of the slag, the size of the bubbles and the number of bubbles. The rate of bubble rupture may be governed by the bubble size, the film thickness between bubbles and the physical properties of the slag. The number of bubbles and the film thickness in the foam are considered to be determined by the gas evolution rate, the bubble size and the slag properties. Therefore if the bubble size, the distribution of the bubbles in the foam and the rupture of bubble films at the top surface of the slag are known, the foam height can be predicted.

The calculations of the configuration of a bubble at the slag/metal interface are based on the resolution of Laplace's equation of capillarity. This equation expresses the difference of pressure across the interface between 1 and 2.

$$\Delta P = \gamma_{12}(1/R_1 + 1/R_2) \qquad \textbf{Eq. 2-55}$$

where $\gamma_{12}$ is the interfacial tension between the two phases and $R_1$ and $R_2$ are the principal radii of curvature of the interface.

At equilibrium this pressure difference is balanced by the difference of static pressure, which is a function of position on the interface, the difference between the densities of the two phases and the gravity. If the descending vertical axis is called Oz, this balance gives at any point of the interface:

$$\begin{aligned}\Delta P &= \gamma_{12}(1/R_1 + 1/R_2) \\ &= (\rho_1 - \rho_2)g(z - z_0) + \gamma_{12}(1/R_{1O} + 1/R_{2O})\end{aligned} \qquad \textbf{Eq. 2-56}$$

where, $\rho_1$ and $\rho_2$ are the densities of the two phases, g is the gravity acceleration and O is a point of reference where the principal radii of curvature are known.

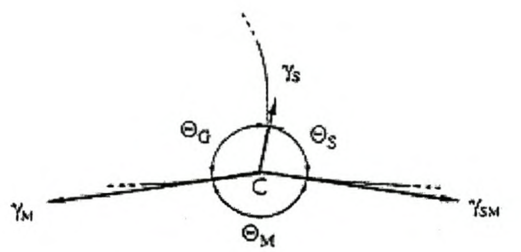


**Figure 2-27. Schematic drawing of the joining point between three phases (Ogawa 1993)**

At the joining point of the three phases, if the interfacial tensions are considered as force vector (sketch), the angles formed by the three phases are expressed by the relationship:

$$\cos(\Theta_G) = (-\gamma_M^2 - \gamma_S^2 + \gamma_{SM}^2)/2\gamma_S\gamma_M \qquad \textbf{Eq. 2-57}$$

$$\cos(\Theta_M) = (-\gamma_M^2 + \gamma_S^2 - \gamma_{SM}^2)/2\gamma_{SM}\gamma_M \qquad \textbf{Eq. 2-58}$$

$$\cos(\Theta_S) = (\gamma_M^2 - \gamma_S^2 - \gamma_{SM}^2)/2\gamma_{SM}\gamma_S \qquad \textbf{Eq. 2-59}$$

where $\gamma_S$, $\gamma_M$ and $\gamma_{SM}$ are the interfacial tensions of gas/slag , gas/metal and slag/metal respectively. The angle $\Theta_S$ is commonly referred to as the contact angle between slag and metal.

Next the equations at each of the three interfaces must be defined. The gas/slag interface is studied first.

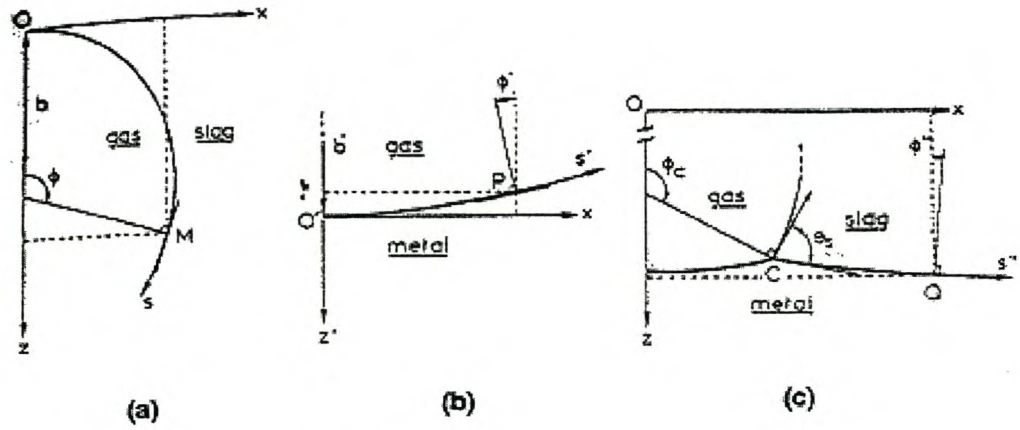


**Figure 2-28. Schematic drawing of the interface between two phases. a) gas/slag interface, b) gas/metal interface, c)slag/metal interface (Ogawa 1993)**

The bubble is assumed to be axis-symmetric as show in figure 2-22 a). At the apex O of the bubble, the two radii of the curvature are equal to the same value, b. ($R_{1O}$=$R_{2O}$=b)
A point M(x, z) may be associated with an angle $\Phi$ between the normal at the interface and the vertical axis. If the curvilinear abscissa on the interface is called s, the two principal radii of the curvature of the interface are such that:

$$1/R_1 = \partial\Phi / \partial s \text{ and } 1/R_2 = \sin\Phi / x \qquad \textbf{Eq. 2-60}$$

Thus, the gas/slag interface can be described by combining equations 2-55, 2-56 and 2-60 into:

$$\partial\Phi / \partial s = -\sin\Phi / x + \frac{(\rho_G - \rho_s)g}{\gamma_s} \cdot z + 2/b \qquad \textbf{Eq. 2-61}$$

and seeing from the geometry that

$$\partial x / \partial s = \cos\Phi \quad \text{and} \quad \partial z / \partial s = \sin\Phi \qquad \textbf{Eq. 2-62}$$

with the initial conditions at the apex O: x=z=s=$\Phi$=0.

We can now define the equations describing the gas metal interface. It is possible to show that the curvature of this interface has an opposite sign compared to that of the gas/slag interface as shown in figure 2-22 b). Let O'(0,h) be the position (unknown) of the bottom of the bubble and b' the value of the two radii of curvature at this point. The generic equation is written in the reference axis (O'x,O'z) where z'=z-h.

The shape of the gas/metal interface is described by the following system:

$$\partial\Phi'/\partial s' = -\sin\Phi/x + \frac{(\rho_G - \rho_M)g}{\gamma_M}\cdot z' + 2/b' \qquad \textbf{Eq. 2-63}$$

and seeing from the geometry that

$$\partial x/\partial s' = \cos\Phi' \quad \text{and} \quad \partial z'/\partial s' = \sin\Phi' \qquad \textbf{Eq. 2-64}$$

with the initial conditions at the apex O': x=z'=s'=Φ'=0.

Lastly, we have to describe the slag/metal interface. For this interface, the joining point C is the reference point as is shown in figure 2-22 c). The shape of the slag/metal interface can be computed by resolution of the system:

$$\begin{aligned}\partial\Phi''/\partial s'' = -\sin\Phi''/x + \frac{(\rho_M - \rho_S)g}{\gamma_{SM}}\cdot z + \\ (2\gamma_S/b - 2\gamma_M/b' + (\rho_G - \rho_M)g\cdot h)/\gamma_{SM}\end{aligned} \qquad \textbf{Eq. 2-65}$$

and seeing from the geometry that

$$\partial x/\partial s'' = \cos\Phi'' \quad \text{and} \quad \partial z/\partial s'' = \sin\Phi'' \qquad \textbf{Eq. 2-66}$$

with the initial conditions at point C: $x=x_C$; $z=z_C$; s"=0;Φ"= $\Phi_c+\Theta_S-\pi$

For each one of the three interfaces, the positions of the successive points spaced at fixed distance δs apart, are calculated step by step. In order to compute the displacement (dx/dz) corresponding to the relative position of the two successive points, Taylor series expansion is used.

An iterative procedure is then used to compute the maximum volume of a bubble, which exists stably at the slag metal interface. The size of the bubble was obtained from this volume, assuming that the bubble is spherical.

X-ray observations of slag foaming showed the emergence of two superposed layers in the slag:

1. in the lower layer, the bubbles seemed to move freely and the void fraction is low,
2. in the upper layer, they formed a dense packed bed where the void fraction is much higher.

A theoretical model proposed for two-phase flows evaluates the void fractions of the two layers. The model is based on the assumptions of a flat velocity profile and that the rise velocity W   in an infinite medium follows the modified Stokes law:

$$W_\infty = \frac{(\rho_L - \rho_G) g R^2}{3\mu_L} \qquad \textbf{Eq. 2-67}$$

where $\rho_L$ and $\rho_G$ are the densities of liquid and gas, $\mu_L$ is the viscosity of the liquid and R is the radius of the bubbles.

From the relationship between the actual and the superficial gas velocities, two values of the void fraction ($\alpha_1$ and $\alpha_2$), which correspond to two layers, are theoretically obtained.

$$\alpha_1 = (1 + \sqrt{1 - 4 v_g / W_\infty})/2 \quad \text{and} \quad \alpha_2 = 1 - \alpha_1 \qquad \textbf{Eq. 2-68}$$

where $v_g$ is the superficial gas velocity as defined in section 2-3.2.

As it is difficult to calculate the rate of film rupture directly for a bubble at the top of a foam, it was assumed that the film life of a bubble at the top of a foam is the same as that at the top surface of slag without foam. The Volume of Fluid (VOF) method was adopted to calculate the film rupture of the bubble. In this method the free surface is treated by introduction of a function F. The value of F in a cell is equal to the fractional volume of the cell occupied with fluid. By calculating F, the new free surface orientation in each cell is determined. In the cell with F value between 0 and unity, the curvature of the free surfaces is obtained from F values of neighbouring cells. The pressure and velocity fields are calculated with use of the surface tension of the liquid and this curvature.

#### *2.5.3.1 Evaluation of the model*

This model is based on a very fundamental approach. This led to the development of a complex set of equations that require iterative operations to solve. The model is also limited to slag foams where bubbles are formed due to a reaction at the metal/liquid interface, therefore excluding foams where gas injection and coal-based reduction reactions leads to bubble formation.

### 2.5.4 A model for slag foaming for the in-bath smelting process (Lin, 1995)

Modelling experiments suggest a complex dependence of foam height on bubble flow regimes. These, in turn, are dependent on the sizes of the bubbles, superficial gas rates and physical properties of the liquids. To obtain a general relationship characterising foaming behaviour, one can consider that the total foam volume of gas in a foam is related to increase in foam height, according to continuity:

$$V_g = \Delta h \cdot A \qquad \textbf{Eq. 2-69}$$

where $\Delta h$ is the bath height increment and A is the cross-sectional area of the column.

On the other hand, the total volume of the gas can also be described as:

$$V_g = (\text{number of bubbles in foam bed}) \cdot \mathrm{V_b} \qquad \textbf{Eq. 2-70}$$

where $V_b$ is the volume of a single bubble of average bubble size.

The number of bubbles, $N_b$, can be defined as

$$N_b = (\text{frequency of bubble formation}) \times (\text{mean residence time of bubbles in foam bed}):$$

$$N_b = \frac{Q_g}{V_b} \cdot \frac{(h + \Delta h)}{v_s} \qquad \textbf{Eq. 2-71}$$

By combining equations 2-70 and 2-71 we find that

$$V_g = Q_g \cdot \frac{(h + \Delta h)}{v_s} \qquad \textbf{Eq. 2-72}$$

where $v_s$ is the average slip velocity of the bubbles in the foam bed.

$\frac{(h+\Delta h)}{v_s}$ represents the mean residence time of the bubbles in the foam bed. Since $Q_g = v_g \cdot A$, we can combine equation 2-69 with equation 2-72 to show that

$$\Delta h = \frac{v_g}{v_s - v_g} \cdot h \qquad \textbf{Eq. 2-73}$$

Equation 2-73 was derived from volume continuity and it signifies that the foam height is not only dependent on the superficial gas velocity, but also on the average slip velocity of the bubbles and on the initial depth of liquid (h). The average slip velocity of the bubbles can further be influenced by sizes of the bubbles, the physical properties of the liquid and interaction between the bubbles. If the bubble size is small, as in most kugelschaum, their corresponding average rise velocity is also very small. Based on equation 2-73, a large foam height would be expected even at low superficial gas velocity, since $v_s$ $v_g$ in the denominator. For the other case, where bubbles are large and have a high rise velocity, only a small foam height may be achieved even at large gas flow rates. This has been observed for the churn-turbulent flow regime (Lin 1995).

Equation 2-73 can also be rewritten to clarify the relationship between the superficial gas velocity and the average slip velocity of the bubbles.

$$v_s = \frac{v_g}{\varepsilon} \qquad \textbf{Eq. 2-74}$$

where $\varepsilon = \frac{\Delta h}{\Delta h + h}$ is, by definition, the average hold up of the gas within the foam and $v_g$, the superficial gas velocity.

Its physical significance is that the average slip velocity of the bubbles is equal to the interstitial gas velocity in a fraction, ε, of the cross-sectional area of the foam bed.

Experimental studies on steelmaking slags showed a remarkably constant ε value of approximately 0.8 even though superficial gas velocities increased form 2.0m/s to 4.0m/s. Based on these results, $v_s$ could be readily estimated from equation 2-74. Large values for $v_s$ obtained by Lin (1995) indicate the presence of large bubbles in the foam bed.

To predict the amount of gas hold up in the foaming slag, equation 2-74 is not enough, because it contains two unknowns ($v_s$ and $\varepsilon$). Other equations to determine $\varepsilon$ have been proposed.

In general, the commonly accepted correlations for slip velocity have the following form:

$$v_s = v_T(1-\varepsilon)^{m-1} \qquad \textbf{Eq. 2-75}$$

where $v_T$ is the terminal rise velocity of a single bubble of average size and m = 2 for small bubbles and m = 0 for large bubbles.

When a single bubble rises through a large body of stationary liquid, its terminal velocity can be obtained by equating the drag force and buoyancy force:

$$\tfrac{1}{2}\rho_L v_T^2 A C_D = \frac{\pi}{6} D_b^3(\rho_L - \rho_g)g \qquad \textbf{Eq. 2-76}$$

The area of one bubble can be described as $A = \pi \frac{D_b^2}{4}$ and therefore we can simplify equation 2-76 to

$$v_T = \sqrt{\frac{4gD_b}{3C_D}} \qquad \textbf{Eq. 2-77}$$

### *2.5.4.1 Terminal velocity for small bubbles*

For small bubbles, which can be considered as rigid spheres, the drag coefficient is $C_D$=24/$Re_b$, where $Re_b$ is the Reynolds number for a single bubble of average size. In this case equation 2-79 reduces to Stoke's solution:

$$v_T = \frac{(\rho_L - \rho_G)gD_b^2}{18\mu_L} \qquad \textbf{Eq. 2-78}$$

By combining equations 2-74, 2-75 and 2-78 we can express $v_s$ in terms of the physical properties of the liquid, the average bubble size and the superficial gas velocity.

#### 2.5.4.2 *Terminal velocity for large bubbles*

For large bubbles Lin (1995) assumed that $C_D$=8/3. This assumption is only valid for slags with a viscosity smaller than 5.0g/s.cm. As a result equation 2-77 reduces to:

$$v_T = \sqrt{0.5 g D_b} \qquad \textbf{Eq. 2-79}$$

By combining equations 2-74, 2-75 and 2-79 we can express $v_s$ in terms of the average bubble size and the superficial gas velocity.

#### 2.5.4.3 *Estimation of average bubble size in slag foaming*

If however it is possible to determine the average slip velocity and gas hold up experimentally, these equations can be rewritten to estimate the average bubble size. Using the equations for large bubbles we find:

$$D_b = \frac{2}{g}\left(\frac{1-\varepsilon}{\varepsilon} v_g\right)^2 \qquad \textbf{Eq. 2-80}$$

#### 2.5.4.4 *Evaluation of the model*

This is a fundamental model based on volume continuity. The model does not predict the foam index, but rather the change in foam height as function of the gas void fraction or gas hold up, the superficial gas velocity and the gas average slip velocity. There is some uncertainty about the true value of the drag coefficient.

The model is very easy to use if a constant gas void fraction can be assumed and only slightly more difficult if the void fraction has to be estimated.

### 2.5.5 Multiphase fluid mechanics approach to gas hold-up in bath smelting processes (Gou, 1996)

In this model, equations are written for mass and momentum conservation in the vertical direction or the gas phase only. The equations are averaged over the cross-section of the vessel.

The gas continuity equation,

$$\frac{d}{dz}(\rho_G \cdot \varepsilon \cdot v_s) = 0 \qquad \textbf{Eq. 2-81}$$

simply states that the mass flux is unchanged in the vertical direction. The momentum equation for the gas phase shows that the acceleration of the gas is due to the balance of the buoyancy and drag forces:

$$\frac{d}{dz}(\rho_G \cdot \varepsilon \cdot {v_s}^2) = F_B - F_D \qquad \textbf{Eq. 2-82}$$

The buoyancy force is

$$F_B = (\rho_L - \rho_G) g \varepsilon \qquad \textbf{Eq. 2-83}$$

The interphase drag force between gas and liquid can be written as

$$F_D = \frac{3}{4}\frac{C_D}{D_B} {v_s}^2 \rho_m \varepsilon = f_D {v_s}^2 \rho_m \varepsilon \qquad \textbf{Eq. 2-84}$$

$f_D$ is called the drag factor.

The mixture density, $\rho_m$, is defined as

$$\rho_m = \rho_G \varepsilon + \rho_L (1 - \varepsilon) \qquad \textbf{Eq. 2-85}$$

in which the local gas density is calculated from the ideal gas law

$$\rho_G = \frac{PMr}{RT} \qquad \textbf{Eq. 2-86}$$

The total pressure, P, is the hydrostatic pressure due to the mixture

$$P = P_{atm} + g \rho_m (h - z) \qquad \textbf{Eq. 2-87}$$

where h is the total mixture height.

It is assumed that the vessel is tall enough and that there is no loss of liquid from the system. Consequently the weight of the liquid is conserved before and during gas injection, which is expressed mathematically as

$$M_L = A\int_{0-}^{h}\rho_L(1-\varepsilon)dz = Ah_0\rho_L \qquad \textbf{Eq. 2-88}$$

Equations 2-81 through 2-84 can be manipulated to obtain the differential equation for the gas velocity over the vessel height:

$$\frac{dv_s}{dz} = \frac{g(\rho_L - \rho_G)}{v_s\rho_G} - \frac{f_D v_s \rho_m}{\rho_G} \qquad \textbf{Eq. 2-89}$$

The gas void fraction is determined from equation 2-74.

As it has been observed in industry, the void fraction and the gas velocity are virtually constant throughout the expanded slag. Equation 2-89 can therefore be simplified by setting $\frac{dv_s}{dz} = 0$. Also, the gas density is much less than that of the liquid, $(\rho_L - \rho_G) \quad \rho_L$ and $\rho_m \quad \rho_L(1-\varepsilon)$ and this permits further simplification of equation 2-89 to

$$f_D = \frac{g\varepsilon^2}{v_g^{\,2}(1-\varepsilon)} \qquad \textbf{Eq. 2-90}$$

Combining equation with an empirical regression equation for $f_D$ determined by (Gou 1996) to eliminate $f_D$, a simple expression between the superficial gas velocity and the gas void fraction are obtained:

$$\frac{\varepsilon^2}{1-\varepsilon} = 0.91 v_g^{\,0.57} \qquad \textbf{Eq. 2-91}$$

In figure 2-29 Gou showed how an expanded slag foams (high gas velocities) behave differently from slag foams generated by low gas flow rates.

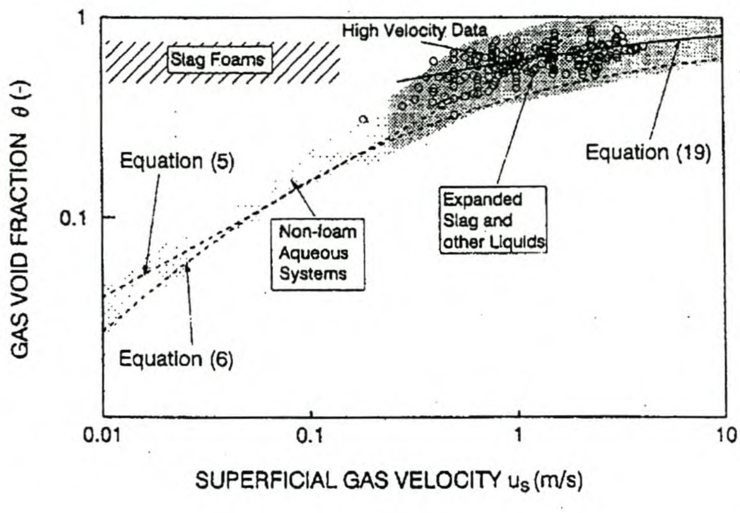


**Figure 2-29. Relationship between superficial gas velocity and void fraction for three groups of data: slag foams from small-scale experiments, non-foaming aqueous systems and aqueous systems (Gou 1996)**

#### *2.5.5.1 Evaluation of the model*

This is a model based on mass and momentum conservation for the gas phase. The drag factor had to be experimentally determined before the model could be solved. Results showed good agreement with slag foam and aqueous foam data.

### 2.5.6 Dynamic model of slag foaming in oxygen steelmaking converters (Mishra, 1998)

This model was based on observation of slag foaming and emulsification in oxygen steel making converters. The model strives to include the effect of metal droplets within the slag in a model of slag foaming behaviour. In steelmaking converters oxygen is injected into the converter through a lance.

The system consisting of gas, slag and metal droplets are described by the Emulsion number, En, defined as:

$$\text{En} = \frac{\text{Mean residence time of metal droplets in slag, } (\tau_\text{d})}{\text{Mean residence time of gas bubbles in the slag, } (\tau_\text{b})} \qquad \textbf{Eq. 2-92}$$

$$= \frac{h / v_d}{h / v_g} = \frac{v_g}{v_d}$$

The settling velocity of the metal droplets, $v_d$, can be calculated as

$$v_d = \frac{(\rho_m - \rho_{SG}) g D_m^2}{18 \mu_{SG}} \Delta_{SM} \qquad \textbf{Eq. 2-93}$$

where the factor $\Delta_{SM}$ accounts for the inter-particle interactions of the ensemble of droplets ($\Delta_{SM}$ >1)

$$\Delta_{SM} = \frac{3\mu_{SG}(1-\varepsilon_m{}^{1/3})(1-\varepsilon_m{}^{5/3}) + [3 - \frac{9}{2}(\varepsilon_m{}^{1/3} - \varepsilon_m{}^{5/3}) - 3\varepsilon_m{}^2]\mu_m}{2\mu_{SG}(1-\varepsilon_m{}^{5/3}) + (3 + 2\varepsilon_m{}^{5/3})\mu_m} \qquad \textbf{Eq. 2-94}$$

and the average diameter of droplets , $D_m$, can be calculated by knowing the limiting diameter of droplets, $D_{lim}$, ejected from the jet impact zone

$$D_m = 0.2 D_{\lim} \qquad \textbf{Eq. 2-95}$$

where

$$D_{\lim} = 5.513 \times 10^{-6} \left[ 10 \left( \frac{D_t}{x_{lance}} \right)^2 P_{at} \left\{ 1.27 \left( \frac{P_O}{P_{at}} \right) - 1 \right\} \cos\theta_{nozzle} \right]^{1.206} \qquad \textbf{Eq. 2-96}$$

where $D_t$ is the throat diameter of the lance nozzle (m), $x_{lance}$ in the lance height (m), $P_{at}$ is the ambient pressure (Pa), $P_O$ is the supply pressure of the CO in the gas phase (Pa) and $\theta_{nozzle}$ is the angle of the divergent part of the nozzle (radians)

The term $\mu_{SG}$ represents the viscosity of the slag in the presence of gas bubbles. Previously $\mu_{SG}$ was calculated by using the equation

$$\mu_{SG} = \frac{2\mu_S(1-\varepsilon)}{3(1-\varepsilon^{1/3})} \qquad \textbf{Eq. 2-97}$$

Comparing the resulting $v_d$ values showed that they were approximately two orders of magnitude greater than values of $v_d$ reported from laboratory experiments. It was suspected that the high gas void fraction in the slag substantially increased the viscosity of the slag/gas continuous phase and this led to much slower values of $v_d$ than expected from equations 2-93 to 2-97. To correct this, the equation for $\mu_{SG}$ was modified in the following manner:

$$\mu_{SG} = \mu_S \left[ 1 + \frac{1.25}{(1-\varepsilon)} \right]^2 \qquad \textbf{Eq. 2-98}$$

The resulting values of the droplet velocity seem to be fairly close to the reported experimental values.

Bubble velocity is calculated using the following equation:

$$v_g = \frac{(\rho_{SM} - \rho_G) g D_b^2}{12\mu_{SM}} (1 - \varepsilon^{1/3}) \qquad \textbf{Eq. 2-99}$$

where the average bubble diameter is calculated using the following expression

$$D_b = \frac{1}{2}\left[ 2\left(\frac{6}{\varepsilon}\right)^3 \frac{\sigma}{0.52 g (\rho_G \rho_{SM}{}^2)^{1/3}} \right]^{1/2} \qquad \textbf{Eq. 2-100}$$

### *2.5.6.1 Evaluation of the model*

This model has been compared with other models (Mishra 1998). It was found that the bubble velocity is inversely proportional to viscosity for this model as well as the model proposed by Jiang (1991). However the predictions of the two models were contradictory about the effect of the gas void fraction on bubble velocity. The model of Ogawa (1993) does agree with Mishra (1998) on the influence of the gas void fraction on the bubble velocity. The model proposed by Gou (1996) showed a trend similar to that based on the model of Jiang (1991).

## 2.5.7 Model development of slag foaming (Ghag, 1998)

Ghag (1998) developed three models to determine the most important stability mechanism in foaming. The models are based on dimensional analysis.

### *2.5.7.1 Model 1 – Surface tension depression*

The motivation for this model is based on the fact that pure liquids do not foam. The addition of a surface active agent is necessary before foam will form. Noting that the surface tensions of liquid differ, it is clear that the stability of foam films is a function of lowering of the solutions surface tension on the addition of the surfactant, the surface tension depression ($\Delta\sigma$), rather than the absolute value of the surface tension. The dimensional analysis problem was simplified looking the variables ($\rho g$) as a single term:

$$\Sigma = f(\rho g, D_b, \Delta\sigma, \mu) \qquad \textbf{Eq. 2-101}$$

The analysis resulted in two dimensionless numbers, which are related as follows:

$$\frac{\Sigma \cdot \Delta\sigma}{\mu D_b} = k\left(\frac{\Delta\sigma}{(\rho g)D_b^{\,2}}\right)^{\delta} \qquad \textbf{Eq. 2-102}$$

The coefficients were determined from data of the physical modelling of water glycerol solutions to be $\delta$=2.32 and k=$2\times10^6$ respectively.

When the correlation was used to determine the gas residence times for calcium silicate slags however, the results were not within the same order of magnitude as the values observed.

Clearly to be applicable to a range of systems, the model of foaming must take into account the mechanisms of foam stabilisation and their implications. Accordingly, to develop a model for wet spherical foams that is not system specific, the viscoelastic forces resulting from the adsorption of surface active species are examined and incorporated into the relationship.

#### 2.5.7.2 Model 2 Surface elasticity

The elasticity of a surface can be expressed as

$$E = \frac{d\sigma}{d(\ln A)} \qquad \textbf{Eq. 2-103}$$

where $d\sigma$ is the change in equilibrium surface tension and A is the surface area

Equation 2-103 shows that the surface elasticity is proportional to the change in the surface tension with fractional change in surface area. Noting that the surface tension depression ($\Delta\sigma$) is equal to the difference in the surface tension of the solvent ($\sigma_o$) and the solution ($\sigma$):

$$\Delta\sigma = \sigma_o - \sigma \qquad \textbf{Eq. 2-104}$$

the elasticity of a single surface can be expressed as :

$$E = -\frac{d\sigma}{d(\ln\Gamma_i)}\frac{d\ln\Gamma_i}{d\ln A} \qquad \textbf{Eq. 2-105}$$

where $\Gamma_i$ is the Gibbs relative surface excess energy of the surface active species. For a film oscillating at high frequencies such that there is no mass transfer between the surface and the bulk solution, the total quantity of adsorbed surface active species in the surface is constant:

$$\Gamma_i A_s = \text{constant} \qquad \textbf{Eq. 2-106}$$

and the surface behaves as an insoluble monolayer. In this case the elasticity is at a maximum, referred to as the Marangoni dilational modulus. Substitution of equation 2-106 into equation 2-105 results in the following expression for the Marangoni dilational modulus ($E_M$):

$$E_M = \frac{d\Delta\sigma}{d\ln\Gamma_i} \qquad \textbf{Eq. 2-107}$$

The Marangoni dilational modulus can be readily determined from equation 2-107 once the equation of state for the surface of the system is known. Equations 2-108 and 2-109 are the results of Langmuir and Frumkin behaviour of the system respectively:

$$\mathrm{E_M} = \frac{RT\,\Gamma_{i,\infty}\Gamma_i}{(\Gamma_{i,\infty} - \Gamma_i)}$$ **(Langmuir isotherm)** **Eq. 2-108**

$$\mathrm{E_M} = \frac{RT\,\Gamma_{i,\infty}\Gamma_i}{(\Gamma_{i,\infty} - \Gamma_i)} - 2a'\left(\frac{\Gamma_i}{\Gamma_{i,\infty}}\right)^2$$ **(Frumkin isotherm)** **Eq. 2-109**

It can be seen from equation 2-107 that the Marangoni dilational modulus and the surface depression are identical, and, given that the Marangoni dilational modulus represents the maximum elasticity of the film, it is argued that it is appropriate that in dimensional analysis the Marangoni dilational modulus should be substituted for the surface tension depression. The following relationship is obtained between the resulting dimensionless numbers:

$$\frac{\Sigma \cdot E_M}{\mu D_b} = k\left(\frac{E_M}{(\rho g)D_b^2}\right)^{\delta}$$ **Eq. 2-110**

Least squares regression analysis results in the following relationship between the significant system properties:

$$\Sigma = 5.43 \times 10^5\,\mu \frac{E_M^{0.89}}{(\rho g)^{1.89} D_b^{2.78}}$$ **Eq. 2-111**

However, the overall fit of the data was poorer than for the analysis in terms of the surface tension depression.

In the derivation of equation 2-111 it has been assumed that the elasticity of the bubble films is at its maximum value. In practice, the effective elasticity can drop below this maximum as a result of lower than equilibrium surface concentration of the surfactant prior to film deformation, and reduction of the surface tension gradients generated on deformation by surfactant mass transfer from the bulk solution.

#### *2.5.7.3 Model 3 Effective elasticity*

Data for solutions with effective elasticities within 90-100% of the Marangoni dilational modulus was plotted in the form:

$$\log\left(\frac{\Sigma \cdot E_{eff}}{\mu D_b}\right) = \delta \log\left(\frac{E_{eff}}{(\rho g)D_b^2}\right) + \log k \qquad \textbf{Eq. 2-112}$$

least squares regression analysis of the data gives δ=1.92 and $k=9.01\times10^5$. Taking the uncertainty in the elasticities into consideration the relationship can be simplified to:

$$\frac{\Sigma \cdot E_{eff}}{\mu D_b} = 1\times10^6\left(\frac{E_{eff}}{(\rho g)D_b^2}\right)^2 \qquad \textbf{Eq. 2-113}$$

Equation 2-113 can be expressed as:

$$\frac{\Sigma \cdot \rho g D_b^2}{\mu D_b} = 1\times10^6\left(\frac{E_{eff}}{(\rho g)D_b^2}\right) \qquad \textbf{Eq. 2-114}$$

The right hand side dimensionless number is the ration of a surface tension related force per unit length and a hydrostatic pressure force per unit length, representing the condition for the rupture of liquid films within the foam – the elastic force counter film rupture, while the hydrostatic pressure determines the rate of film drainage.

A physical interpretation of the left hand side dimensionless number is not so readily apparent. However, if it is assumed that the excess liquid resulting from the rupture of the film drains down the foam through capillaries of radius R and length $D_b$, such that, the mean velocity of liquid flow (v) is described by the Haggen-Poiseuille equation for flow resulting from a hydrostatic head, $\rho g D_b$:

$$v = \frac{\rho g R^2}{8\mu} \qquad \textbf{Eq. 2-115}$$

The capillary drainage time ($\Sigma_{cap}=D_b/v$) is proportional to:

$$\Sigma_{cap} \propto \frac{\mu D_b}{\rho g R^2} \qquad \textbf{Eq. 2-116}$$

and under steady state conditions represents the time required for the underlying film to drain the excess liquid resulting from the rupture of a bubble film without altering the structure of the foam.

The relationship between the film thickness (2R), the bubble diameter ($D_b$), and the gas fraction ($\varepsilon$) for close packed spherical foams is described by the following equation:

$$2R = \left(\frac{1}{\varepsilon} - 1\right)\frac{D_b}{3} \qquad \textbf{Eq. 2-117}$$

Substituting for the capillary radius in 2-116:

$$\Sigma_{cap} \propto \frac{\mu D_b}{\rho g {D_b}^2}\left(\frac{1}{\varepsilon} - 1\right)^{-2} \qquad \textbf{Eq. 2-118}$$

and substituting 2-118 into 2-114 results in the following relationship:

$$\left(\frac{\Sigma}{\Sigma_{cap}}\right)\left(\frac{1}{\varepsilon} - 1\right)^{-2} = k_1\left(\frac{E_{eff}}{\rho g {D_b}^2}\right) \qquad \textbf{Eq. 2-119}$$

The left hand side dimensionless number in equation 2-119 is the product of the ratio of the gas retention and the film drainage time, and a dimensionless number representing the geometry of the foam.

#### *2.5.7.4 Evaluation of the model*

This model is a modification of the model proposed by Jiang (1991) and considers the effect of the dynamic adsorption of surface active species on foaming, rather than indirectly through the equilibrium surface tension or the surface tension depression. The model applies to spherical foams.

## 2.6 Summary of Literature Study

In this chapter the definition of foams, foam classification and terms often used to describe foaming behaviour is reviewed and explained.

Mechanisms of foam stabilisation are discussed and the liquid surface tension and viscosity as well as the degree of ionisation of the liquid are identified as important properties influencing these mechanisms.

The measurement of foam stability is reviewed and the foam index is chosen as measure of foaminess, as it relates more to the foam height than the foam decay rate. In this study the foam height is of more importance than the foam decay rate.

The following conclusions were reached in literature on slag foaming:

- Foaming decreases with increasing slag basicity, possibly due to lowering viscosity or the adsorption of silica at low basicity, which leads to decreased drainage rates of the liquid films.
- Slags tend to show decreased foaming at high FeO concentrations due to the lowering of slag viscosity.
- Surface active components promotes the stability of the foam.
- Carbonaceous particles decrease foaming due to their non-wetting characteristics.
- Second phase particles is believed to cause an increase in slag viscosity and therefore increased foaming.
- Foaming depends on bubble size, but bubble size is dependent on liquid properties. However, some models still treat the bubble size as independent of liquid physical properties.
- The molecular size and shape of a gas are of more relevance to foaming than the gas density. Increased pressure does not influence foaming behaviour.

Of the models proposed for slag foaming, the empirical models describing the foam index are found to be easier to use and more applicable to slag foaming in general than complicated fundamental models. However, most of these models were derived for basic steelmaking slags and need to be evaluated for slags not in this range. This is an objective in this study.

The next chapter deals with the preparation and set-up for the experiments conducted in this study.

# 3 Experimental techniques and procedures

This chapter explains the experimental set-up for both the room temperature experiments and molten slag experiments of foaming. It also includes summaries of published set-ups that served as background knowledge in setting up the experiments.

As experiments with aqueous mixtures were used to develop a concrete understanding of foams in general, these experiments will be described first.

## *3.1 Experiments in two-phase aqueous systems*

Physical modelling is a standard modelling method in pyrometallurgy to study fluid dynamic behaviour of simulated melts and has been used by a number of researchers (Ogawa 1993; Worczok 1994; Ghag 1998).

Physical modelling in two-phase systems is important to determine the underlying influence of the physical properties of the liquid (or simulated slag). Various aqueous mixtures were used to test a variety of surface tension and viscosity properties. Addition of ethanol and a flotation frother (MIBC) to water were used to change the surface tension of the liquid without really influencing the density or viscosity of the mixture. Glycerol and sucrose mixtures were used to investigate the effect of changes in viscosity and density without influencing the surface tension significantly. The various mixtures were chosen after literature of previous studies on the physical modelling of slag foaming were reviewed.

### 3.1.1 Background

Various studies have been done to develop a model for slag foaming by studying foaming at room temperature in various liquid systems. The conditions for some of these studies are summarised in tabular form:

**Table 3-1. Experimental set-up of various studies published on the physical modelling of slag foaming**

| Author | Column Diameter (m) | Column Height (m) | Liquid phase | Gas phase | Bubble generation method |
|---|---|---|---|---|---|
| Ogawa (1993) | 0.037<br>0.060 | 1.0 | Water + saccharose with 2% ethanol | Nitrogen and argon | Glass sinters with various pore sizes |
| Worczok (1994) | 0.055 x 0.075 rectangular | 0.3 | Water-glycerol<br>Water- ethanol<br>Water-alcohol | air | Top lance<br>Bottom lance<br>Porous disc |
| Gou (1996) | --- | --- | water | air | Sieve plate |
| Lin (1995) | 0.075 | --- | Various liquids (unspecified) | Nitrogen and argon | Porous metal disc |

The various solutions studies were not chosen because their physical properties agrees with that of pyrometallurgical slags, in fact their properties vary substantially from those of molten slags. Liquids with physical properties comparable to those of molten slags are seldom available and very expensive. The various solutions are therefore chosen for economic and practical purposes (not toxic) as well as availability.

The conclusions reached in these studies can shortly be summarised as follows.

Ogawa found that the rupture rate of bubbles, the size and the number of bubbles determine gas escape rate. The bubble size, the film thickness and the physical properties of the slag may govern the rupture rate of bubbles. Moreover, the gas evolution rate, the bubble size and the slag properties determine the number of bubbles and the film thickness in the foam. Therefore if the bubble size, the distribution of the bubbles in the foam and the rupture rate of the bubble films at the top surface of the slag are known, the foam height can be predicted.

Worczok found that foaming behaviour depends on

1. gas injection velocity
2. superficial gas velocity
3. mode of injection
4. physicochemical properties of the liquid

Initially the foam stability increased with further additions of the surface-active component. After reaching a maximum value, the foam stability decreased with further additions of the surface-active component until finally no foaming will occur.

When operating in the region of decreasing foam stability with increasing gas injection rate, it was shown that the foam height would decrease when additional gas was injected into the foam layer.

Gou found that the behaviour of the solutions subjected to high rates of gas injection, greater than 1.0 m/s, is distinctly different from classical foaming observed at low rates of injection, below 1.0 m/s. As this has already been reviewed in Chapter 2.2.2.4, no further discussion is needed.

Lin found that foam height is dependent on bubble flow regimes.

The bubble flow regime is dependent on:

1. size of bubbles
2. superficial gas rates

3. physical properties of liquids

Foam height is not only dependent on the superficial gas velocity but also on the average slip velocity of bubbles in the foam bed and on the initial depth of liquid.

Average slip velocity is influenced by:

1. size of bubbles
2. physical properties of liquid
3. interaction between bubbles

### 3.1.2 Systems investigated

The liquids used in the experiment were made up according to mass percentages. The physical properties of the liquids (density, viscosity and surface tension) were obtained in literature, except for the surface tension of the sugar solutions and the water with frother additions. The surface tensions of these solutions were obtained by using the Wilhelmy Plate Method (using the force at contact and the contact angle of the liquid with a reference object to determine the surface tension). The viscosities of saturated solutions were determined with a Haake rotoviscometer.

**Table 3-2. Properties of various mixtures investigated**

| Key | Mixture | μ [mPa.s] | σ [mN/m] | ρ [g/cm$^3$] |
|---|---|---|---|---|
| 1 | Water | 0.89 | 72.75 | 0.998 |
| 2 | 10% EtOH | 1.32 | 37.70 | 0.982 |
| 3 | 40% EtOH | 2.35 | 31.89 | 0.935 |
| 4 | 60% EtOH | 2.24 | 27.56 | 0.891 |
| 5 | 10% Glycerol | 1.15 | 69.13 | 1.022 |
| 6 | 40% Glycerol | 3.18 | 67.47 | 1.099 |
| 7 | 60% Glycerol | 8.82 | 66.06 | 1.154 |
| 8 | 20% Sucrose | 1.92 | 71.69 | 1.118 |
| 9 | 40% Sucrose | 5.98 | 71.95 | 1.235 |
| 10 | 60% Sucrose | 58.50 | 76.09 | 1.353 |
| 11 | MIBC 1 | 0.89 | 64.81 | 0.998 |
| 12 | MIBC 2 | 0.89 | 73.09 | 0.998 |
| 13 | EtOH | 1.07 | 22.75 | 0.789 |
| 14 | Saturated $MgSO_4$ | 7.80 | 68.27 | 1.290 |
| 15 | Saturated Starch | 2.19 | 66.68 | 1.000 |

### 3.1.3 Evolution of experimental set-up for aqueous mixtures

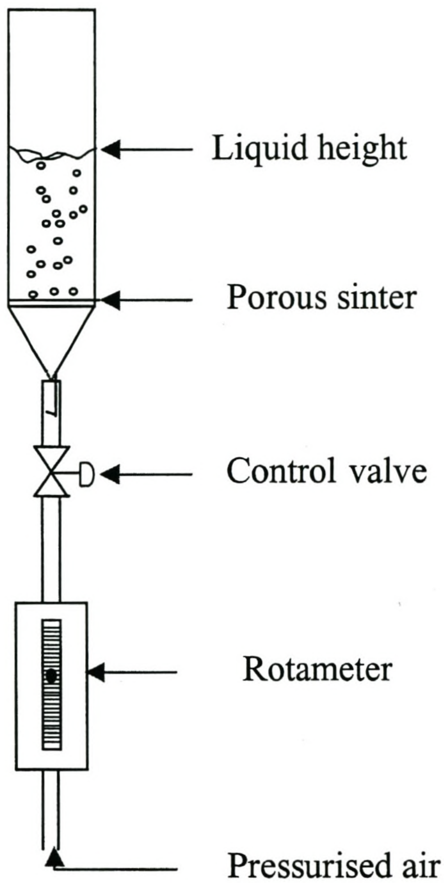


**Figure 3-1. Sketch of original experimental configuration**

In the first experimental set-up, glass columns with sinter disks were used. The diameters of the columns were 32mm and 68mm. The porous sinters were type 4 (13μm pores) and type 2 (70μm pores).

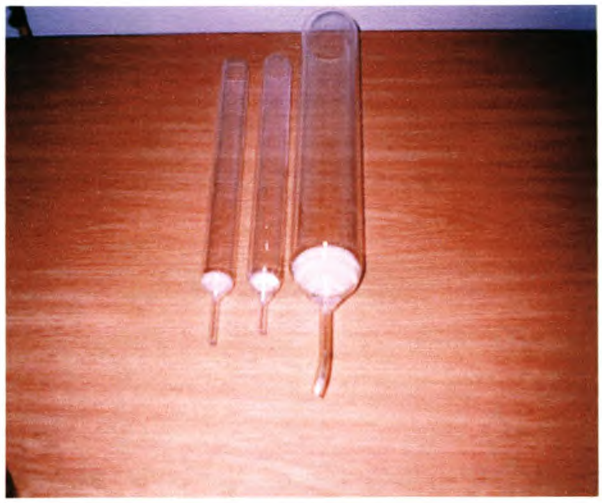

**Figure 3-2. Columns used in first experiments**

The flow rate of the pressurised air was determined by a rotameter and controlled by a small valve. This set-up was limited by the fact that the columns were only 28cm high. At high velocities the foam height would exceed the height of the narrow columns (32mm diameter) and the data in this foam region could not be obtained. The rotameter also limited the investigation, due to the fact that the required superficial gas velocity (m/s) comparable to that obtained in the narrow columns (32mm diameter) could not be obtained in the wider column (68mm).

To address these issues, new columns were designed and constructed. These columns were made of clear perspex and had a height of 2m and diameters of 60mm and 100mm. Air distribution was achieved by fine steel mesh, secured in a flange and sealed with silicone sealer. A new rotameter was obtained and calibrated to register higher flow rates. These columns were also used to investigate the effect of solid precipitates on foaming and were modified to obtain bubble size distributions for various liquids.

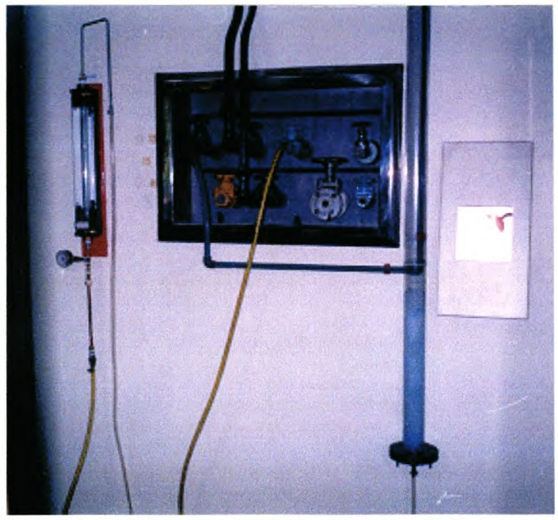

**Figure 3-3. Improved Perspex column with foam generation by pressurised air**

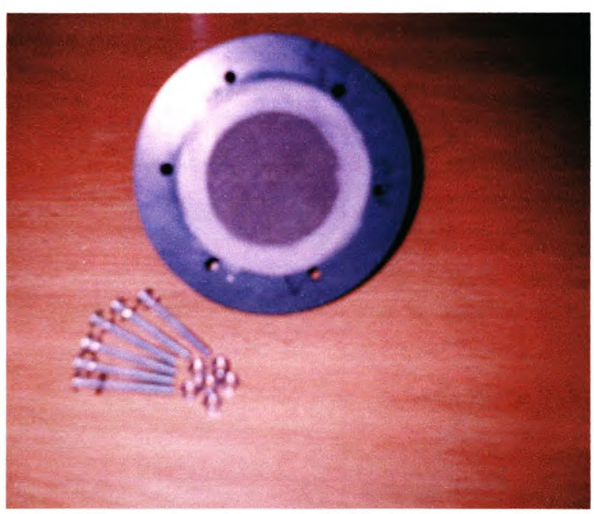

**Figure 3-4. Bottom flange of Perspex column showing stainless steel mesh used as gas distributor**

### 3.1.4 Experiments in three-phase aqueous systems

Supersaturated solutions of $MgSO_4$ and starch were used to investigate the effect of solid particles on foaming. $MgSO_4$ were chosen to simulate an ionic melt and starch to simulate a silicate rich slag (acidic) where silicate chains predominate. Supersaturation was necessary to ensure a constant quantity of solids in the foam. MIBC was also added to the $MgSO_4$ system to see if frother additions influence the system significantly.

The viscosities of the saturated and supersaturated solutions were determined in a Haake rotoviscometer. The surface tensions of these mixtures were obtained by using the Wilhelmy Plate Method (using the force at contact and the contact angle of the liquid with a reference object to determine the surface tension).

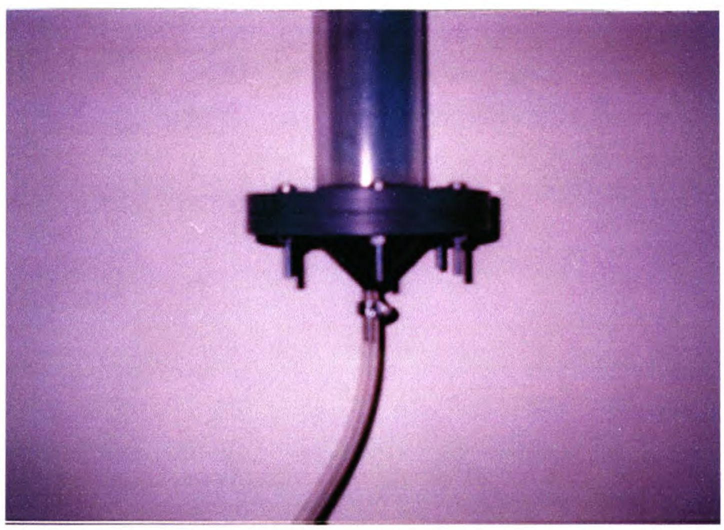

**Figure 3-5. PVC column with bolted flange for two- and three-phase systems**

The last section dealing with aqueous systems concerns the determination of the bubble size distribution in various foamy mixtures.

### 3.1.5 Bubble size distribution

Various authors have noted the importance of the bubble size distribution in slag foaming (Ogawa, 1993; Zhang, 1995; Lin, 1995). In experiments with foaming slags the measurement of the bubble size distribution is extremely difficult and prone to large experimental error. The most common method of determining the bubble size distribution is to quench the foam and then study a cross-section of the quenched slag foam. With physical modelling most problems in measuring the bubble size distribution are eliminated.

Bubble size distributions were measured using the UCT bubble size analyser. The operation of this instrument aspires the bubbles into a capillary tube, where the liquid gas interface is optically detected. The bubble size analyser was coupled to a glass probe and inserted through the wall of the PVC column. Tucker (1994) discloses more details on the working of the bubble size analyser.

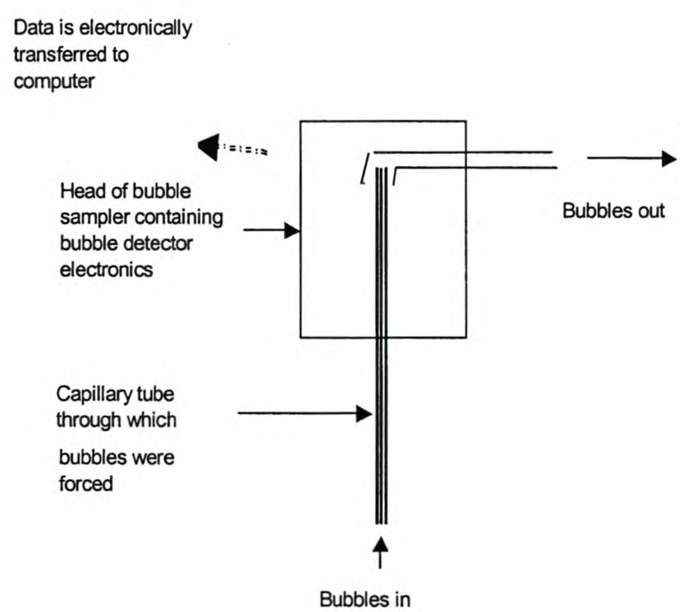


**Figure 3-6. The bubble sampler of the bubble size analyser**

The liquids used in the experiment were made up according to mass percentages. The surface tensions of these solutions were obtained by using the Wilhelmy Plate Method (using the force at contact and the contact angle of the liquid with a reference object to determine the surface tension). The viscosities of saturated solutions were determined in a Haake rotoviscometer.

Led by the results of the room temperature experiments and literature study, factors identified as influencing slag foaming were identified. These include the slag basicity, physical properties of the slag, namely viscosity, surface tension and density, the formation of particles due to under-cooling of the slag and the FeO concentration in the slag. The next section deals with the set-up and experiments investigating slag foaming.

## 3.2 *Slag foaming experiments*

Before the experiments on slag foaming were conducted, a detailed study of previous studies of slag foaming was done. The experimental set-up was then based on the information published. The aim of these experiments was to test if models proposed for basic slag foaming would perform equally well in acid slag foaming systems. Data was therefore necessary in order to fit the models and evaluate their parameters.

### 3.2.1 Background

On the next page, the information obtained from the literature study is contained in tabular form, as it assisted in the experimental set-up chosen for this study. The $Al_2O_3$-CaO-'FeO'-$SiO_2$ slag system has been chosen for the study as it contains the compounds most commonly found in industrial slags. A non-oxidising atmosphere is required when conducting experiments to prevent the FeO from oxidising to $Fe_2O_3$. The experiments were therefore conducted in an argon atmosphere and foaming was simulated by argon injection into the molten slag through an alumina lance. Detection of the liquid/foam height was done with electrical probes and the slags were contained in alumina crucibles. A vertical SiC resistance heated furnace was used for the slag foaming experiments.

**Table 3-3. Summary of literature on the set-up for slag foaming experiments**

| **Author** | Hara (1986) | Ito (1989) | Gudenau (1992) | Zamalloa (1992) | Utigard (1993) | Koch (1994) | Ren (1994) | Zhang (1995) | Ozturk (1995) | Yi (1997) |
|---|---|---|---|---|---|---|---|---|---|---|
| **Crucible diameter (m)** | 0.020 | 0.032 to 0.050 | --- | 0.040 | 0.040 | --- | --- | 0.041 to 0.050 | 0.041 | 0.040 |
| **Crucible Height (m)** | 0.120 | 0.200 | --- | 0.160 | 0.160 | --- | --- | --- | 0.300 | 0.200 |
| **Crucible material (m)** | Alumina | Alumina | Alumina | Alumina | Alumina | Graphite/ Alumina | Graphite | Alumina | Alumina | MgO or graphite |
| **Probe material** | Iron | Stainless steel | --- | Mo | Mo | Photo-electric cell | Photo-electric cell | Mo | Mo | X-ray fluoroscopy |
| **Slag system** | FeO-$SiO_2$-CaO | FeO-$SiO_2$-CaO | FeO-$Fe_2O_3$-$SiO_2$-CaO | FeO-$SiO_2$-CaO | FeO-$SiO_2$-CaO | $Fe_2O_3$-$SiO_2$-CaO | $Fe_2O_3$-$SiO_2$-CaO | CaO-$SiO_2$-CaF | CaO-$SiO_2$-$Al_2O_3$-FeO | FeO-$SiO_2$ |
| **$CaO/SiO_2$ ratio** | --- | 0.43 to 1.00 | 1.34 to 2.53 | 0.4 to 1.0 | 0.53 to 1.36 | 0.10 to 1.80 | 0.10 to 2.70 | 0.50 | --- | --- |
| **Atmosphere** | Argon | Argon | $O_2$ or $N_2$ | Argon | Argon | 40%CO, 60% $N_2$ | 40%CO, 60% $N_2$ | Argon | Argon | --- |

### 3.2.2 Slag systems investigated

Due to uncertainty about the amount of alumina that would dissolve from the crucible into the slag, slags were sent for XRF-analysis to determine the true composition of the melt. The results for successful experiments are shown in table 3-4. The total amount of iron in the slag, whether present as FeO, $Fe_2O_3$ or $Fe_3O_4$, is expressed as "FeO".

**Table 3-4. Summary of slags investigated**

| Slag | Composition wt% | | | |
|---|---|---|---|---|
| Number | $SiO_2$ | $Al_2O_3$ | "FeO" | CaO |
| 1 | 45.5 | 10.5 | 23.7 | 20.3 |
| 2 | 47.5 | 9.7 | 22.8 | 20.0 |
| 3 | 41.4 | 6.0 | 19.9 | 32.8 |
| 4 | 45.1 | 7.1 | 28.0 | 19.8 |
| 5 | 41.0 | 15.4 | 25.9 | 17.8 |
| 6 | 53.5 | 6.8 | 20.4 | 19.3 |
| 7 | 46.9 | 19.2 | 24.2 | 9.7 |
| 8 | 43.8 | 5.0 | 25.0 | 25.3 |
| 9 | 51.9 | 10.0 | 9.3 | 28.8 |
| 10 | 52.9 | 8.4 | 13.9 | 24.8 |
| 11 | 42.8 | 17.1 | 8.6 | 31.5 |

The $Fe^{2+}/Fe^{3+}$ ratios were determined with the hot acid method where $K_2Cr_2O_7$ is used to indicate the critical point of the titration. The resulting ratios are shown in table 3-5. These results were used in all thermodynamic simulations and property calculations for the slags. The high amount of $Fe_2O_3$ in slag 5 indicates the ingress of air into the furnace. This was probably due to a crack in the furnace tube. The tube was replaced and subsequent experiments showed low levels of $Fe_2O_3$.

**Table 3-5. The state of oxidation of iron in slags**

| Slag | $SiO_2$ | $Al_2O_3$ | FeO | $Fe_2O_3$ | CaO | $Fe^{2+}/Fe^{3+}$ |
|---|---|---|---|---|---|---|
| | wt% | Wt% | wt% | wt% | wt% | |
| 1 | 45.3 | 10.5 | 20.7 | 3.2 | 20.2 | 7.1 |
| 2 | 47.4 | 9.6 | 20.8 | 2.2 | 20.0 | 10.6 |
| 3 | 41.2 | 5.9 | 16.3 | 3.9 | 32.7 | 4.7 |
| 4 | 44.9 | 7.1 | 23.4 | 4.9 | 19.7 | 5.3 |
| 5 | 40.3 | 15.1 | 10.4 | 16.7 | 17.5 | 0.7 |
| 6 | 53.5 | 6.8 | 18.9 | 1.6 | 19.2 | 12.9 |
| 7 | 46.9 | 19.2 | 23.1 | 1.2 | 9.7 | 21.2 |
| 9 | 51.9 | 10.0 | 9.1 | 0.3 | 28.8 | 35.4 |
| 10 | 52.9 | 8.4 | 13.5 | 0.5 | 24.8 | 32.7 |
| 11 | 42.8 | 17.1 | 8.3 | 0.3 | 31.5 | 30.7 |

### 3.2.3 Evolution of slag foaming experiments

The experiments were conducted in a vertical tube furnace. The slags were contained in alumina crucibles and stainless steel probes protected by alumina tubes measured the slag height. Argon gas was injected through another alumina tube to create foam.

### 3.2.4 Preparation of slag

To prepare the slag, chemically pure amounts of $SiO_2$, CaO and $Al_2O_3$ were melted in a carbon crucible using an induction furnace. The amounts of $Al_2O_3$ were set at 5% or 10% and acted as a precaution to the dissolution of alumina from the final crucible to the slag. The relative amounts of $SiO_2$ and CaO were based on predetermined slag basicities. The resulting slag were ground to powder and left overnight in a muffle furnace (800 C) to burn off any traces of carbon that might have been picked up from the carbon crucible. This carbon-free slag was then mixed with FeO just before being placed in the tube furnace with the argon atmosphere. The FeO was prepared separately to prevent it from oxidising.

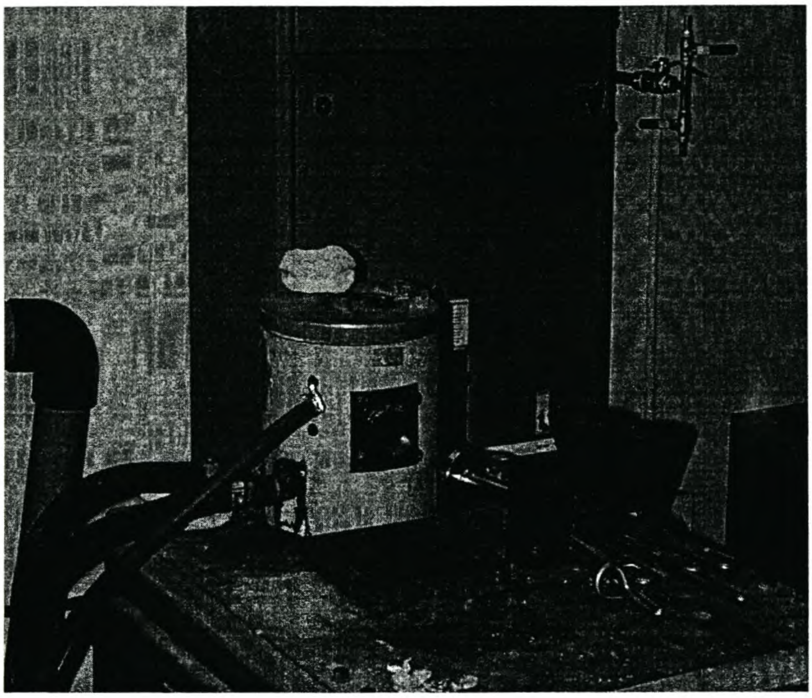

**Figure 3-7. Induction furnace used in the preparation of the slag**

FeO was prepared by mixing stoichiometric amounts of Fe and $Fe_2O_3$. This mixture was then pressed into pellets and heated at 900 C for approximately 10 hours in an argon atmosphere, using the vertical tube furnace. FeO was stored in a non-oxidising atmosphere until it was mixed with the other slag components.

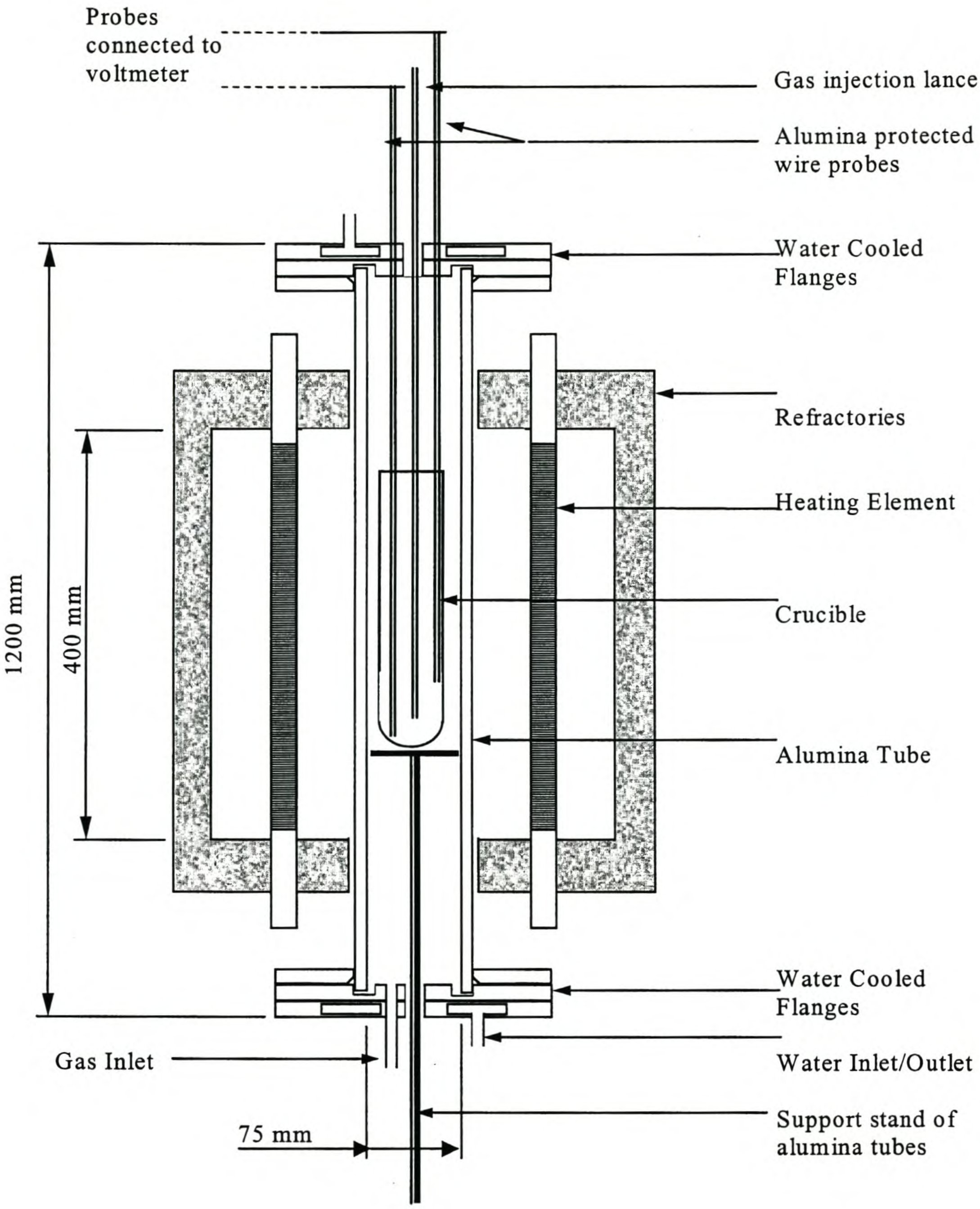


**Figure 3-8. Sketch of furnace showing crucible positioning (Not according to scale)**

### 3.2.5 Furnace set-up

On the previous page the experimental arrangement is shown. The slag was contained in an alumina crucible (i.d. 45mm, height 280mm). The crucible was wrapped in alumina wool to keep it vertical for the duration of the experiment. The crucible rested on a pedestal made of alumina and supported by alumina tubes.

The electrical probes were made of stainless steel. It was found that molybdenum probes were difficult to protect from traces of air and would rapidly oxidise at the temperatures where experiments were conducted. For experiments near the melting point of stainless steel, thicker stainless steel rods were used as the thinner wires tended to partially dissolve or break.

When slags containing 5% alumina were found to dissolve the alumina rods protecting the electrical probes and also the gas injection tube, the concentration of alumina in the slag were raised to 10%.

One of most severe limitations of the experimental set-up was found to be excessive foaming of the slag, leading to slag overflow. Slag overflow made the removal of the crucible increasingly difficult, as it would cement the crucible to the furnace tube. Contact with slag also weakens the furnace tube and eventually leads to irreparable damage. If any foaming within 5cm of the top of the crucible were detected, the experiment would be interrupted and continued at a lower gas velocity or different temperature in an effort to avert slag overflow.

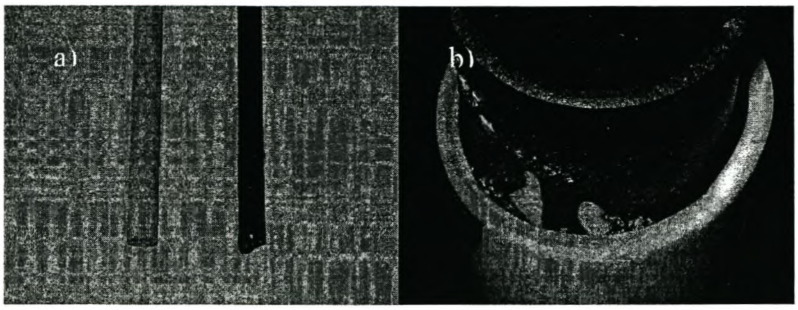


**Figure 3-9. a) Comparison of new alumina tube and one damaged by slag attack,**

**b) Crucible cemented to alumina tube due to slag overflow**

Having described the experimental set-up and problems, the next step is the processing of data generated through the experiments. Chapters 4 and 5 deal with the physical modelling and the slag foaming experiments respectively.

# 4 Results and discussions – Physical modelling

The definition of the foam index is given as

$$\Sigma = \frac{\Delta H}{V} \qquad \textbf{Eq. 4-1}$$

where $\Sigma$ is the foam index [s]

$\Delta H$ is the change in liquid height [mm]

and $V$ is the superficial gas velocity [mm/s]

When plotting $\Delta H$ against $V$, then the gradient, $\frac{\Delta H}{\Delta V}$, can be seen as an averaged foam index value for the mixture and geometry of the system. When investigating such plots, it was found that the relationship between $\Delta H$ and $V$ could be best fit with a quadratic polynomial equation. In Figure 4.1, such fits for one specific geometry and mixture are shown. The equation for the best polynomial fit is also shown on the figure.

Any quadratic polynomial can be written in the following general form

$$y = ax^2 + bx + c \qquad \textbf{Eq. 4-2}$$

The gradient at any point on the polynomial is equal to the derivative of polynomial at that point. The derivative of the general function, eq. 4-2, is

$$\frac{dy}{dx} = 2ax + b \qquad \textbf{Eq. 4-3}$$

If however the coefficient a is very small and x is small as well, the first term can be neglected and eq. 4-3 will simplify to

$$\frac{dy}{dx} \approx \mathrm{b} \qquad \textbf{Eq. 4-4}$$

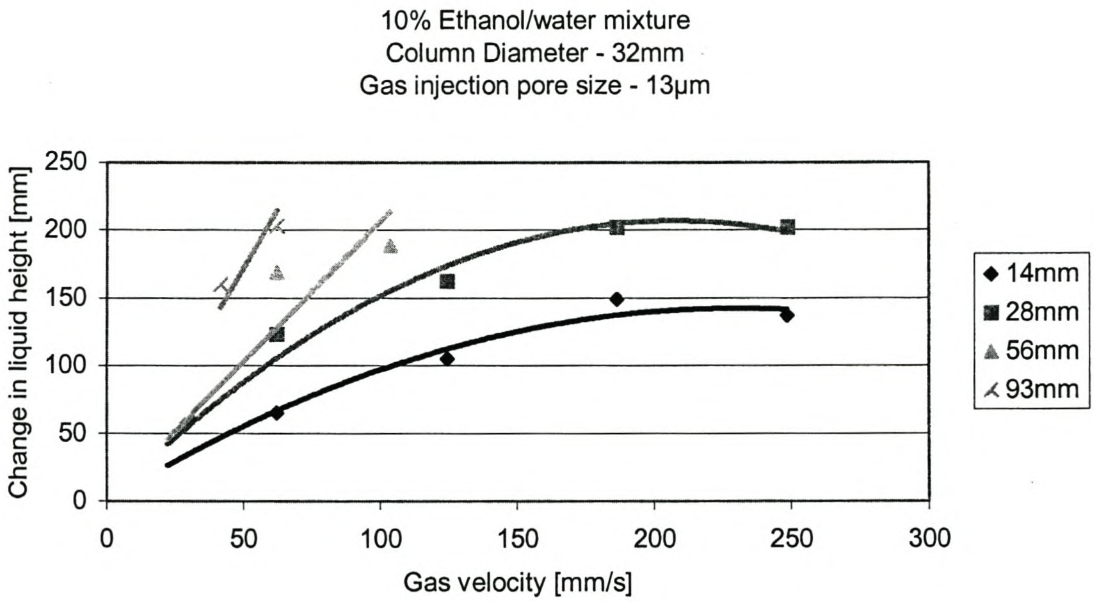


**Figure 4-1 Determining the average foam index as the gradient of curves shown.**

As we are interested in later comparing physical modelling results with the foam data measured for slag systems ($V \leq$ 50mm/s) the simplified equation, eq. 4-4, was used to determine the foam index. The foam index values for the 10% ethanol/water mixture is given in Table 4-1.

**Table 4-1. Summary of data for 10% ethanol/water mixture**

| Column diameter | Gas injection pore size | Initial liquid depth | Foam Index ($\Sigma$) |
|---|---|---|---|
| [m] | [μm] | [mm] | [s] |
| 0.0320 | 13 | 14 | 1.240 |
| 0.0320 | 13 | 28 | 2.000 |
| 0.0320 | 13 | 56 | 2.060 |
| 0.0320 | 13 | 93 | 3.450 |
| 0.0320 | 70 | 14 | 1.130 |
| 0.0320 | 70 | 28 | 1.800 |
| 0.0320 | 70 | 56 | 2.360 |
| 0.0320 | 70 | 93 | 2.490 |
| 0.0600 | 75 | 14 | 0.310 |
| 0.0600 | 75 | 24 | 0.722 |
| 0.0600 | 75 | 50 | 1.290 |
| 0.0600 | 75 | 90 | 1.755 |
| 0.0600 | 75 | 186 | 2.691 |
| 0.0600 | 197 | 14 | 0.438 |
| 0.0600 | 197 | 26 | 0.647 |
| 0.0600 | 197 | 53 | 0.999 |
| 0.0600 | 197 | 90 | 1.342 |
| 0.0600 | 197 | 186 | 1.723 |
| 0.0680 | 13 | 14 | 2.433 |
| 0.0680 | 13 | 28 | 2.364 |
| 0.0680 | 13 | 56 | 3.385 |
| 0.0680 | 13 | 93 | 3.641 |

From Table 4-1 it is possible to get a clear picture of the influence of the initial liquid depth (liquid volume) on the foam index. The data are graphically represented in figure 4-2.

There is a positive correlation between the initial liquid depth and the average foam index. An increase in the liquid depth leads to a higher foam index. The pore size of the gas injection openings also influences the foam index. It appears as if a smaller pore size leads to a higher foam index in a given column.

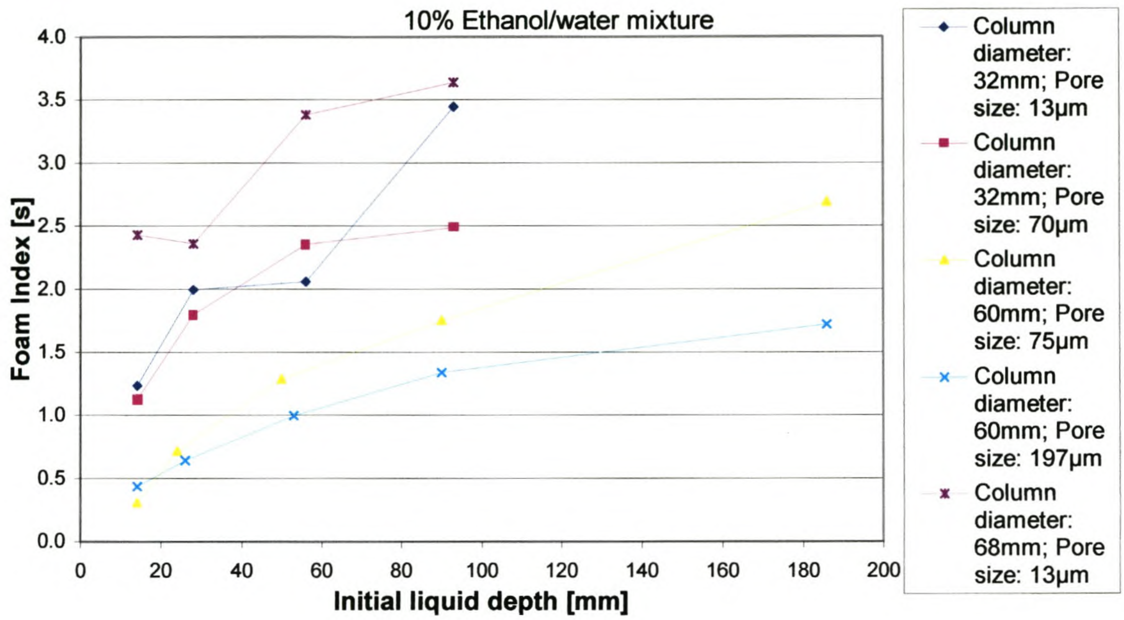


**Figure 4-2. Influence of initial liquid depth on foam index for 10% ethanol/water mixture**

Following the same procedure, it is possible to extract the similar relationships from data for other mixtures. The complete data figures and tables will be given in appendix B.

In the following paragraphs the final figures for each mixture will be discussed in terms of the influence of the initial liquid depth on the foam index.

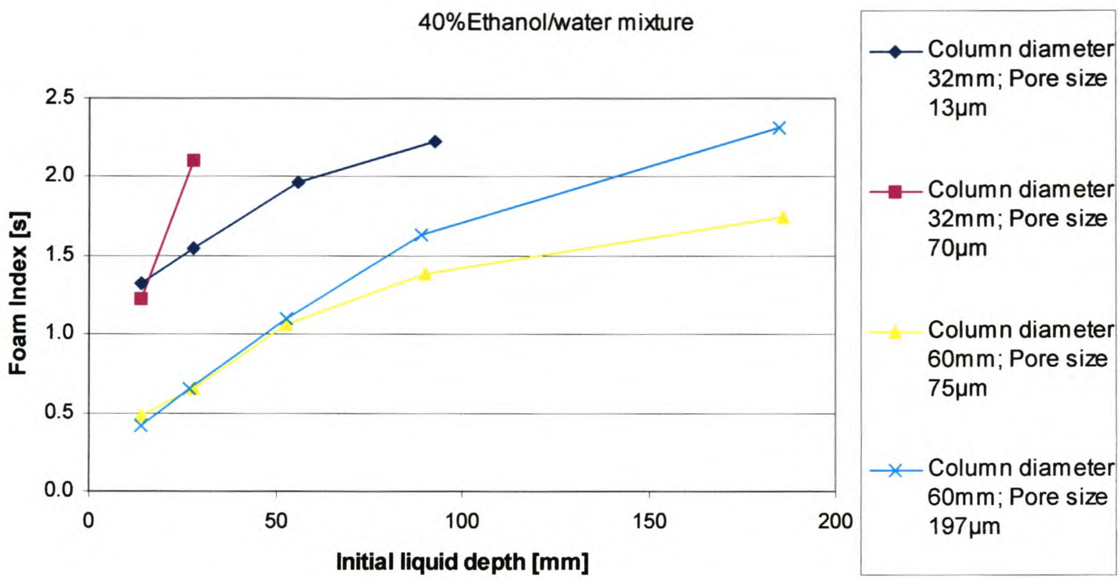


**Figure 4-3 Influence of initial liquid depth on foam index for 40% ethanol/water mixture**

Once again higher values for the foam index are observed when experiments were conducted with a bigger liquid reservoir. In figure 4-3 the foam index seems to be lower for smaller gas injection pore size in the 32mm column.

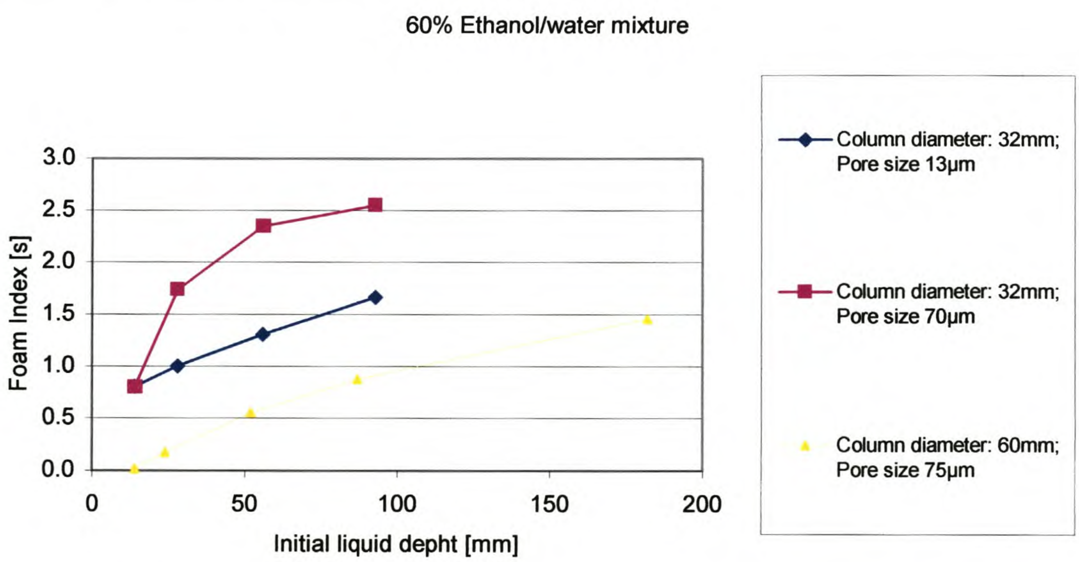


**Figure 4-4 Influence of initial liquid depth on foam index for 60% ethanol/water mixture**

For the 60% ethanol-water mixture the positive relationship between the foam index and the liquid volume holds true. For the 32mm diameter column the highest foam index values obtained were with 70μm pore size.

Of all the ethanol-water mixtures, the highest foam index values were observed for the 10%ethanol mixture. This value was approximately 3.5 s.

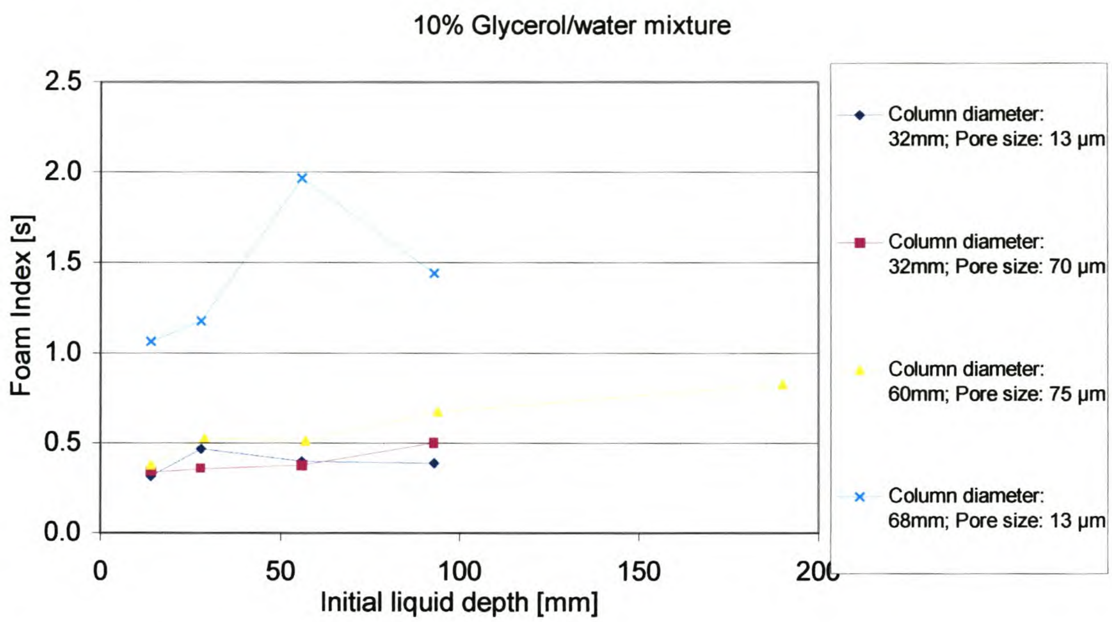


**Figure 4-5 Influence of initial liquid depth on foam index for 10% glycerol/water mixtures.**

As for the ethanol-water mixtures, the 10%glycerol-water mixture shows a positive correlation between the liquid volume and the foam index. Although the effect of pore size on the foam index is not clear for the 32mm column, the 60mm column shows higher foam index values when smaller gas injection pores were used. The highest foam index value, approximately 2 s, is also the highest foam index value obtained for any of the glycerol-water mixtures. The figure for 40%glycerol-water mixture is similar to figure 4-5 and will be shown in the appendix.

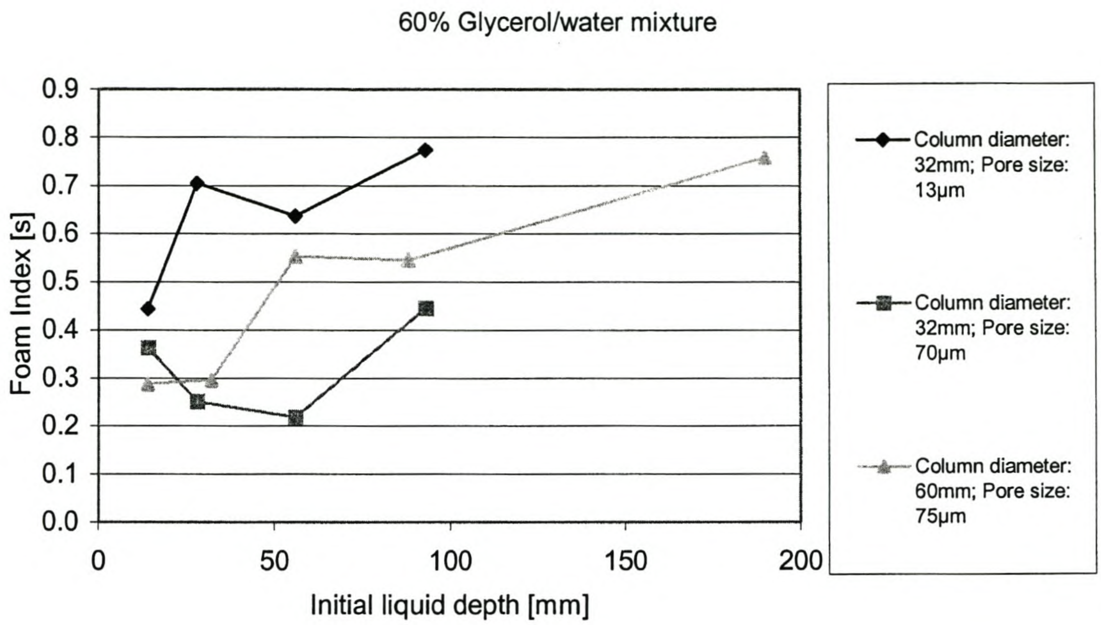


**Figure 4-6 Influence of initial liquid depth on the foam index for 60% glycerol/water mixture.**

Although the trend lines on figure 4-6 also shows a positive relationship to the foam index, it is clear that the data points are more scattered than on previous figures. It was observed that the glycerol-water mixtures did not form stable foam and lower foam index values were observed than for the ethanol-water mixtures. The 60% glycerol-water mixture did however show a marked increase in foaming when gas was injected through smaller pores.

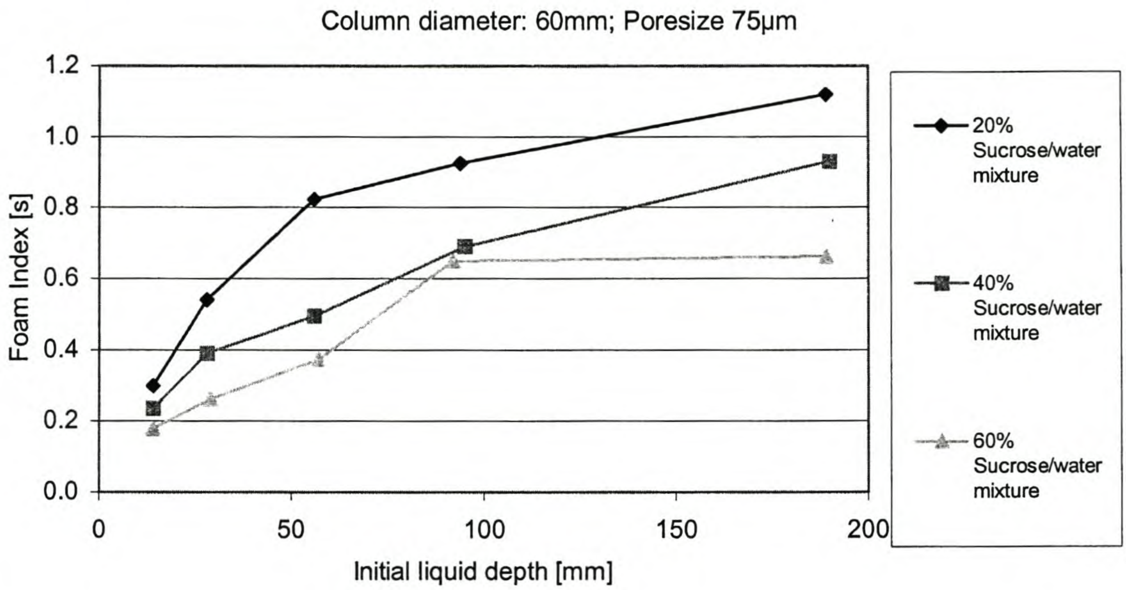


**Figure 4-7 Influence of initial liquid depth on foam index for sucrose/water mixtures**

The results for sucrose/water mixtures are shown in figure 4-7. The solutions were made up to 20-, 40- and 60% weight solutions. The mixtures show a decrease in foam index values obtained when the sucrose content is increased. This is contrary to results with ethanol and glucose mixtures as it implies that an increase in viscosity and density led to a decrease in foamability. As the surface tension of these mixtures does not differ as markedly as the viscosity and density, the difference in foaming behaviour can be explained by noting that the sucrose mixtures did not form true foams consisting of bubbles and only expanded due to churning causes by the gas injection. This indicates that high liquid viscosity and density are not sufficient conditions for foam to form and that surface tension depression is necessary to form a bubbly foam.

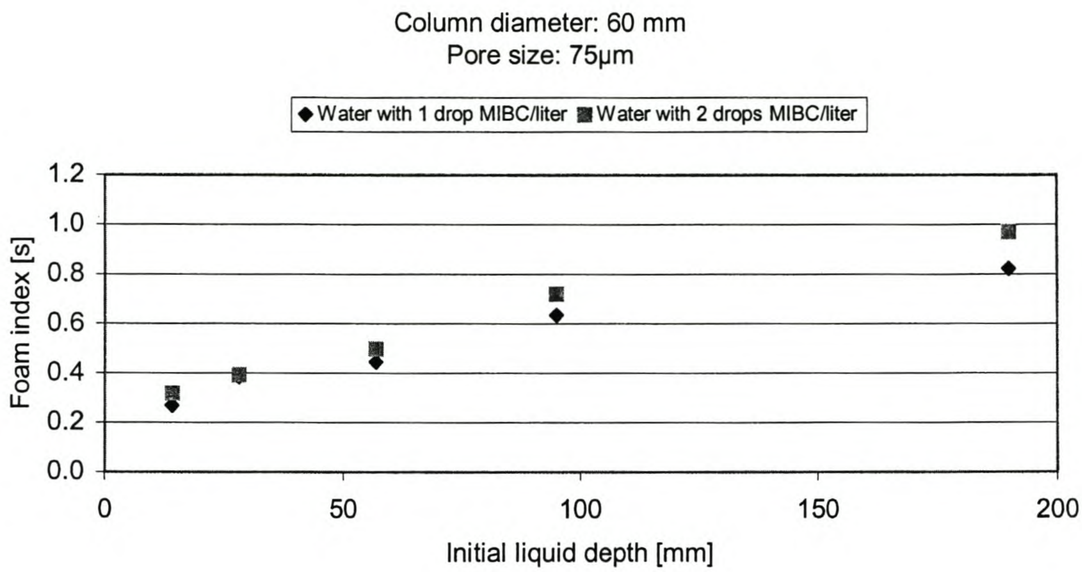


**Figure 4-8 Influence of initial liquid depth on foam index for water with frother addition**

The influence of the addition of a frother, Methyl Iso-Butyl Carbinol (MIBC), to water is shown in figure 4-8. As the small amounts of frother are unlikely to influence the density or viscosity of the liquid, the increase in foam index values can only be ascribed to the change in the surface tension of the liquid.

To test if the results of figures 4-2 to 4-8 are statistically significant, multiple linear regression was done on the collection of data. It was found that the only variable that in the experimental set-up (column diameter, pore size and initial liquid depth) that influences the foam index is the initial liquid depth. The influence of the column diameter and pore size could not be established from the current dataset.

**Table 4-2. Coefficients for regression showing initial liquid depth (ILD) as a variable influencing the foam index (FI)**

**Coefficients[a]**

| Model | | Unstandardized Coefficients | | Standardized Coefficients | t | Sig. | 95% Confidence Interval for B | | Collinearity Statistics | |
|---|---|---|---|---|---|---|---|---|---|---|
| | | B | Std. Error | Beta | | | Lower Bound | Upper Bound | Tolerance | VIF |
| 1 | (Constant) | 1.097 | .240 | | 4.566 | .000 | .621 | 1.572 | | |
| | DIAMETER | -4.284 | 5.107 | -.080 | -.839 | .403 | -14.400 | 5.833 | .816 | 1.226 |
| | PORESIZE | -2930.58 | 1513.906 | -.183 | -1.936 | .055 | -5929.34 | 68.173 | .837 | 1.194 |
| | ILD | 4.932 | 1.287 | .341 | 3.834 | .000 | 2.384 | 7.481 | .947 | 1.056 |

a. Dependent Variable: FI

## *4.1 Effect of solid precipitates*

Supersaturated solutions of $MgSO_4$ and starch were used to investigate the effect of solid particles on foaming. $MgSO_4$ was chosen to simulate an ionic melt and starch to simulate a silicate rich slag (acidic) where silicate chains predominate. A supersaturated starch solution would precipitate starch chains that lead to non-Newtonian rheological properties. It is suspected that acidic slags form similar chains upon cooling below their solidus temperature. Supersaturation was necessary to ensure a constant quantity of solids in the foam. MIBC was also added to the $MgSO_4$ system to see if frother addition influences the system significantly.

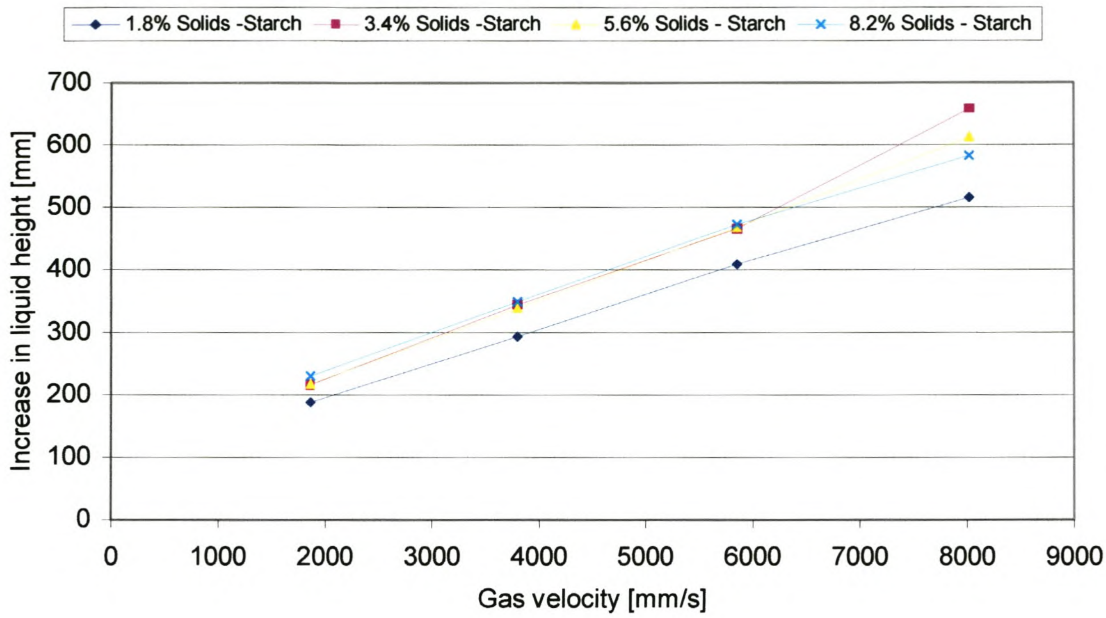


**Figure 4-9 Influence of solids on supersaturated starch foaming behaviour**

Following the same methodology as described in 4.1, the average foam index values for 3-phase foaming systems are derived. Figure 4-9 shows the data for the supersaturated starch system. Once again the other relevant figures are in appendix B.

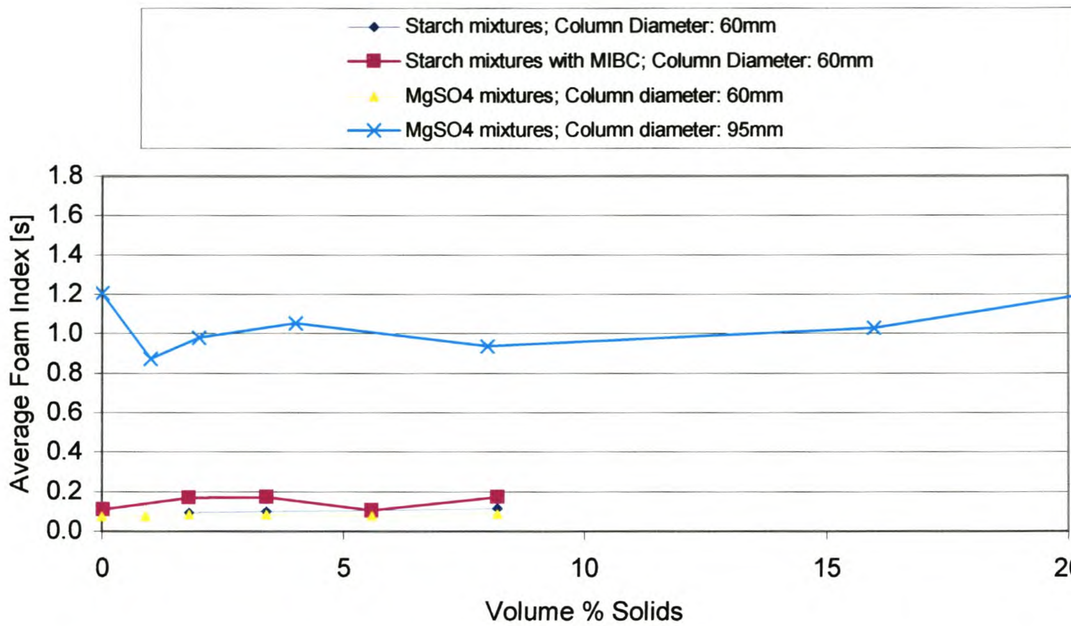


**Figure 4-10 Influence of solid particles on the foam index**

Figure 4-10 summarises the results obtained from the 3-phase systems studied. In all the systems studied, the average foam index increased with an increasing amount of solids in the system. The gradient of increase is however very small and more work are recommended before conclusions are definite. From the data gathered for Figure 4-10, the influence of solids particles on the foam index is statistically insignificant.

The gradient for the starch system is approximately equal to that for the starch-with-added-frother system. This suggests that the influence of additional starch particles is the same and that the difference in foaming behaviour is mainly due to the frother addition.

## 4.2 Influence of bubble size

Bubble size analyses were done for water and aqueous mixtures of ethanol. The results of these analyses clearly show the effect of ethanol addition on the bubble size and the foam characteristics. For pure water, the foam is turbulent and churning with large bubbles. As the bubble size analyser can only measure bubbles up to 5mm in diameter accurately, the confidence in this data (Figure 4-11) is not as high as the data for the 10% ethanol system. The addition of ethanol leads to a turbulent churning foam with many fine bubbles (Figure 4-12).

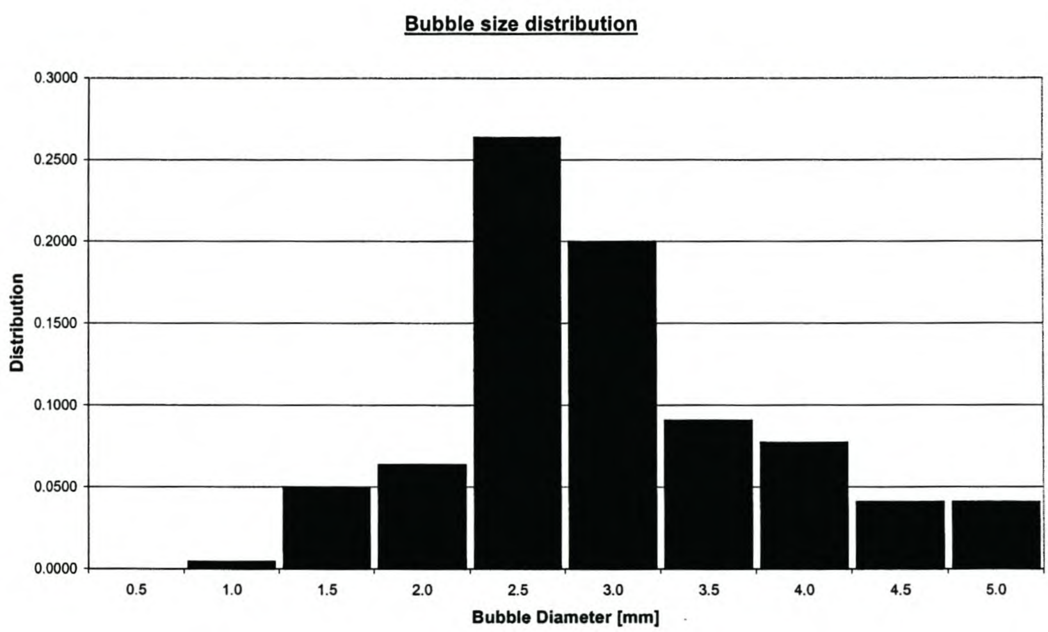


**Figure 4-11 Distribution for water with 0% Ethanol - Gas velocity 0.3m/s**

For pure water a mean bubble diameter of 3.0 mm was measured with a standard deviation of 3.0 mm. A 10% ethanol solution had a bubble size distribution with mean diameter of 3.3 mm and standard deviation of 1.2mm. The bubble size distributions in figures 4-10 and 4-11 were obtained for the same gas velocity.

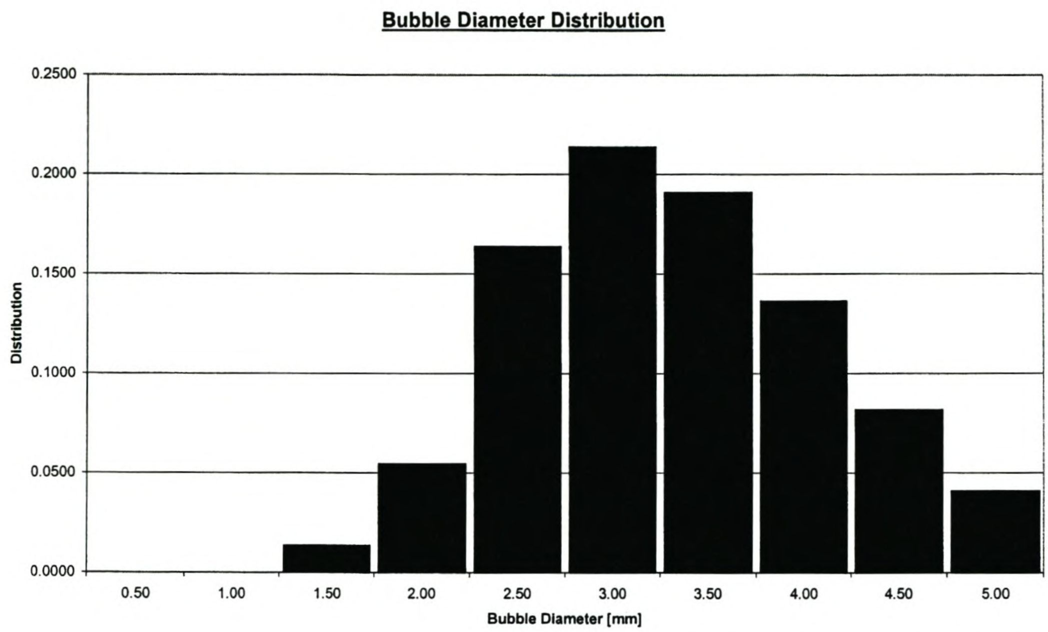


**Figure 4-12 Distribution for water with 10% Ethanol - Gas velocity 0.3m/s**

The mean bubble diameter for the 10% ethanol mixture is slightly bigger than that for the pure water system. This is due to the lower surface tension of the ethanol mixture. The pure water system had a larger standard deviation and showed no stable foam formation. The 10% ethanol system showed a normal distribution with a smaller standard deviation in bubble size measurements.

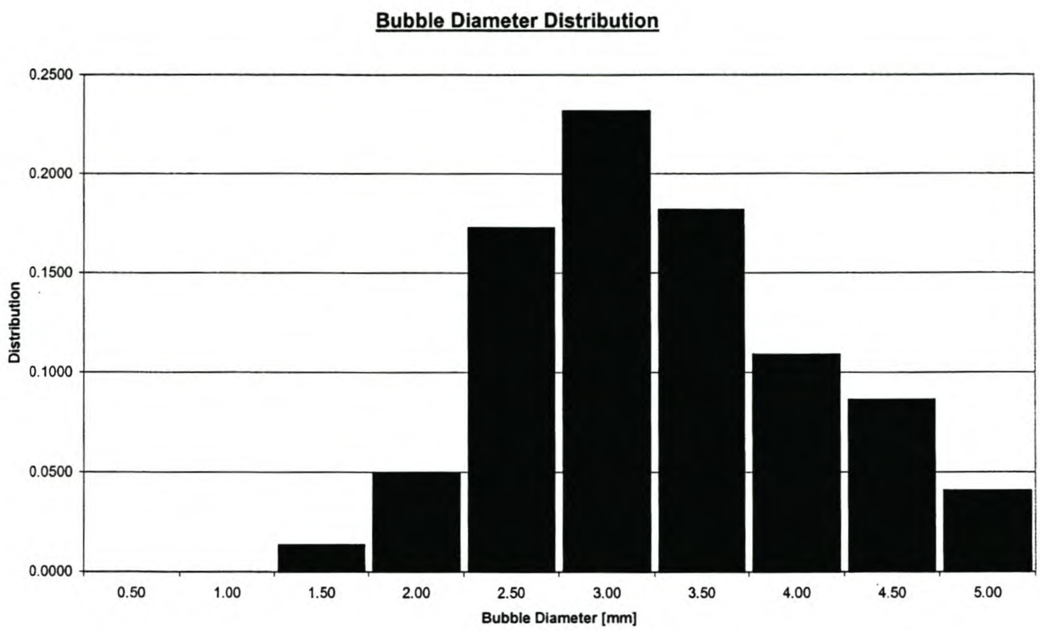


**Figure 4-13 Distribution for water with 10% Ethanol Gas velocity 0.6m/s**

For higher gas velocities (Figure 4-13) the mean bubble diameter obtained was 3.3 mm with a standard deviation of 0.8 mm. The bubble diameter seems much the same as that obtained for the lower gas velocity. In this case the increase in turbulence did not lead to bubble breakdown into smaller bubbles. Smaller bubbles increase the foam stability and can therefore lead to increased foam height due to built-up of foam.

Attempts to establish the bubble size distribution for ethanol-water mixtures with higher ethanol content failed. The data obtained had low confidence levels and this could be attributed to a high percentage of bubbles falling outside the analyser sensor range. The same difficulties were experienced when higher gas velocities were investigated. It was however possible to obtain bubble size distribution data for three different gas velocities for a mixture consisting of 10% ethanol, 10% glycerol and 80% water. The results are given in figure 4-14 and table 4-3.

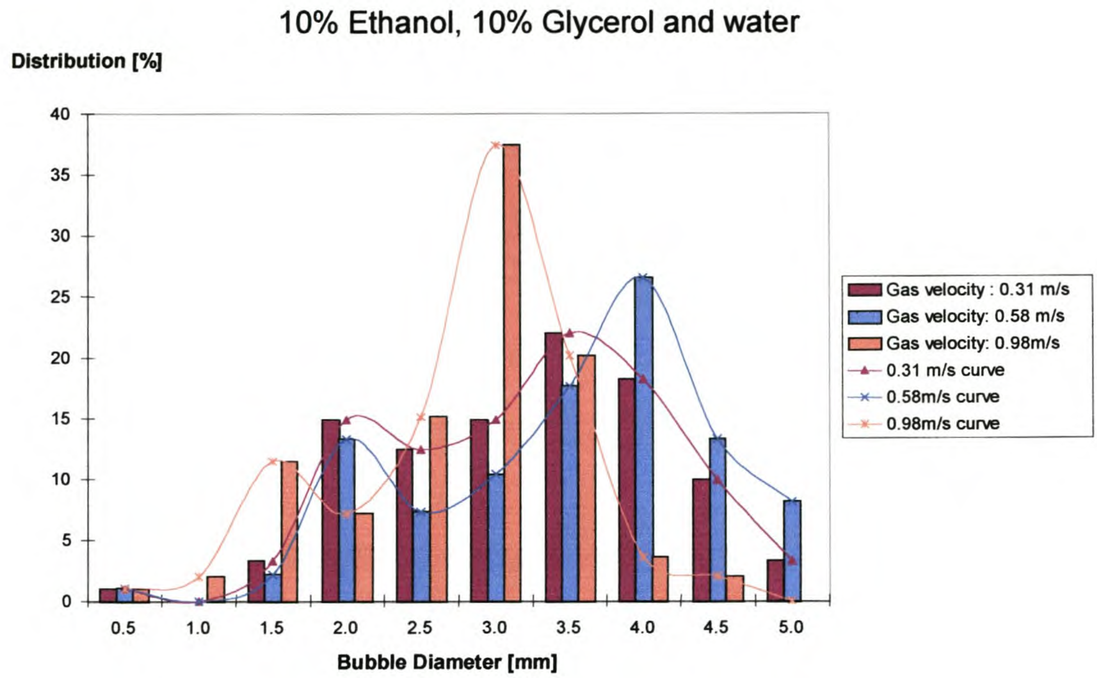


**Figure 4-14 Comparison of bubble size distribution for different gas velocities**

**Table 4-3. Statistics for 10% ethanol-10% glycerol-water mixture**

| Gas velocity [m/s] | Mean bubble diameter [mm] | Standard deviation of bubble diameter [mm] | Discrepancy in readings [%] |
|---|---|---|---|
| 0.31 | 2.55 | 0.99 | 1.22 |
| 0.58 | 2.82 | 1.02 | 2.66 |
| 0.98 | 2.08 | 0.70 | 2.09 |

From table 4-3 it can be observed that the smallest mean bubble diameter resulted from the highest gas velocity and that the smallest standard deviation of bubble diameter was also obtained from the highest gas velocity. The bubble size distribution is however, no longer normal. A small secondary peak on the left of the mean bubble diameter is visible for all three datasets. This peak may be the result of the break-up of bigger bubbles due to turbulence.

## 4.3 Modelling

In the study of slag foaming the foam index is often modelled with empirical correlations. One of the methods most often used is based on dimensionless analysis and was first proposed by (Ito 1989). The dimensionless groups they identified were

$$\Pi 1 = \frac{\Sigma g \mu}{\sigma} \qquad \textbf{Eq. 4-5}$$

where $\Sigma$ is the foam index [s]

$g$ is the gravitational constant [m/s$^2$]

$\mu$ is the melt viscosity [Pa.s]

$\sigma$ is the melt surface tension [N/m$^2$]

and

$$\Pi 2 = \frac{\rho \sigma^3}{\mu^4 g} \qquad \textbf{Eq. 4-6}$$

where $\rho$ is the melt density [kg/m$^3$]

By separating the data into groups according to the geometry of the set-up and the liquid height, it is possible to model the foaming behaviour for a range of mixtures in a specific experimental set-up. The column diameter and gas injection pore size as well as the liquid volume were therefore constant for each model fit.

The parameters for the model are found by plotting the logarithms of the dimensionless numbers against each other and fitting a line through the resulting points.

Figure 4-15 is an example of this exercise. The other figures are given in appendix B.

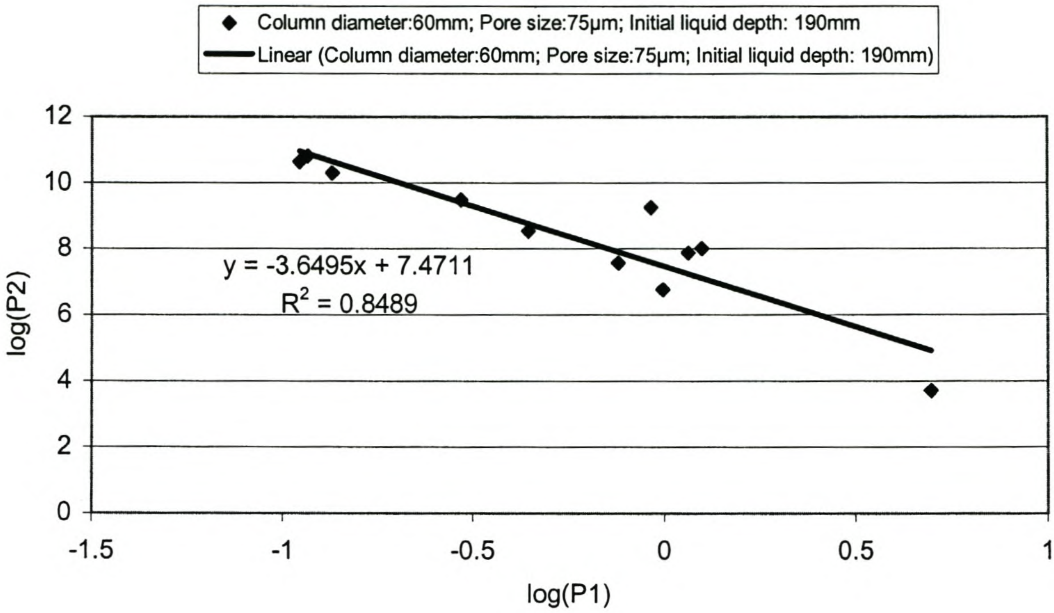


**Figure 4-15 Example of dimensionless group model fit**

Once the parameters have been established, the resulting equation is manipulated to express the foam index in terms of the liquid/melt physical properties. This equation is in the following form

$$\Sigma = K\frac{\rho^{q}\sigma^{r}}{\mu^{s}g^{t}} \qquad \textbf{Eq. 4-7}$$

where K, q, r, s and t are constants determined from the model.

The results of these operations are given in table 4-4.

**Table 4-4. Results for dimensionless analysis on physical modelling data**

| Column diameter [mm] | Pore size [µm] | Initial liquid depth [mm] | q | r | s | t | K |
|---|---|---|---|---|---|---|---|
| 32 | 13 | 14 | -0.46 | -0.39 | -0.85 | 0.54 | 2944 |
| 32 | 13 | 28 | -0.46 | -0.37 | -0.82 | -0.54 | 3420 |
| 32 | 13 | 56 | -0.51 | -0.53 | -1.05 | 0.49 | 11236 |
| 32 | 13 | 93 | -0.59 | -0.77 | -1.36 | 0.41 | 65346 |
| 32 | 70 | 14 | -0.54 | -0.62 | -1.15 | 0.46 | 10458 |
| 32 | 70 | 28 | -0.84 | -1.52 | -2.36 | 0.16 | 4895630 |
| 32 | 70 | 56 | -0.88 | -1.65 | -2.53 | 0.12 | 13368785 |
| 32 | 70 | 93 | -0.60 | -0.80 | -1.40 | 0.40 | 74403 |
| 60 | 75 | 14 | -0.24 | 0.29 | 0.05 | 0.76 | 15 |
| 60 | 75 | 28 | -0.24 | 0.27 | 0.03 | 0.76 | 23 |
| 60 | 75 | 56 | -0.27 | 0.19 | -0.08 | 0.73 | 57 |
| 60 | 75 | 94 | -0.27 | 0.18 | -0.09 | 0.73 | 83 |
| 60 | 75 | 190 | -0.27 | 0.18 | -0.10 | 0.73 | 111 |

The results in table 4-4 are discussed in 4.5 in terms of the liquid physical properties. It is however to be noted that the constant K varies over several orders of magnitude. The highest values for K were found with a column diameter of 32mm and a pore size of 70µm. This is also the set-ups where the worst linear fits were found ($R^2$ values from 0.22-0.51). The lowest K values were found for a column diameter of 60mm. These values were obtained from the best linear fits observed ($R^2$ values from 0.85-0.95). It is also interesting to note the resemblance between the K values and the initial liquid depth for this column. This might be an indication that wall effects are no longer influencing the foaming behaviour in the bigger column and that the liquid depth is therefore the most important influence on foaming behaviour - after the liquid properties. K is therefore not truly constant, as is currently defined but is very dependent on liquid depth. With regard to slag operations one may therefore expect deep slags to behave differently from shallow slags.

## *4.4 Effect of physical properties on the foam index*

The following discussion of the influence of physical properties of the liquid on the foam index is based on the results contained in table 4-3.

### 4.4.1 The effect of density

When we look at equation 4-7, we can extract the relationship of density to the foam index as follow

$$\Sigma \propto \rho^{q} \qquad \textbf{Eq. 4-8}$$

The values determined for q ranges from –0.24 to –0.88. They are all negative numbers. This means that the higher the density, the lower the foam index. The weighted average value of q is –0.5. This value is equal to the value obtained for slag foaming by Ito (1989). The weighted average is the average of the three values obtained from averaging over the same column diameter and pore size. The weighted average is rounded to one significant digit. This is in line with physical expectation as the denser the liquid the more the tendency would there be for it to drain.

### 4.4.2 The effect of surface tension

When we look at equation 4-7, we can extract the relationship of surface tension to the foam index as follow

$$\Sigma \propto \sigma^{r} \qquad \textbf{Eq. 4-9}$$

The values determined for r ranges from –0.80 to 0.29. There is a crossover of sign. That means that there are regions where higher the surface tension, the lower the foam index and other regions where the lower the surface tension the higher the foam index. The weighted average value of r is –0.5. This value is equal to the value obtained for slag foaming by Ito (1989).

### 4.4.3 The effect of viscosity

When we look at equation 4-7, we can extract the relationship of surface tension to the foam index as follow

$$\Sigma \propto \mu^{-s} \qquad \textbf{Eq. 4-10}$$

The values determined for s ranges from –2.53 to 0.05. There is a crossover of sign. That means that there are regions where the higher the viscosity, the lower the foam index and other regions where the lower the viscosity the higher the foam index. The weighted average value of s is –1. This value is equal to the value obtained for slag foaming by Ito (1989).

In summary it can therefore be said that while the dimensionless group modelling technique describes the behaviour of any given system with constant geometry and initial liquid depth and set-up well, the parameters determined for each set-up and initial conditions differ markedly. The dimensionless group modelling technique should never be applied to a system with different set-up or physical properties outside of the range for which it was derived. However, the foam index seems to follow general trends in terms of the liquid properties $\sigma$, $\rho$ and $\mu$.

# 5 Results and discussions for slag foaming in metallurgical slags

## 5.1 Objectives

This chapter reports the results of experiments conducted on foaming in metallurgical slags. The results is analysed to clarify the role of solid precipitates, slag basicity and "FeO" concentration on slag foaming. The amount of iron in the system (FeO, $Fe_2O_3$ and $Fe_3O_4$) is expressed as "FeO". This amount would remain constant throughout an experiment unless precipitation of $Fe_3O_4$ occurred. This change in composition of the molten slag due to this precipitation was predicted through thermodynamic simulations and the resulting change in properties was estimated through correlations discussed at the end of this chapter..

Possible explanations for foaming behaviour that differs from that expected according to published articles and data are given. Possible models for slag foaming are compared with data to determine which model is more applicable.

## 5.2 Foam index for different compositions

The foam index is defined in the same manner as in chapter 4.

$$\Sigma = \frac{\Delta H}{\Delta V} \qquad \textbf{Eq. 5-1}$$

where $\Sigma$ is the foam index [s]

$\Delta H$ is the change in liquid height [mm]

and $\Delta V$ is the superficial gas velocity [mm/s]

The foam index is therefore obtained as the gradient of the graph relating the change in liquid height of the slag to the superficial gas velocity. Figure 5-1 is an example of this method of determining the foam index. Implicit in this method of foam characterisation is the assumption that the foam index is independent of the superficial gas velocity. (If gradient of a line fitted through data are used and not all the gradients on a curve fitted through the data.) Although the data may appear non-linear, this is in part due to the uncertainty in the foam height measurements. As the foam data was generated through low gas velocities, the assumption that the foam index is independent of the gas velocity is considered a safer option than over-fitting the data. The foam index is used to interpret the data because it is easy to measure, is used commonly in literature to describe slag foaming and is the basis for several models proposed for slag foaming.

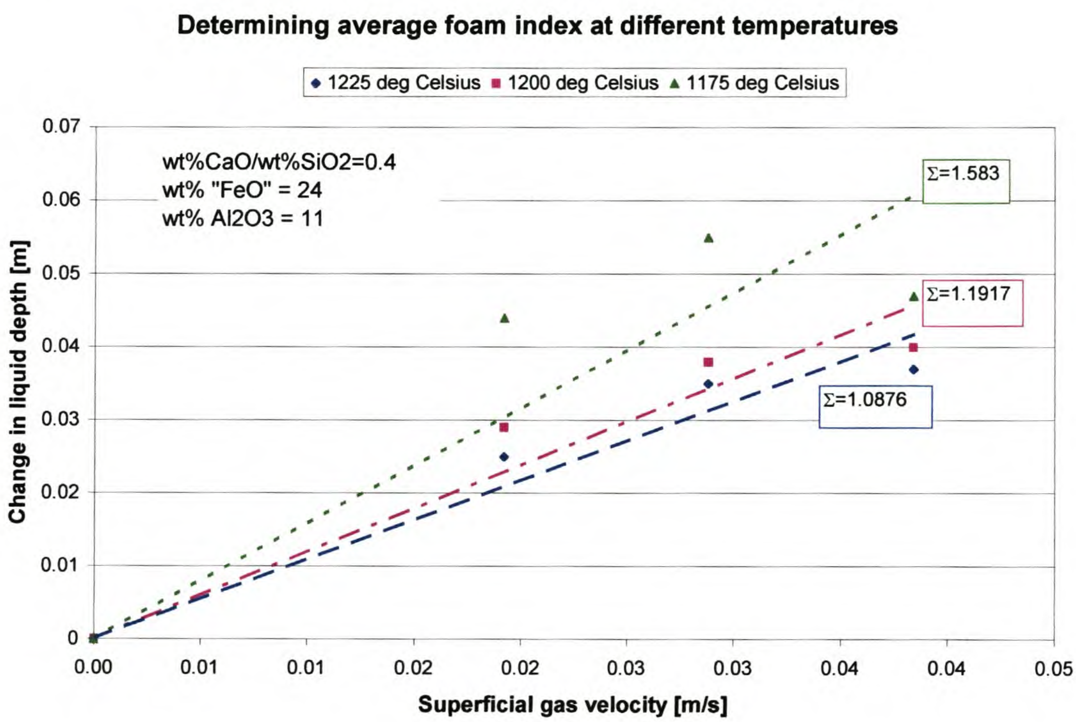


**Figure 5-1. An example of the determination of the average foam index for metallurgical slags at different temperatures**

A summary of the results for all the slags is given in Table 5.1. The composition of each slag system is given, as well as the temperature at which the slag was foamed. To simplify the data analysis, the amount of iron in the system (FeO, $Fe_2O_3$ and $Fe_3O_4$) is expressed as "FeO".

**Table 5-1. Results of average foam index values for metallurgical slags**

| Slag | Temperature | Composition wt% | | | | Foam Index |
|---|---|---|---|---|---|---|
| Number | [K] | $SiO_2$ | $Al_2O_3$ | "FeO" | CaO | [s] |
| 1 | 1448 | 45.5 | 10.5 | 23.7 | 20.3 | 1.6 |
| 1 | 1473 | 45.5 | 10.5 | 23.7 | 20.3 | 1.2 |
| 1 | 1498 | 45.5 | 10.5 | 23.7 | 20.3 | 1.1 |
| 2 | 1413 | 47.5 | 9.7 | 22.8 | 20.0 | 3.6 |
| 2 | 1438 | 47.5 | 9.7 | 22.8 | 20.0 | 2.0 |
| 2 | 1463 | 47.5 | 9.7 | 22.8 | 20.0 | 3.4 |
| 3 | 1413 | 41.4 | 6.0 | 19.9 | 32.8 | 9.6 |
| 3 | 1438 | 41.4 | 6.0 | 19.9 | 32.8 | 8.1 |
| 3 | 1463 | 41.4 | 6.0 | 19.9 | 32.8 | 16.3 |
| 4 | 1384 | 45.1 | 7.1 | 28.0 | 19.8 | 5.4 |
| 4 | 1409 | 45.1 | 7.1 | 28.0 | 19.8 | 4.6 |
| 4 | 1434 | 45.1 | 7.1 | 28.0 | 19.8 | 3.9 |
| 5 | 1473 | 41.0 | 15.4 | 25.9 | 17.8 | 1.9 |
| 5 | 1498 | 41.0 | 15.4 | 25.9 | 17.8 | 2.1 |
| 5 | 1523 | 41.0 | 15.4 | 25.9 | 17.8 | 2.6 |
| 5 | 1573 | 41.0 | 15.4 | 25.9 | 17.8 | 16.3 |
| 5 | 1623 | 41.0 | 15.4 | 25.9 | 17.8 | 18.4 |
| 6 | 1448 | 53.5 | 6.8 | 20.4 | 19.3 | 6.9 |
| 6 | 1498 | 53.5 | 6.8 | 20.4 | 19.3 | 6.6 |
| 7 | 1573 | 46.9 | 19.2 | 24.2 | 9.7 | 7.9 |
| 7 | 1613 | 46.9 | 19.2 | 24.2 | 9.7 | 4.1 |
| 7 | 1638 | 46.9 | 19.2 | 24.2 | 9.7 | 4.1 |
| 7 | 1653 | 46.9 | 19.2 | 24.2 | 9.7 | 9.0 |
| 8 | 1623 | 43.8 | 5.0 | 25.0 | 26.3 | 6.2 |
| 8 | 1673 | 43.8 | 5.0 | 25.0 | 26.3 | 10.4 |
| 9 | 1573 | 51.9 | 10.0 | 9.3 | 28.8 | 9.0 |
| 10 | 1673 | 52.9 | 8.4 | 13.9 | 24.8 | 8.2 |
| 11 | 1673 | 42.8 | 17.1 | 8.6 | 31.5 | 4.5 |

Foam index values obtained ranges from 1.1 seconds to 18.4 seconds. These values are within the range of foam index values reported for metallurgical slags of different composition, ranging from 0.3 seconds to 56 seconds (Roth 1993; Zhang 1995; Zhang 1995; Zhang 1995; Paramguru 1997; Gaskell 2000). The raw data for the determination of the average foam index values are given in the appendix A Table 5.2.

**Table 5-2. The physical properties of metallurgical slags investigated**

| Slag Number | Temp Kelvin | density $kg/m^3$ | viscosity Pa.s | surface tension N/m |
|---|---|---|---|---|
| 1 | 1448 | 3089 | 5.53 | 0.469 |
| 1 | 1473 | 3095 | 4.18 | 0.460 |
| 1 | 1498 | 3102 | 3.14 | 0.451 |
| 2 | 1413 | 3072 | 8.58 | 0.475 |
| 2 | 1438 | 3076 | 6.50 | 0.468 |
| 2 | 1463 | 3081 | 4.94 | 0.461 |
| 3 | 1413 | 3142 | 12.96 | 0.513 |
| 3 | 1438 | 3121 | 8.19 | 0.501 |
| 3 | 1463 | 3106 | 4.33 | 0.486 |
| 4 | 1384 | 3097 | 7.91 | 0.482 |
| 4 | 1409 | 3101 | 6.04 | 0.475 |
| 4 | 1434 | 3106 | 4.36 | 0.468 |
| 5 | 1473 | 3168 | 7.09 | 0.483 |
| 5 | 1498 | 3160 | 5.43 | 0.477 |
| 5 | 1523 | 3151 | 4.35 | 0.470 |
| 5 | 1573 | 3185 | 1.61 | 0.493 |
| 5 | 1623 | 3185 | 1.61 | 0.486 |
| 6 | 1448 | 3005 | 5.58 | 0.446 |
| 6 | 1498 | 3005 | 5.58 | 0.438 |
| 7 | 1573 | 3135 | 5.46 | 0.467 |
| 7 | 1613 | 3135 | 5.46 | 0.461 |
| 7 | 1638 | 3135 | 5.46 | 0.457 |
| 7 | 1653 | 3135 | 5.46 | 0.455 |
| 8 | 1623 | 3121 | 0.90 | 0.480 |
| 8 | 1673 | 3121 | 0.90 | 0.473 |
| 9 | 1573 | 2899 | 7.26 | 0.457 |
| 10 | 1673 | 2941 | 6.18 | 0.438 |
| 11 | 1673 | 2952 | 4.82 | 0.473 |

In the table above, the physical properties for the slags described in table 5-1 are given. The effects of the slag physical properties on the foam index will be discussed after the sections dealing with the effects of solid particles, slag basicity and 'FeO' concentration on slag foaming.

## 5.3 The effect of solid precipitates on slag foaming

Due to the take-up of alumina from the crucible and the fact that FeO contains traces of $Fe_2O_3$, the composition of slags were determined by XRF analyses, and the $Fe^{2+}/Fe^{3+}$ ratio was determined by the hot acid titration method. The results from these tests were used in thermodynamic simulations (FactSage) to determine the amount [g] of solids present in the melt at the different temperatures investigated. These results are summarised in appendix A Table 5-3. The predicted phases of solid particles, according to FactSage, was in agreement with the $FeO$-$Fe_2O_3$-$SiO_2$-$CaO$-$Al_2O_3$ multi-component phase diagrams by (F. Kongoli 2001).

The viscosity of the slag was modified to include the effect of solids according to the equation suggested by (Happel 1957).

$$\frac{\mu}{\mu_0} = 1 + 5.5\varphi\psi \qquad \textbf{Eq. 5-2}$$

where $\varphi$ is the volume fraction of solids in the melt

$\psi$ is an interaction factor dependent on the solids concentration

$\mu$ is the adjusted viscosity of the melt

and $\mu_o$ is the viscosity if the melt without any solids

Having obtained the mass of solid precipitates from FactSage, it was still necessary to obtain the densities of the precipitates to determine the volume fraction of solids in the melt. The densities of solid precipitates were obtained from the FactSage database except for the density of magnetite ($Fe_3O_4$) which was found in (Gray 1971). The precipitates were one or more of magnetite, wollastonite ($FeSiO_3$, $CaSiO_3$) or anorthite ($Ca_2Al_2SiO_7$).

The results obtained are graphically summarised in figure 5.2. Small volume % magnetite in the slag stabilised the foaming, but increasing amounts of wollastonite and anorthite destabilised the foaming behaviour.

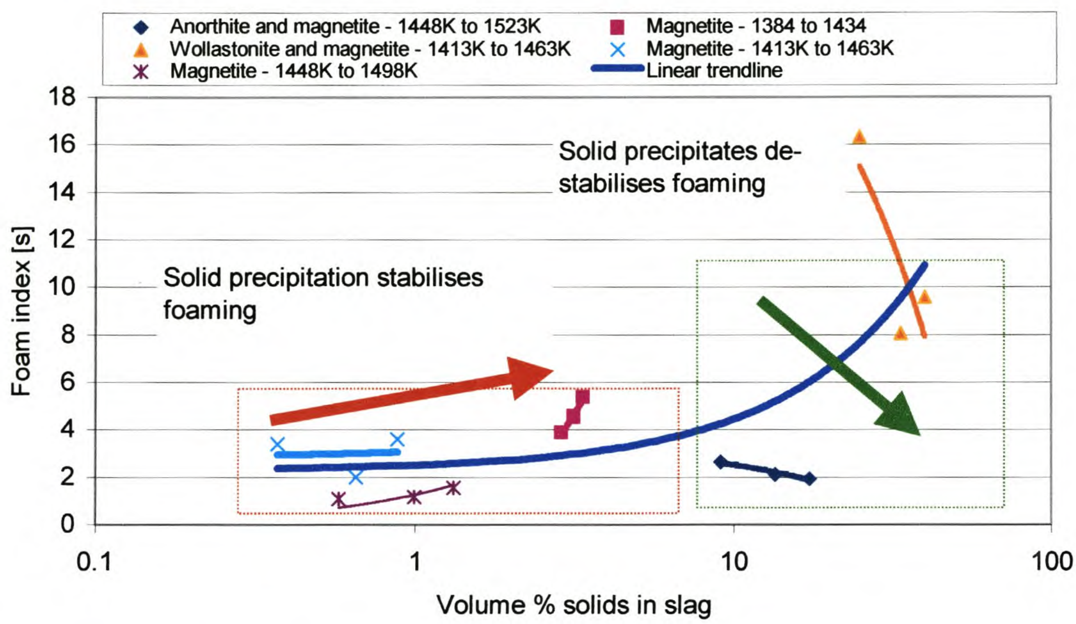


**Figure 5-2. Summary of influence of solid precipitates on slag foaming**

The influence of solids on foaming is therefore not only a function of the amount of solids present in the system, but also of the nature of the solids, such as solid form. $Fe_2O_3$ is isometric while wollastonite and anorthite are elongated. There are also large differences in interfacial properties and densities.

## *5.4 The effect of basicity on slag foaming*

The data obtained in this study confirm the effect of basicity on slag foaming as discussed by (Ito 1989). The foam index decreases with increasing basicity due to the lowering of the slag viscosity. This continues until the precipitation of solids starts and the foam index once again increases. They found that minimum foaming took place with a $CaO/(SiO_2 + Al_2O_3)$ [wt%/wt%] ratio of 1.2. The slags analysed by Ito, et.al contained 30wt% FeO and 3-5wt% $Al_2O_3$ and was studied at 1576K and 1673K.

From figure 5.3 minimum foaming occurred at a $(CaO + Al_2O_3)/SiO_2$ ratio of 0.67. This difference can be explained by the difference in $Al_2O_3$ concentration in the slag. A higher level of $Al_2O_3$ decrease the size of the liquid zone and therefore leads to solids precipitation at lower slag basicity.

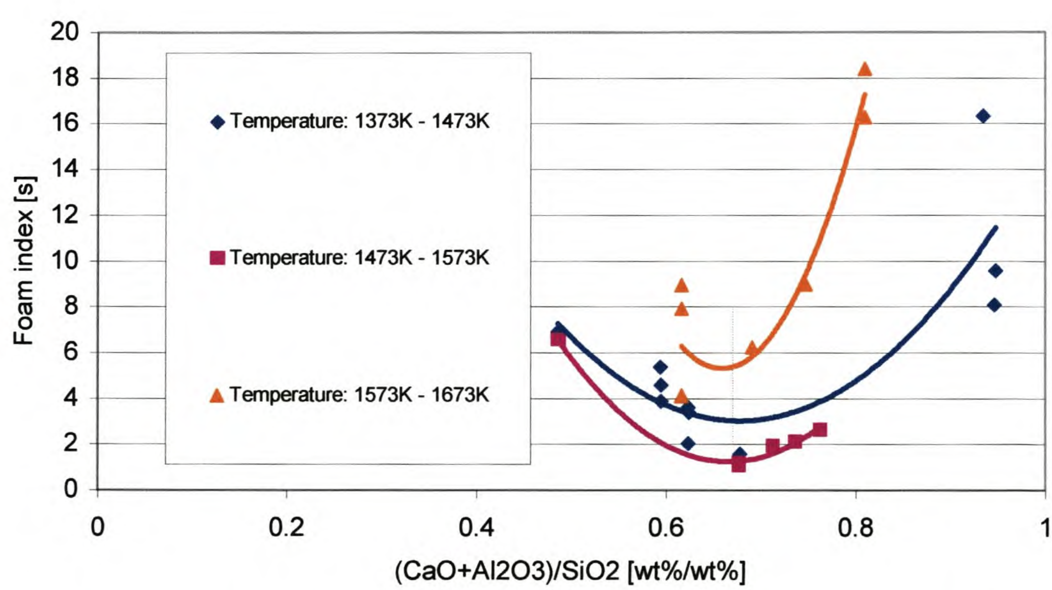


**Figure 5-3. Foaming index data sorted according to temperature and basicity**

## 5.5 The effect of "FeO" concentration on slag foaming

The "FeO" concentration in a slag is defined as the amount of iron oxide present in the slag expressed as FeO.

The $Fe^{2+}/Fe^{3+}$ ratio for the slags vary from 2.1 to 13.0 with an average value of 3.9.

(Jiang 1991) showed that for with 2 – 15 wt% FeO, the average foam index decreases with increasing FeO content at $CaO/SiO_2$ [wt%/wt%] ratios of 1.0 and 1.25. This is explained by the lowering of the liquid viscosity with increased FeO concentration.

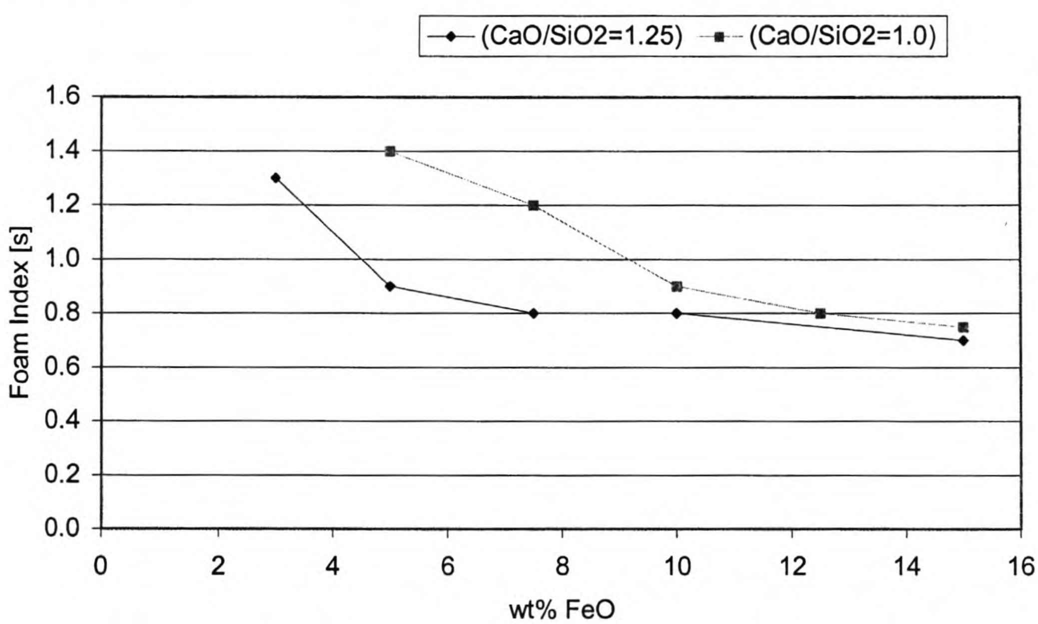


**Figure 5-4. Foaming index for $CaO$-$SiO_2$-$FeO$ slags at 1773K. (Jiang 1991)**

Figure 5.5 shows that the influence of FeO concentration reaches a minimum at approximately 24 wt% FeO. A possible explanation for the increased foaming at higher FeO concentrations could be that solid precipitates has formed and stabilised the foam.

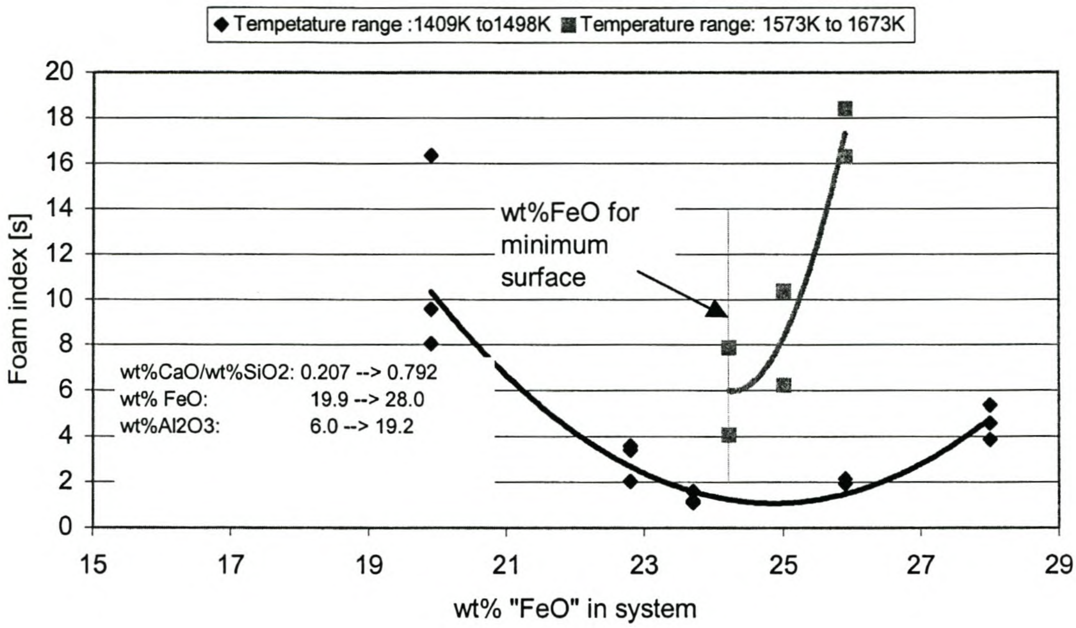


**Figure 5-5. Influence of "FeO" concentration on foaming behaviour**

In Figure 5-6 the amount of solids in the system is plotted against the temperature of the system. Although there is solids present in the temperature range lower than 1500K, there is no solids present in any of the systems above this temperature. As the data for the slags at temperatures above 1500K also shows increased foaming for higher FeO concentrations, investigation eliminated the possibility that solid precipitates is the reason for increased foamability.

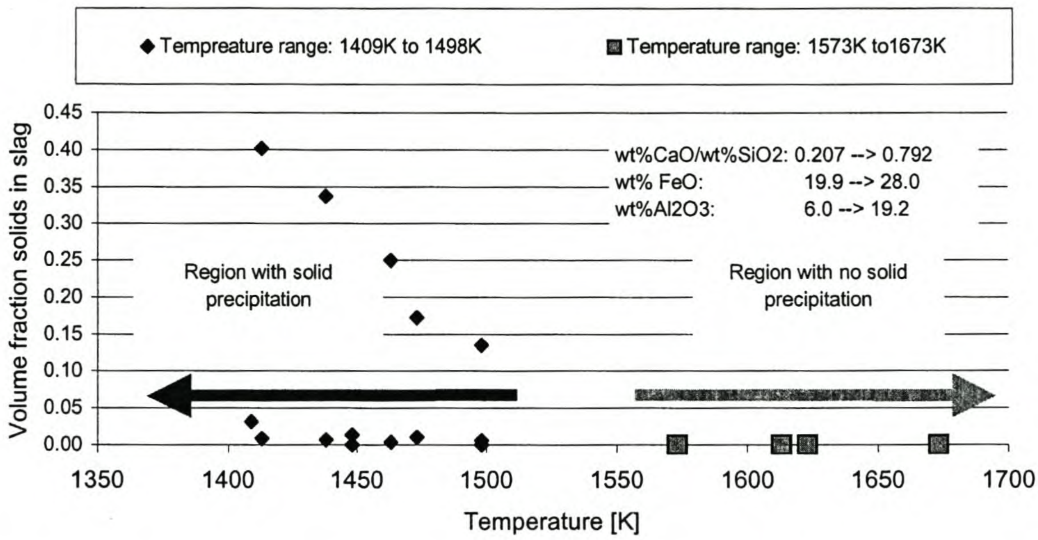


**Figure 5-6. Precipitation of solids in different temperature ranges**

A closer look at the surface tension properties of the slags hinted that the surface tension depression might play a bigger role in stabilising foams with low viscosities. The minimum surface tension for slags showing foam stabilisation with increasing "FeO" concentration is given in Figure 5-7. The minimum surface tension depression was determined from Figure 5-7 and is indicated on Figure 5.5. The surface tension values for the slags were estimated through a correlation that is discussed in section 5.6.4.2. The minimum surface tension depression agrees with the minimum of the foam index. It can therefore be concluded that while an increase of "FeO" concentration lowers the viscosity of slags and this leads to a decrease in the foaming index, the surface tension depression varies with "FeO" concentration and this can lead to an increase in the foam index contrary to that expected when only taking into account the effect of slag viscosity in foaming.

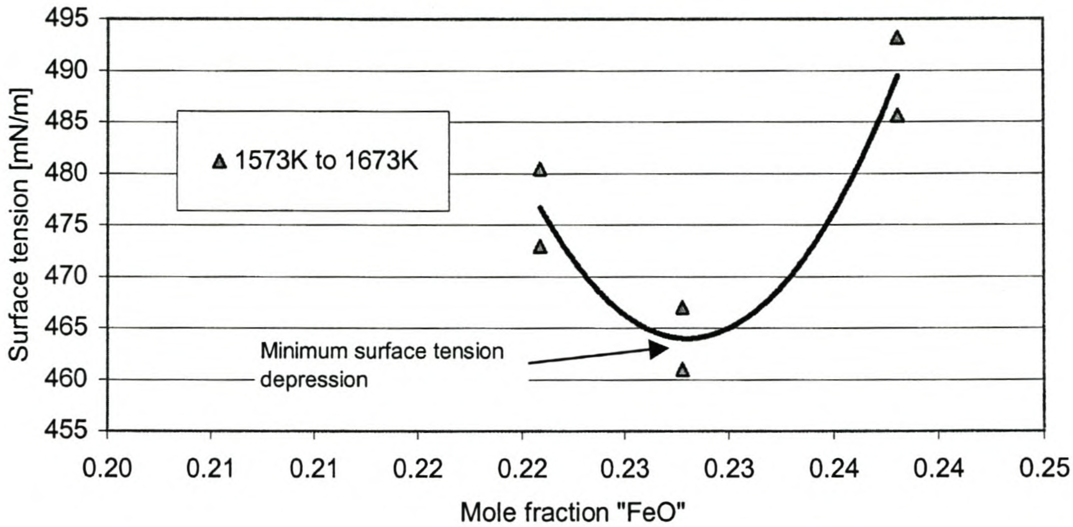


**Figure 5-7. Surface tension values for slags at temperatures of 1573K and 1673K**

In a multi-component system it is difficult to determine the surface tension depression for any given composition and/or temperature. However, by keeping some values constant the system is simplified and the essential relationships between the variables that is of interest, can be extracted. Figure 5-8 shows an example of how to determine the surface tension depression due to the "FeO" concentration. The surface tension depression is the gradient of the plot of surface tension against the molar concentration of the surface-active element, i.e. $\frac{|\partial\sigma|}{\partial \text{mole"FeO"}}$.

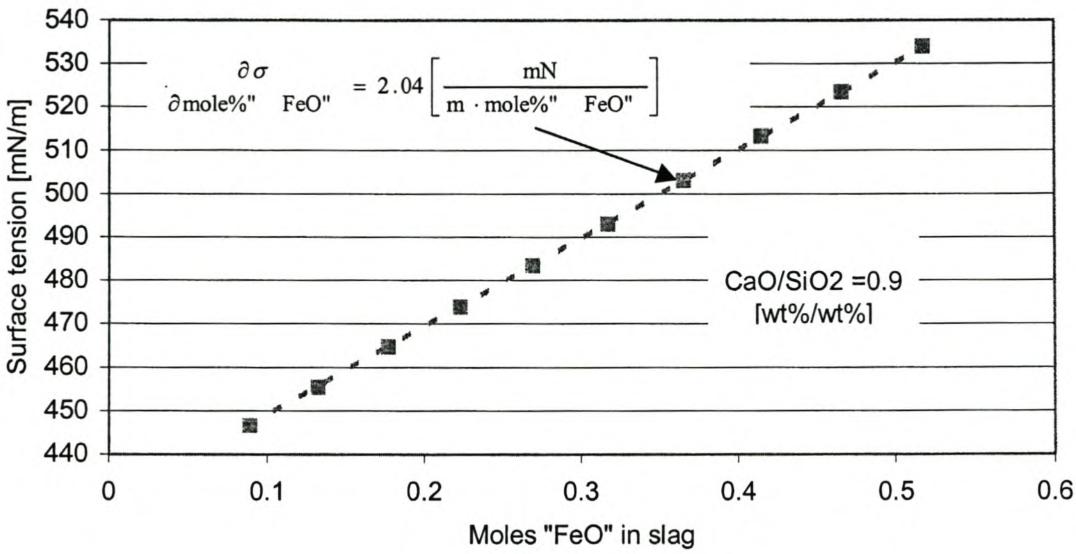


**Figure 5-8. Determining surface tension depression values**

By repeating this process illustrated in figure 5-8, the surface tension depression for "FeO" can be determined over a wide range of compositions. Figure 5-9 shows the change in surface tension depression by "FeO" for acid and basic slags. It is clear

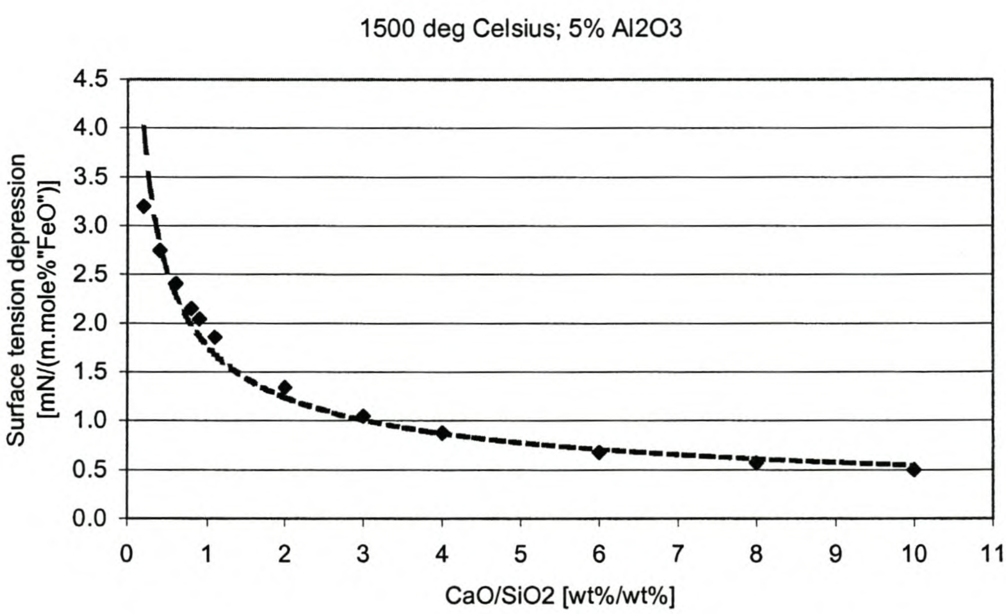


**Figure 5-9. Surface tension depression by "FeO" over wide basicity range**

that the surface tension depression is much more for acid slags and would therefore have greater influence over the foaming behaviour of acid slags compared to basic slags.

## 5.6 Comparison with models and data

Three models were selected to see to what degree they explain the influence of the slag physical properties on the average foam index. These models are empirical in nature and consist of one or more dimensionless numbers, which are related to each other through non-linear regression to determine the model parameters. These dimensionless numbers are identified and the results of the regression exercise are discussed. A more detailed discussion of these models can be found in Chapter 2.

### 5.6.1 Model 1

(Jiang 1991) used the following dimensionless numbers:

$$\Pi_1 = \frac{\Sigma g \mu}{\sigma} \qquad \textbf{Eq. 5-3}$$

$$\Pi_2 = \frac{\rho \sigma^3}{\mu^4 g} \quad \textbf{(Morton number)} \qquad \textbf{Eq. 5-4}$$

The relationship between these dimensionless numbers for basic steelmaking slags were found to be

$$\log(\Pi_2) = -2\log(\Pi_1) + 5.11 \qquad \textbf{Eq. 5-5}$$

Determining the coefficients for acid slags (Figure 5-7) it was found that

$$\log(\Pi_2) = -1.5\log(\Pi_1) + 0.45 \qquad \textbf{Eq. 5-6}$$

The model did not explain the foaming behaviour of acidic slags well. Reasons for this might be the uncertainty of slag properties, but also the fact that the model relies on the surface tension of the slag rather than surface tension depression as an influencing variable. When we rewrite equation 5-5 we get

$$\Sigma = 115\frac{\mu}{\sqrt{\rho\sigma}} \qquad \textbf{Eq. 5-7}$$

Rewriting equation 5-6 gives us

$$\Sigma = 0.93\frac{\mu}{\rho^{2/3}\sigma} \qquad \textbf{Eq. 5-8}$$

It is interesting that both equation 5-7 and 5-8 find the foam index directly proportional to the slag viscosity. Equation 5-8 finds the foam index inversely proportional to the surface tension of the slag, while equation 5-7 found the foam index inversely proportional to the square root of the surface tension of the slag. The influence of density on the foam index is slightly more significant in equation 5-8 having a coefficient of rather than ½ as in equation 5-7.

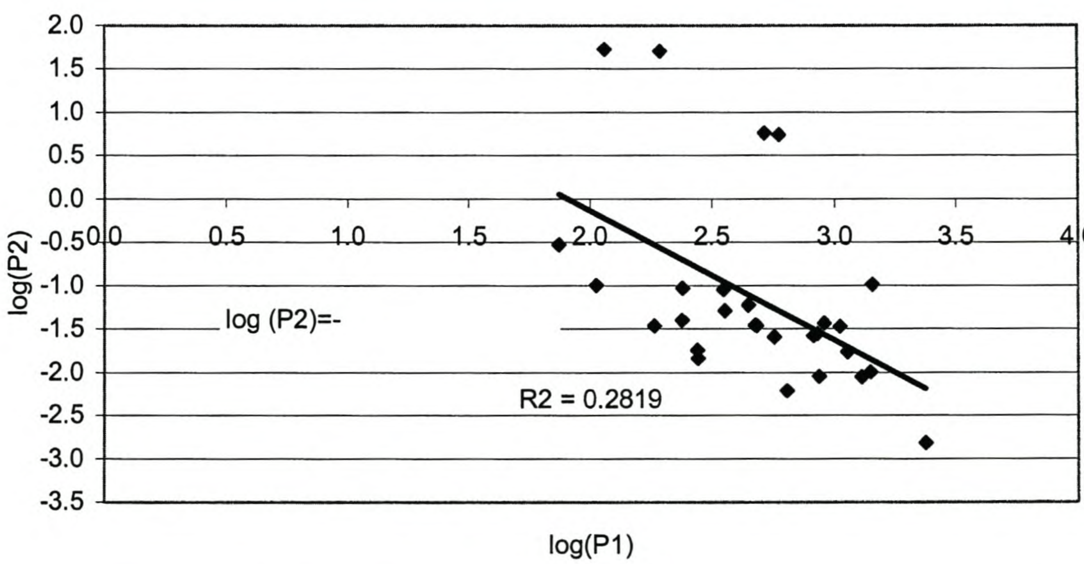


**Figure 5-10. Determining coefficients for acidic slags**

Complete model statistics are given in the appendix. In summary it can be said that although the model does not show a good fit, it satisfies the 95% significance level.

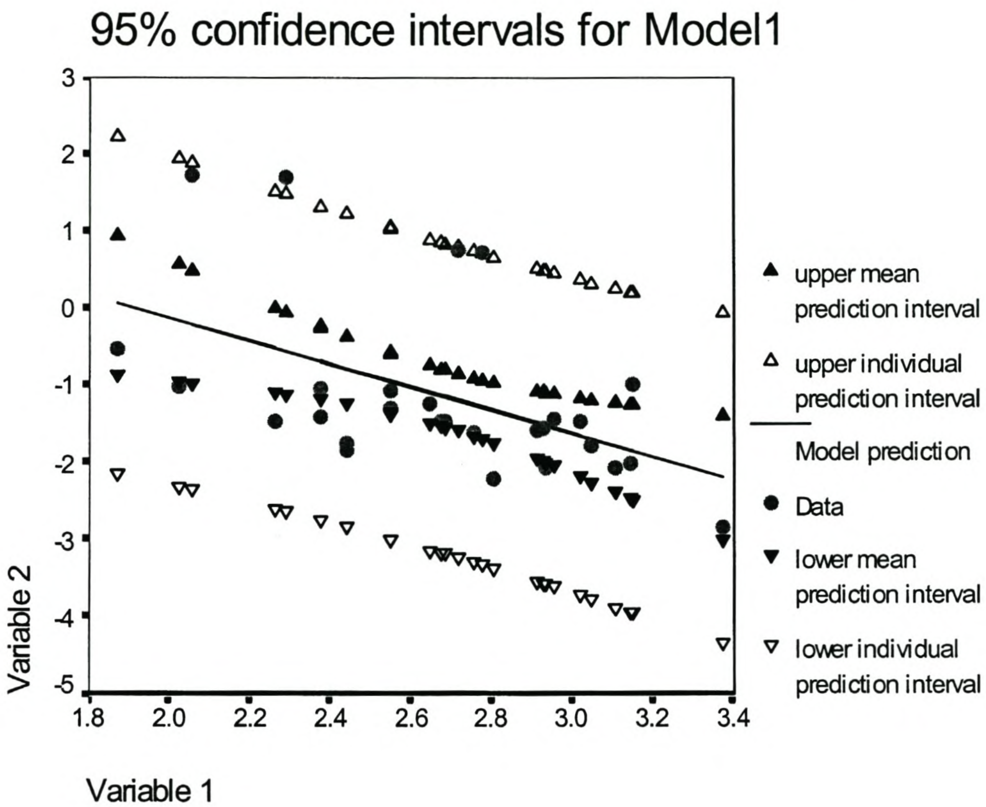


**Figure 5-11. Confidence intervals for model 1. Variable 1=log(Π1) and Variable 2=log(Π2).**

### 5.6.2 Model 2

An empirical model looking at the effect of bubble size on slag foaming was derived by (Zhang 1995). The following three dimensionless numbers were obtained:

$$\Pi_1 = \frac{\Sigma g \mu}{\sigma}$$ **(Denoted as $N_\Sigma$ for convenience)** **Eq. 5-9**

$$\Pi_2 = \frac{\rho \sigma^3}{\mu^4 g}$$ **(Morton number)** **Eq. 5-10**

$$\Pi_3 = \frac{\rho^2 D_b^3 g}{\mu^2}$$ **(Archimedes number)** **Eq. 5-11**

The model was fitted to data for slags with $CaO/SiO_2$=1 and containing 5 to 15% wt% FeO at 1500 C. The relationship between these dimensionless numbers were found to be

$$\log(\Pi_1) = 0.39\log(\Pi_2) - 0.22\log(\Pi_3) + 2.95$$ **Eq. 5-12**

Through non-linear regression, the coefficients for acidic slags were found to be (Figure 5-8)

$$\log(\Pi_1) = 3.71\log(\Pi_2) - 7.72\log(\Pi_3) + 16.99$$ **Eq. 5-13**

Although this model showed a slightly improved fit to that of Jiang (1991), it leaves lots of room for improvement (Figure 5-8).

Once again we can rewrite equations 5-12 and 5-13 to relate the foam index to the physical properties of the slag. Rewriting equation 5-12:

$$\Sigma = 115\frac{\mu^{1.2}}{\sigma^{0.2}\rho D_b^{0.9}}$$ **Eq. 5-14**

Rewriting equation 5-13:

$$\Sigma = 10.3 \times 10^{4} \frac{\sigma^{12}}{\mu^{0.4} \rho^{11.7} D_b^{23}} \qquad \textbf{Eq. 5-15}$$

The importance of the different variables in equations 5-14 and 5-15 as related to the foam index differ to a great extend. Equation 5-14 finds the slag viscosity the variable with the most influence on the foam index values and the slag surface tension the variable with the least influence. In contrast, equation 5-15 gives the bubble size and the slag surface tension as the variables with the most influence on the foam index and gives little importance to the slag viscosity.

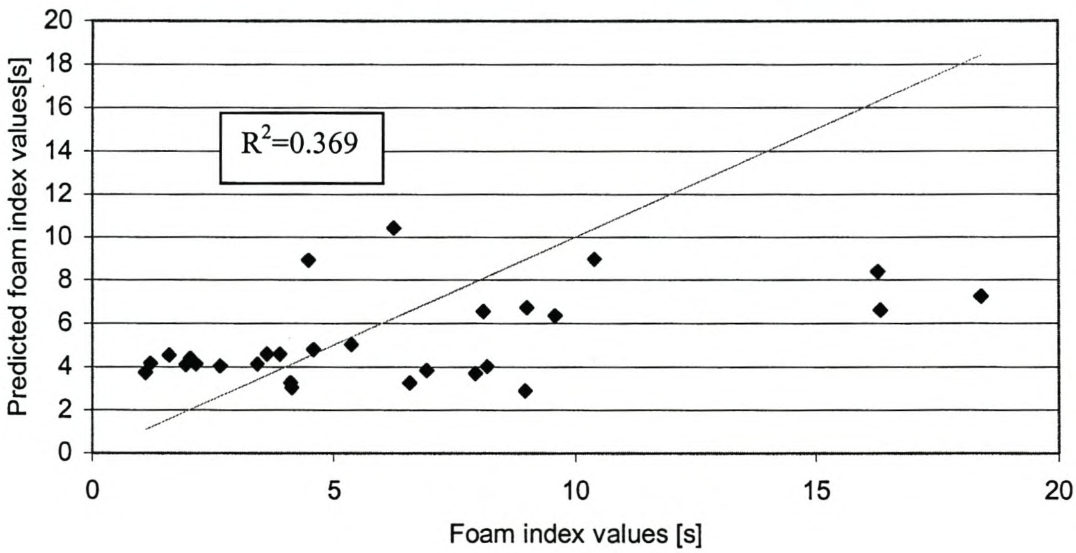


**Figure 5-12. Comparison of measured foam index values with predictions according to Zhang (1995)**

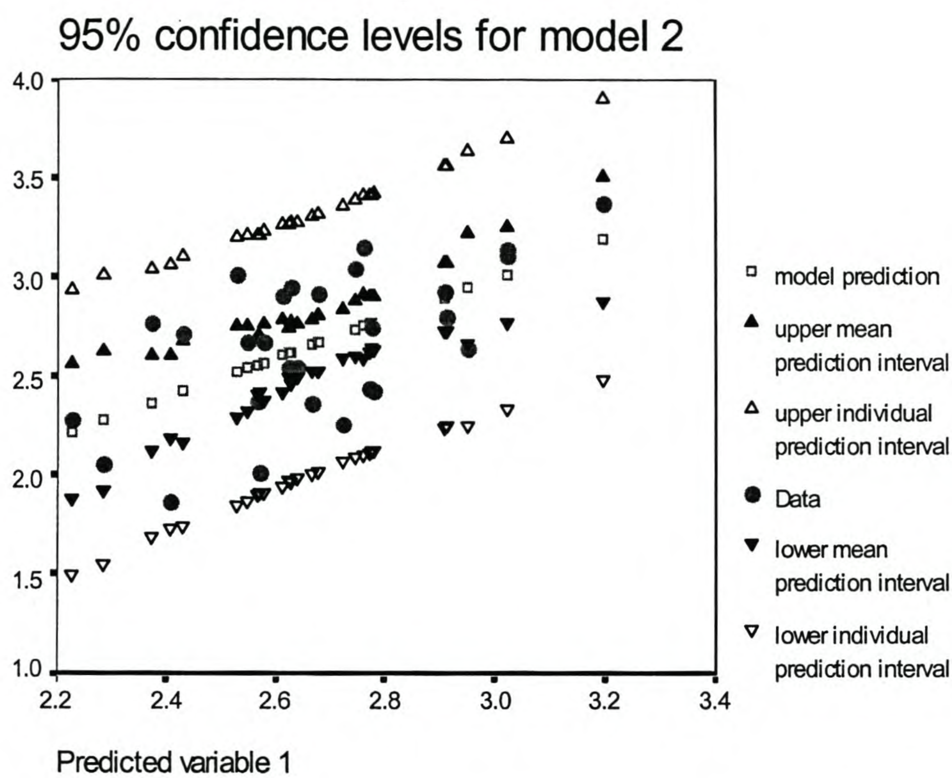


**Figure 5-13. Confidence intervals for model 2. Variable 1=log(Π1)**

Complete model statistics is given in the appendix. In summary it can be said that although the model does not show a good fit, it satisfies the 95% significance level. The variable log(Π2) does not significantly influence the model fit. Collinearity diagnostics indicates that the variables log(Π2) and log(Π3) are dependent on each other, as is expected from the fact that the bubble size is dependent on the liquid/slag physical properties.

**Table 5-3. Collinearity diagnostics for model 2. MODEL2B=log(Π2), MODEL2C=log(Π3), MODEL2A=log(Π1)**

**Collinearity Diagnostics[a]**

| Model | Dimension | Eigenvalue | Condition Index | Variance Proportions | | |
|---|---|---|---|---|---|---|
| | | | | (Constant) | MODEL2B | MODEL2C |
| 1 | 1 | 2.392 | 1.000 | .00 | .00 | .00 |
| | 2 | .608 | 1.984 | .00 | .00 | .00 |
| | 3 | 4.108E-05 | 241.307 | 1.00 | 1.00 | 1.00 |

a. Dependent Variable: MODEL2A

### 5.6.3 Model 3

Ghag (1998) developed three models to determine the most important stability mechanism in foaming. The first of these take into account the surface tension depression in the slag. In order to fit the model, it was assumed that the surface tension depression could be described by the difference between the surface tension of the slag and the surface tension of pure $SiO_2$ at similar conditions. $SiO_2$ were chosen as the pure liquid as it is the component with the highest concentration in the slag. The analysis (Ghag 1998) resulted in 2 dimensionless numbers, which are related as follows:

$$\frac{\Sigma \cdot \Delta\sigma}{\mu D_b} = k\left(\frac{\Delta\sigma}{(\rho g)D_b^{\ 2}}\right)^{\delta}$$ **Eq. 5-16**

$$\text{Number 1} = \frac{\Sigma \cdot \Delta\sigma}{\mu D_b}$$ **Eq. 5-17**

$$\text{Number 2} = \frac{\Delta\sigma}{(\rho g)D_b^{\ 2}}$$ **Eq. 5-18**

The coefficients determined by Ghag (1998) for water glycerol solutions were

$$\frac{\Sigma \cdot \Delta\sigma}{\mu D_b} = 2\times10^{6}\left(\frac{\Delta\sigma}{(\rho g)D_b^{\ 2}}\right)^{2.32}$$ **Eq. 5-19**

Coefficients determined for acidic slags (Figure 5-9) are

$$\frac{\Sigma \cdot \Delta\sigma}{\mu D_b} = 7\times10^{13}\left(\frac{\Delta\sigma}{(\rho g)D_b^{\ 2}}\right)^{7.6}$$ **Eq. 5-20**

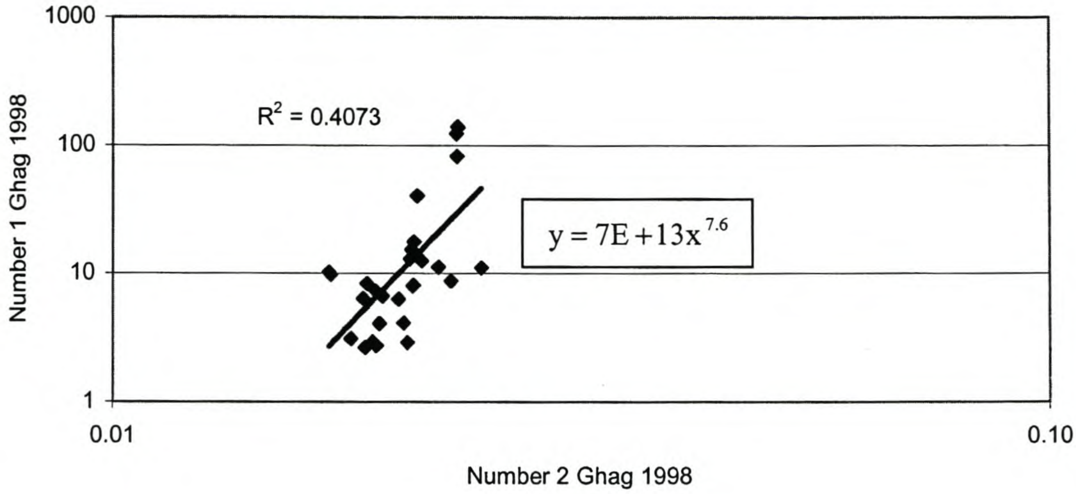


**Figure 5-14. Determining coefficients for equation 5-16**

Comparing equations 5-19 and 5-20, we find that both equations find the foam index directly proportional to the slag viscosity. Equation 5-20 however indicates a stronger influence of the surface tension depression and the bubble size on the foam index than equation 5-19. The model (equation 5-16) describes the foaming behaviour better than the models proposed by Zhang and Jiang (Figure 5-14). This might be because it takes into account the effect of bubbles size as well as surface tension depression. The model satisfies the 95% significance level.

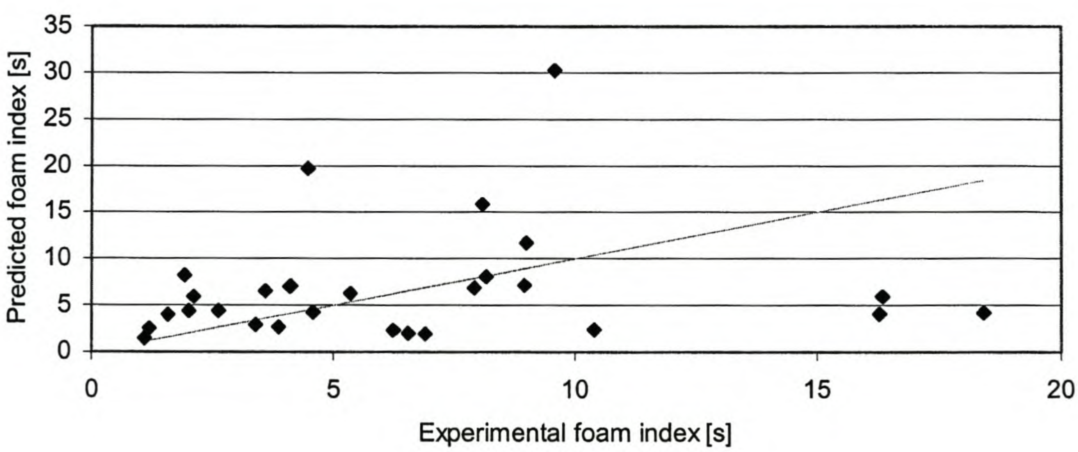


**Figure 5-15. Measured values of the foam index compared with predictions by equation 5-16**

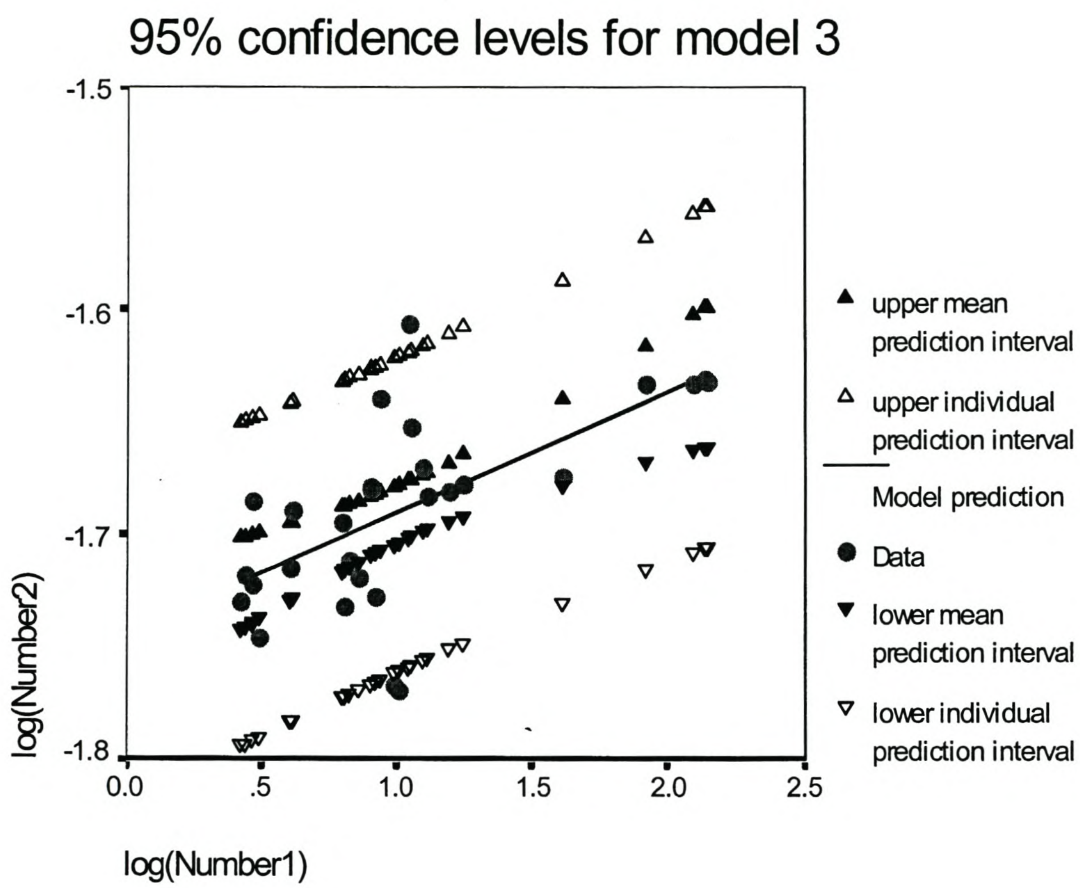


**Figure 5-16.Confidence intervals for model 3**

The following section provides an overview of the influence of slag viscosity and slag surface tension depression on slag foaming for the slags studied (Table 5-1) as well as the methods used to estimate slag physical properties.

### 5.6.4 Determining liquid physical properties

Due to the gaps in experimental data available describing the physical properties of multi-component slag systems, the use of various empirical models to determine the physical properties of slags are a common occurrence in the pyrometallurgical industry. The various models used in this study is explained in the following sections.

#### *5.6.4.1 Density*

The liquid density, ρ, is related to its molar volume, V, by the equation,

$$\rho = \frac{M_1 x_1 + M_2 x_2 + M_3 x_3 + \cdots}{V} \qquad \textbf{Eq. 5-21}$$

where $M_i$ and $x_i$ are the molar weight and the mole fractions of the slag component i. The slag molar volume is the addition of molar volumes of each component, $\overline{V}_1$, $\overline{V}_2$ and $\overline{V}_3$, etc.

**Table 5-4. Partial molar volume for various slag constituents at 1500 C**

| Slag component | $\overline{V}$ [cm$^3$/mole] |
|---|---|
| $Al_2O_3$ | $28.31+32x_{Al2O3}-31.45x^2_{Al2O3}$ |
| CaO | 20.7 |
| FeO | 15.8 |
| $Fe_2O_3$ | 38.4 |
| $SiO_2$ | $19.55+7.966x^2_{SiO2}$ |

The temperature dependence of the molar volume, V, of many slag systems can be considered to have an average value, $\frac{\partial V}{V \cdot \partial T} = 0.01\%K^{-1}$.

##### *5.6.4.2 Surface tension*

The calculation of the liquid slag surface tension is determined by the equation:

$$\sigma = x_1\overline{\sigma}_1 + x_2\overline{\sigma}_2 + x_3\overline{\sigma}_3 + \ldots \quad \textbf{(Zhang 1992)} \qquad \textbf{Eq. 5-22}$$

where $x_i$ indicates the mole fraction of component *i*.

and $\overline{\sigma}_i$ indicates the partial molar surface tension for different slag components.

**Table 5-5. Partial molar surface tension for different slag components at 1500 C**

| Oxide | $Al_2O_3$ | CaO | FeO | MgO | MnO | $SiO_2$ | BaO |
|---|---|---|---|---|---|---|---|
| $\sigma$ [mN/m] | 655 | 625 | 645 | 635 | 645 | 260 | 366 |

For temperatures different from 1500 C, an average value of $\frac{\partial\sigma}{\partial \mathrm{T}} = -0.15\mathrm{mN/m}\cdot\mathrm{K}$ is used.

##### *5.6.4.3 Viscosity*

Slag viscosities were determined from a modified Urbain equation published by Kondratiev (2001).

$$\mu = \mathrm{AT}\exp\left(\frac{1000\mathrm{B}}{\mathrm{T}}\right) \qquad \textbf{Eq. 5-23}$$

where $-\ln\mathrm{A} = m\mathrm{B} + n$

$$B = \sum\nolimits_{i=0}^{3} b_i^0 X_S^i + \sum\nolimits_{i=0}^{3}\sum\nolimits_{j=0}^{2}\left(b_i^{Cj}\frac{X_C}{X_c + X_F} + b_i^{Fj}\frac{X_F}{X_c + X_F}\right)\alpha^j X_S^i \qquad \textbf{Eq. 5-24}$$

where $\alpha = \frac{X_C + X_F}{X_C + X_F + X_A}$

and $X_A$, $X_C$, $X_F$ and $X_S$ are the molar fractions of $Al_2O_3$, CaO, 'FeO' and $SiO_2$ respectively.

And $\quad m = m_A X_A + m_C X_C + m_F X_F + m_S X_S$

**Table 5-6. Viscosity Model Parameters ($10^{-1}$ Pa.s)**

| | j/i | 0 | 1 | 2 | 3 | |
|---|---|---|---|---|---|---|
| $b_i^0$ | 0 | 13.31 | 36.98 | -177.70 | 190.03 | n= 9.322 |
| $b_i^{Cj}$ | 1 | 5.50 | 96.20 | 117.94 | -219.56 | $m_F$= 0.665 |
| | 2 | -4.68 | -81.60 | -109.80 | 196.00 | $m_C$= 0.587 |
| $b_i^{Fj}$ | 1 | 34.30 | -143.64 | 368.94 | -254.85 | $m_A$= 0.370 |
| | 2 | -45.63 | 129.96 | -210.28 | 121.2 | $m_S$= 0.212 |

### 5.6.5 The influence of slag physical properties on slag foaming

In figure 5-17, the effect of physical properties on the foam index can be evaluated. It is clear that an increase in viscosity does leads to higher foam index values for almost all the data. There is also a region where foam stabilisation can be enhanced by Gibbs' and Marangoni surface tension effects. At higher viscosities, foam stabilisation is dominated through viscosity and surface viscosity effects, which retard fluid drainage from the liquid lamella and surface tension effects does not significantly influence foaming behaviour.

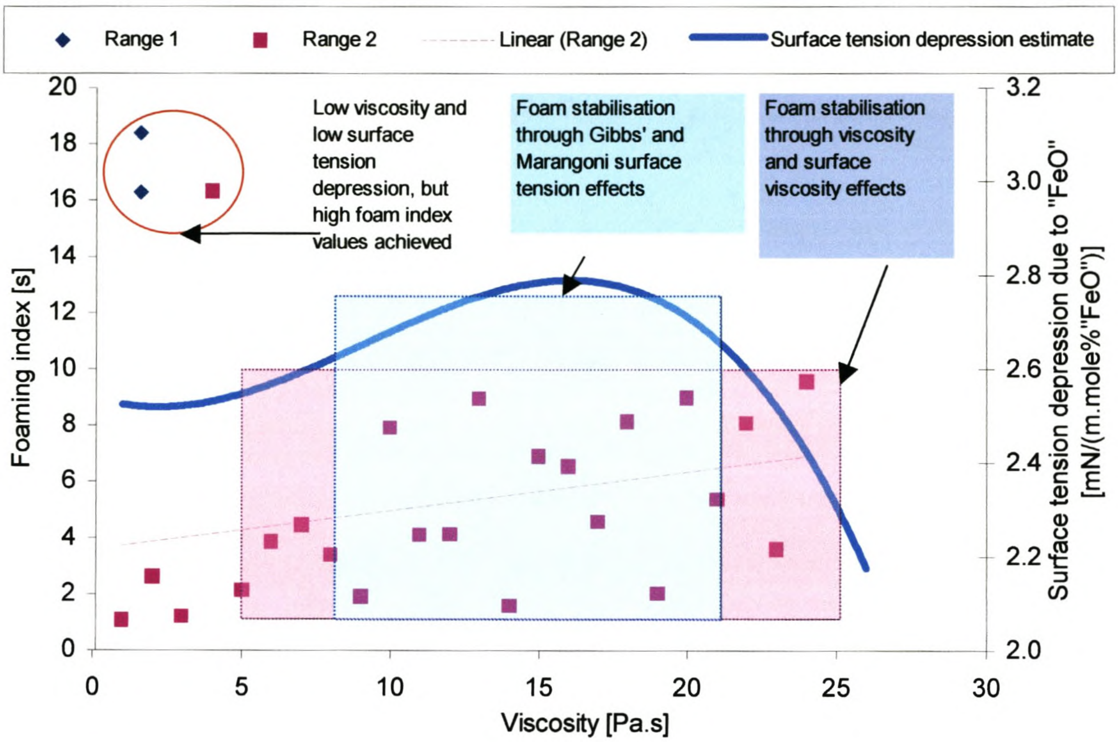


**Figure 5-17. Physical properties and foam stabilisation**

There are however some data-points where a high foaming index was measured, but the slag has a low viscosity and low surface tension depression. It is possible that another foam stabilisation mechanism applies there. Low viscosity and low surface tension depression would lead to very thin bubble lamella. It is therefore possible that the high foam index values in this region is due to the adsorption of ionic surface-active solutes and that electrical double layer repulsion is the foam stabilisation mechanism in this instance.

## 5.7 Summary

In summary we can conclude that

1. Solid precipitates can have positive or a negative influence on the foam index, according to the nature of the precipitates
2. For increasing basicity, the foaming index decreases until precipitation of solids occurs. Then the foaming index increases with increasing basicity.
3. For increasing "FeO" concentration the foam index will decrease due to lower viscosity, but higher surface tension depression may lead to increased foam index values at high "FeO" concentrations.
4. Models derived for the foaming of basic steelmaking slags does not satisfactorily describe the foaming behaviour of acidic slags.

In the following chapter the conclusions reached in various previous chapters will be summarised.

# 6 Conclusions

The main conclusions drawn from the experiments conducted at both room temperature and with metallurgical slags are listed below.

## 6.1 Physical modelling of slag foaming in 2-phase systems

- The foam index is not independent of the superficial gas velocity, but can be approximated as such at low gas velocities.
- An increase in the initial liquid depth leads to increased foaming.
- Glycerol-water mixtures do not form a stable foam and indicates that the lowering of the liquid surface tension is not a sufficient condition for foam formation.
- Gas injection through smaller pores generally leads to increased foaming. This may be attributed to the formation of smaller bubbles.

## 6.2 Influence of bubble size on foaming behaviour of aqueous mixtures

- Smaller mean bubble sizes are achieved at higher gas injection velocities.
- The smallest standard deviation is also achieved at higher gas velocities.
- The bubble size distribution is usually normal, but a secondary peak may appear due to the breakdown of bubbles at high gas injection rates.

## 6.3 Influence of physical properties on foaming of aqueous mixtures

The following conclusions were reached by determining coefficients for an empirical dimensional model.

- Data gathered from the column with the largest diameter show less scatter and it is concluded that this is the result of less influence of wall effects on foaming.
- Higher liquid density leads to lower foam index values.

- The influence of the liquid surface tension is dependent on the system investigated and may have a positive or negative result on foaming.
- The influence of the liquid viscosity is dependent on the system investigated and may have a positive or negative result on foaming.
- The empirical model should only be applied to the property range and geometric set-up for which it was derived, as coefficients may vary greatly for different systems.

## 6.4 Influence of solid precipitates on slag foaming

- Small amounts of magnetite stabilises slag foaming.
- Precipitates of wollastonite and anorthite decreased foaming
- As precipitation of magnetite lowers the slag density and precipitation of wollastonite and anorthite increases the slag density, it is suspected that the liquid density may indicate the positive or negative effect of solid precipitates on slag foaming, unless the magnetite remains suspended.
- The surface structure and interficial tension between the precipitate and the slag also seem to have a significant influence.

## 6.5 Influence of slag basicity on slag foaming

The foam index decreases with increasing basicity due to the lowering of the slag viscosity. This continues until the precipitation of solids starts and the foam index once again increases.

## 6.6 Influence of FeO concentration on slag foaming

For increasing "FeO" concentration the foam index will decrease due to lower viscosity, but higher surface tension depression may lead to increased foam index values at high "FeO" concentrations.

## *6.7 Influence of slag properties on foaming behaviour*

The following conclusions are based on the same empirical model as was used to evaluate foaming of aqueous mixtures.

- Higher foam index values were obtained for slags with lower densities. The empirical relationship observed is $\Sigma \propto \rho^{-\frac{2}{3}}$.
- Higher foam index values were obtained for slags with higher viscosity. The empirical relationship observed is $\Sigma \propto \mu$.
- Higher foam index values were obtained for slags with lower surface tensions. The empirical relationship observed is $\Sigma \propto \sigma^{-1}$.

Models derived for the foaming of basic steelmaking slags does not satisfactorily describe the foaming behaviour of acidic slags.

The physical properties of the slag influence the foam stabilisation mechanism.

In conclusion, it can be said that much is unknown regarding the foaming of non-ferrous slag systems. It is expected that the complex non-Newtonian rheology of the slags still requires further investigation.

# Appendix A.

**Table 6-1. Raw data for determining foam index values**

| Slag No. | Temperature [ C] | Superficial gas velocity [m/s] | Change in liquid depth [m] |
|---|---|---|---|
| 1 | 1225 | 0.02 | 0.025 |
| 1 | 1225 | 0.03 | 0.035 |
| 1 | 1225 | 0.04 | 0.037 |
| 1 | 1200 | 0.02 | 0.029 |
| 1 | 1200 | 0.03 | 0.038 |
| 1 | 1200 | 0.04 | 0.040 |
| 1 | 1175 | 0.02 | 0.044 |
| 1 | 1175 | 0.03 | 0.055 |
| 1 | 1175 | 0.04 | 0.047 |
| 2 | 1190 | 0.01 | 0.045 |
| 2 | 1190 | 0.02 | 0.080 |
| 2 | 1190 | 0.03 | 0.084 |
| 2 | 1165 | 0.01 | 0.018 |
| 2 | 1165 | 0.02 | 0.040 |
| 2 | 1165 | 0.03 | 0.058 |
| 2 | 1140 | 0.01 | 0.065 |
| 2 | 1140 | 0.02 | 0.075 |
| 2 | 1140 | 0.03 | 0.090 |
| 3 | 1190 | 0.01 | 0.157 |
| 3 | 1165 | 0.01 | 0.102 |
| 3 | 1165 | 0.02 | 0.143 |
| 3 | 1140 | 0.01 | 0.092 |
| 4 | 1161 | 0.01 | 0.045 |
| 4 | 1161 | 0.02 | 0.091 |

| | | | |
|---|---|---|---|
| 4 | 1161 | 0.03 | 0.098 |
| 4 | 1136 | 0.01 | 0.071 |
| 4 | 1136 | 0.02 | 0.092 |
| 4 | 1136 | 0.03 | 0.120 |
| 4 | 1111 | 0.01 | 0.092 |
| 4 | 1111 | 0.02 | 0.120 |
| 4 | 1111 | 0.03 | 0.130 |
| 5 | 1350 | 0.006 | 0.094 |
| 5 | 1350 | 0.01 | 0.184 |
| 5 | 1300 | 0.006 | 0.103 |
| 5 | 1300 | 0.01 | 0.151 |
| 5 | 1250 | 0.006 | 0.021 |
| 5 | 1250 | 0.01 | 0.172 |
| 5 | 1225 | 0.01 | 0.028 |
| 5 | 1225 | 0.02 | 0.051 |
| 5 | 1225 | 0.03 | 0.075 |
| 5 | 1200 | 0.01 | 0.027 |
| 5 | 1200 | 0.02 | 0.038 |
| 5 | 1200 | 0.03 | 0.052 |
| 5 | 1175 | 0.01 | 0.038 |
| 5 | 1175 | 0.02 | 0.055 |
| 5 | 1175 | 0.03 | 0.046 |
| 6 | 1225 | 0.01 | 0.104 |
| 6 | 1225 | 0.02 | 0.161 |
| 6 | 1225 | 0.03 | 0.152 |
| 6 | 1175 | 0.01 | 0.080 |
| 6 | 1175 | 0.02 | 0.126 |
| 7 | 1380 | 0.01 | 0.086 |
| 7 | 1365 | 0.01 | 0.083 |
| 7 | 1365 | 0.02 | 0.086 |

| | | | |
|---|---|---|---|
| 7 | 1365 | 0.03 | 0.100 |
| 7 | 1340 | 0.01 | 0.092 |
| 7 | 1340 | 0.02 | 0.096 |
| 7 | 1340 | 0.03 | 0.089 |
| 7 | 1300 | 0.01 | 0.076 |
| 8 | 1400 | 0.01 | 0.100 |
| 8 | 1350 | 0.01 | 0.060 |
| 9 | 1300 | 0.01 | 0.092 |
| 9 | 1300 | 0.013 | 0.117 |
| 10 | 1400 | 0.01 | 0.085 |
| 10 | 1400 | 0.013 | 0.105 |
| 11 | 1400 | 0.01 | 0.046 |
| 11 | 1400 | 0.015 | 0.033 |
| 11 | 1400 | 0.02 | 0.113 |

**Table 6-2. Summary for FactSage results to determine the amount of solid precipitation. Base of 100g slag used**

| | | Liquid Phase | Solid Phase | | | | |
|---|---|---|---|---|---|---|---|
| Slag | Temperature | Slag | $Fe_3O4$ | $FeSiO_3$ | $CaSiO_3$ | $CaAl_2Si_2O_8$ | Total solids |
| - | [?C] | [g] | [g] | [g] | [g] | [g] | [g] |
| 1 | 1175 | 97.8 | 2.21 | 0.00 | 0.00 | 0.00 | 2.2 |
| 1 | 1200 | 98.3 | 1.66 | 0.00 | 0.00 | 0.00 | 1.7 |
| 1 | 1225 | 99.0 | 0.96 | 0.00 | 0.00 | 0.00 | 1.0 |
| 2 | 1140 | 98.5 | 1.48 | 0.00 | 0.00 | 0.00 | 1.5 |
| 2 | 1165 | 98.9 | 1.10 | 0.00 | 0.00 | 0.00 | 1.1 |
| 2 | 1190 | 99.4 | 0.62 | 0.00 | 0.00 | 0.00 | 0.6 |
| 3 | 1140 | 60.1 | 5.32 | 1.35 | 33.27 | 0.00 | 39.9 |
| 3 | 1165 | 66.4 | 4.52 | 0.99 | 28.10 | 0.00 | 33.6 |
| 3 | 1190 | 75.1 | 3.34 | 0.00 | 21.57 | 0.00 | 24.9 |
| 4 | 1111 | 94.4 | 5.55 | 0.00 | 0.00 | 0.00 | 5.6 |
| 4 | 1136 | 94.8 | 5.19 | 0.00 | 0.00 | 0.00 | 5.2 |
| 4 | 1161 | 95.3 | 4.74 | 0.00 | 0.00 | 0.00 | 4.7 |
| 5 | 1175 | 78.5 | 5.13 | 0.00 | 0.00 | 16.42 | 21.5 |
| 5 | 1200 | 81.6 | 4.92 | 0.00 | 0.00 | 13.52 | 18.4 |
| 5 | 1225 | 85.2 | 4.64 | 0.00 | 0.00 | 10.16 | 14.8 |
| 5 | 1250 | 89.6 | 4.23 | 0.00 | 0.00 | 6.19 | 10.4 |

## *A.1 Model 1 – Statistics*

See Section 5.6.1

Model1B = log(Π2)

Model1A = log(Π1)

**Model Summary[a,b]**

| | Variables | | | | | |
|---|---|---|---|---|---|---|
| Model | Entered | Removed | R | R Square | Adjusted R Square | Std. Error of the Estimate |
| 1 | MODEL1A[c,d] | . | .507 | .257 | .229 | .9659 |

a. Dependent Variable: MODEL1B

b. Method: Enter

c. Independent Variables: (Constant), MODEL1A

d. All requested variables entered.

**ANOVA[a]**

| Model | | Sum of Squares | df | Mean Square | F | Sig. |
|---|---|---|---|---|---|---|
| 1 | Regression | 8.408 | 1 | 8.408 | 9.011 | .006[b] |
| | Residual | 24.258 | 26 | .933 | | |
| | Total | 32.666 | 27 | | | |

a. Dependent Variable: MODEL1B

b. Independent Variables: (Constant), MODEL1A

**Coefficients[a]**

| Model | | t | 95% Confidence Interval for B | | Collinearity Statistics | |
|---|---|---|---|---|---|---|
| | | | Lower Bound | Upper Bound | Tolerance | VIF |
| 1 | (Constant) | 2.121 | .088 | 5.603 | | |
| | MODEL1A | -3.002 | -2.512 | -.470 | 1.000 | 1.000 |

a. Dependent Variable: MODEL1B

## A.2 Model 2- Statistics

See Section 5.6.2

Model2B = log(Π2)

Model2A = log(Π1)

Model2C = log(Π3)

**Model Summary[a,b]**

| Model | Variables | | R | R Square | Adjusted R Square | Std. Error of the Estimate |
|---|---|---|---|---|---|---|
| | Entered | Removed | | | | |
| 1 | MODEL2C, MODEL2B[c,d] | . | .607 | .369 | .319 | .3090 |

a. Dependent Variable: MODEL2A

b. Method: Enter

c. Independent Variables: (Constant), MODEL2C, MODEL2B

d. All requested variables entered.

**ANOVA[a]**

| Model | | Sum of Squares | df | Mean Square | F | Sig. |
|---|---|---|---|---|---|---|
| 1 | Regression | 1.396 | 2 | .698 | 7.309 | .003[b] |
| | Residual | 2.387 | 25 | 9.5E-02 | | |
| | Total | 3.783 | 27 | | | |

a. Dependent Variable: MODEL2A

b. Independent Variables: (Constant), MODEL2C, MODEL2B

**Coefficients[a]**

| Model | | Unstandardized Coefficients | | Standardized Coefficients | t | Sig. | 95% Confidence Interval for B | | Collinearity Statistics | |
|---|---|---|---|---|---|---|---|---|---|---|
| | | B | Std. Error | Beta | | | Lower Bound | Upper Bound | Tolerance | VIF |
| 1 | (Constant) | 16.990 | 6.902 | | 2.462 | .021 | 2.775 | 31.206 | | |
| | MODEL2B | 3.712 | 1.848 | 10.907 | 2.008 | .056 | -.094 | 7.518 | .001 | 1168.434 |
| | MODEL2C | -7.725 | 3.674 | -11.419 | -2.103 | .046 | -15.291 | -.159 | .001 | 1168.434 |

a. Dependent Variable: MODEL2A

## *A.3 Model3 - Statistics*

See Section 5.6.3

Model3B = log(Number 2)

Model3A = log(Number 1)

**Model Summary[a,b]**

| Model | Variables Entered | Variables Removed | R | R Square | Adjusted R Square | Std. Error of the Estimate |
|---|---|---|---|---|---|---|
| 1 | MODEL3A[c,d] | . | .638 | .407 | .384 | 3.37E-02 |

a. Dependent Variable: MODEL3B

b. Method: Enter

c. Independent Variables: (Constant), MODEL3A

d. All requested variables entered.

**ANOVA[a]**

| Model | | Sum of Squares | df | Mean Square | F | Sig. |
|---|---|---|---|---|---|---|
| 1 | Regression | 2.0E-02 | 1 | 2.0E-02 | 17.864 | .000[b] |
| | Residual | 2.9E-02 | 26 | 1.1E-03 | | |
| | Total | 5.0E-02 | 27 | | | |

a. Dependent Variable: MODEL3B

b. Independent Variables: (Constant), MODEL3A

**Coefficients[a]**

| Model | | Unstandardized Coefficients | | Standardized Coefficients | t | Sig. | 95% Confidence Interval for B | |
|---|---|---|---|---|---|---|---|---|
| | | B | Std. Error | Beta | | | Lower Bound | Upper Bound |
| 1 | (Constant) | -1.744 | .015 | | -118.695 | .000 | -1.774 | -1.714 |
| | MODEL3A | 5.4E-02 | .013 | .638 | 4.227 | .000 | .028 | .080 |

a. Dependent Variable: MODEL3B

# Appendix B. Physical modelling of foaming data

## B.1 Determining the average foam index

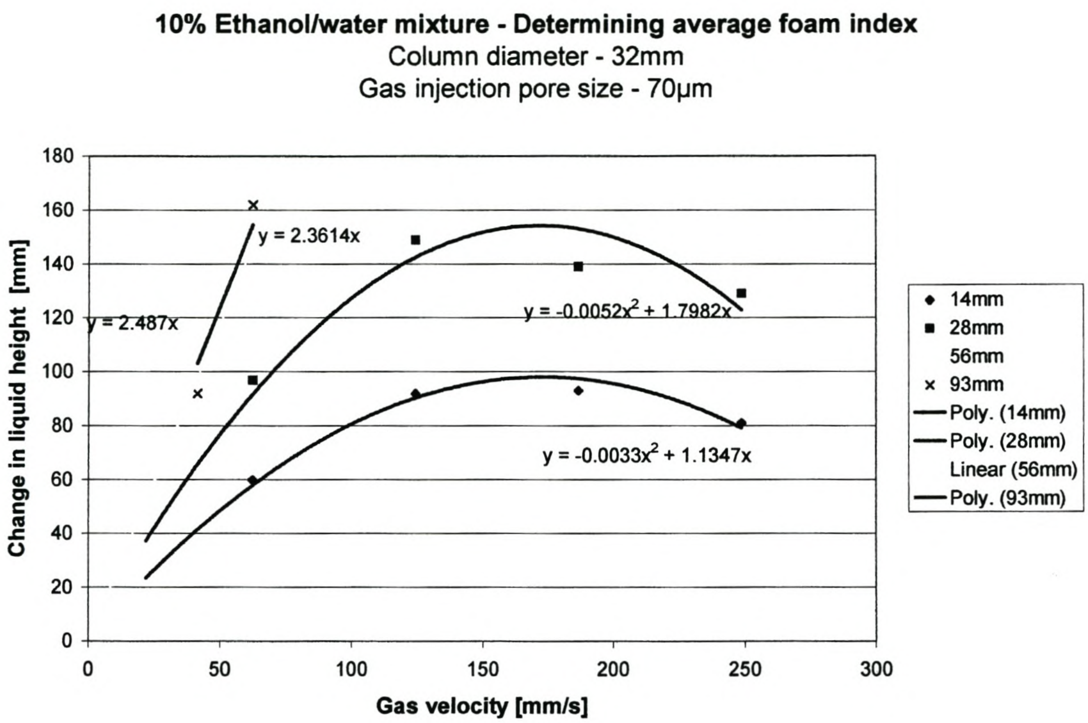


Appendix B. Figure 1

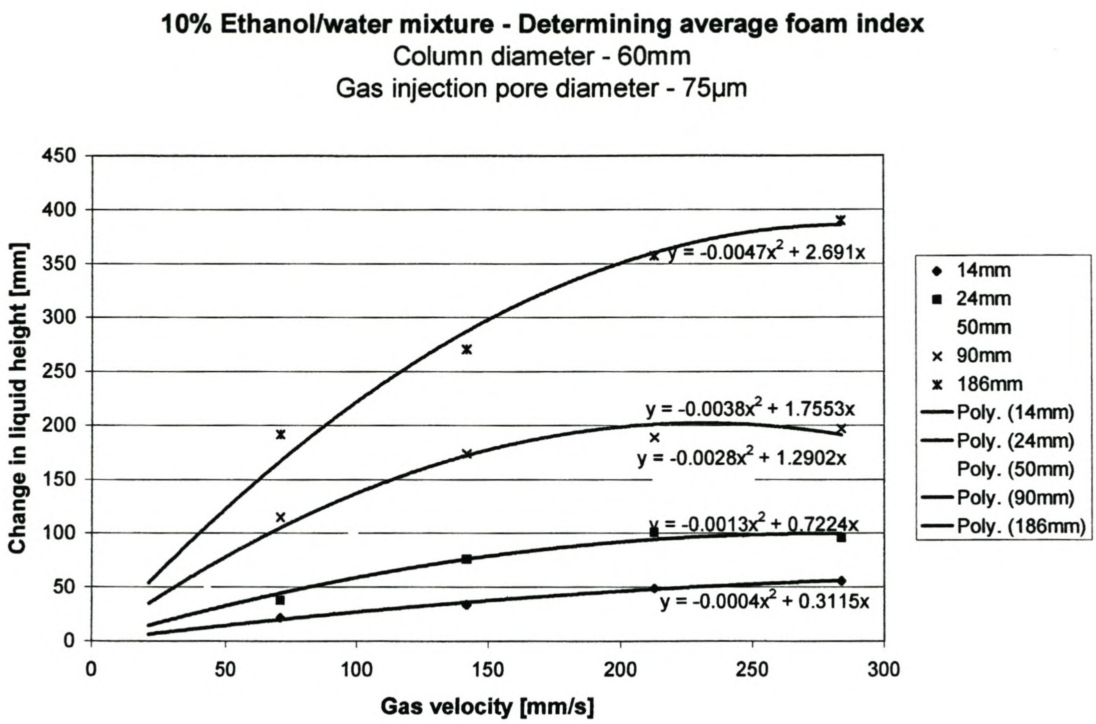


**Appendix B. Figure 2**

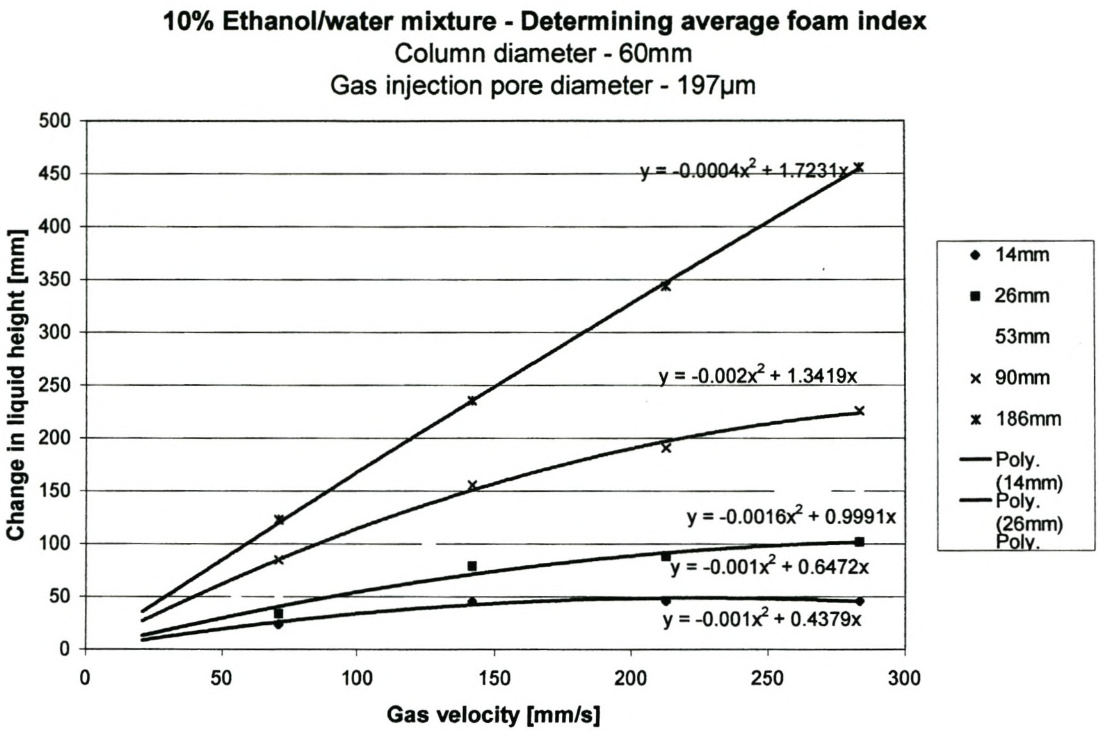


**Appendix B. Figure 3**

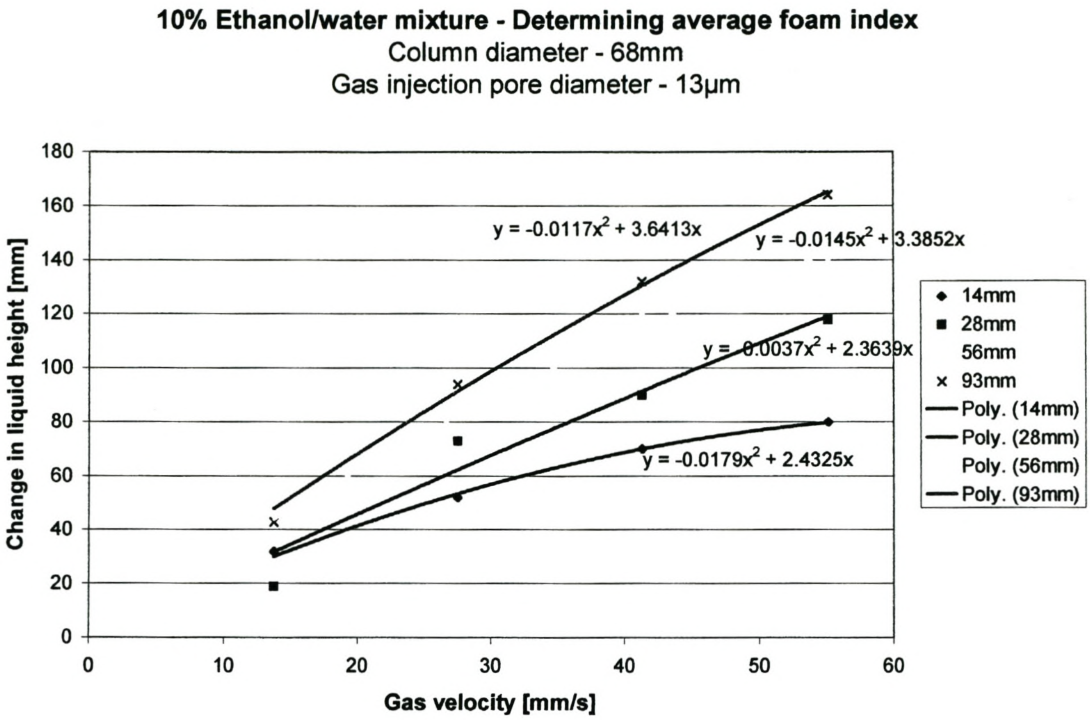


**Appendix B. Figure 4**

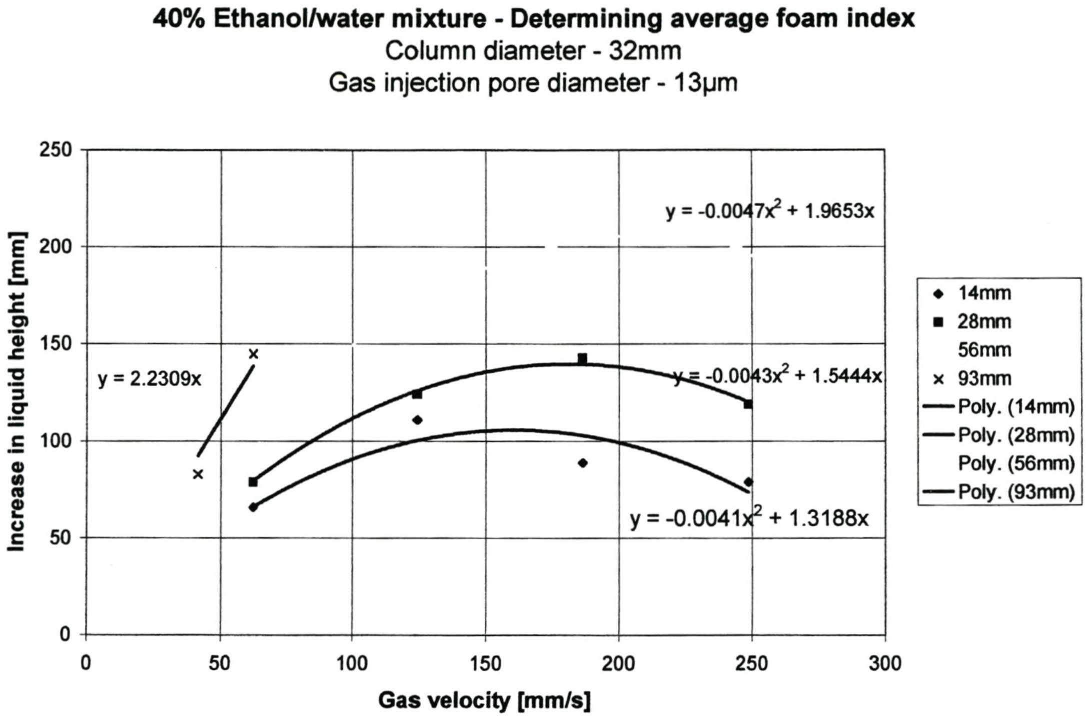


**Appendix B. Figure 5**

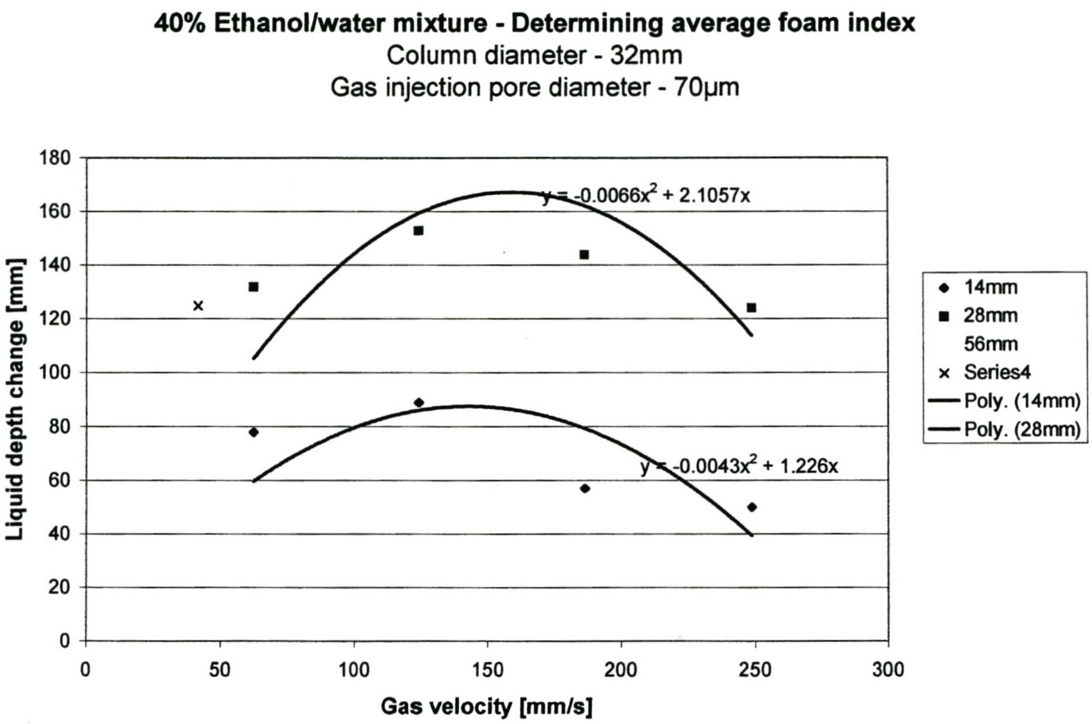


**Appendix B. Figure 6**

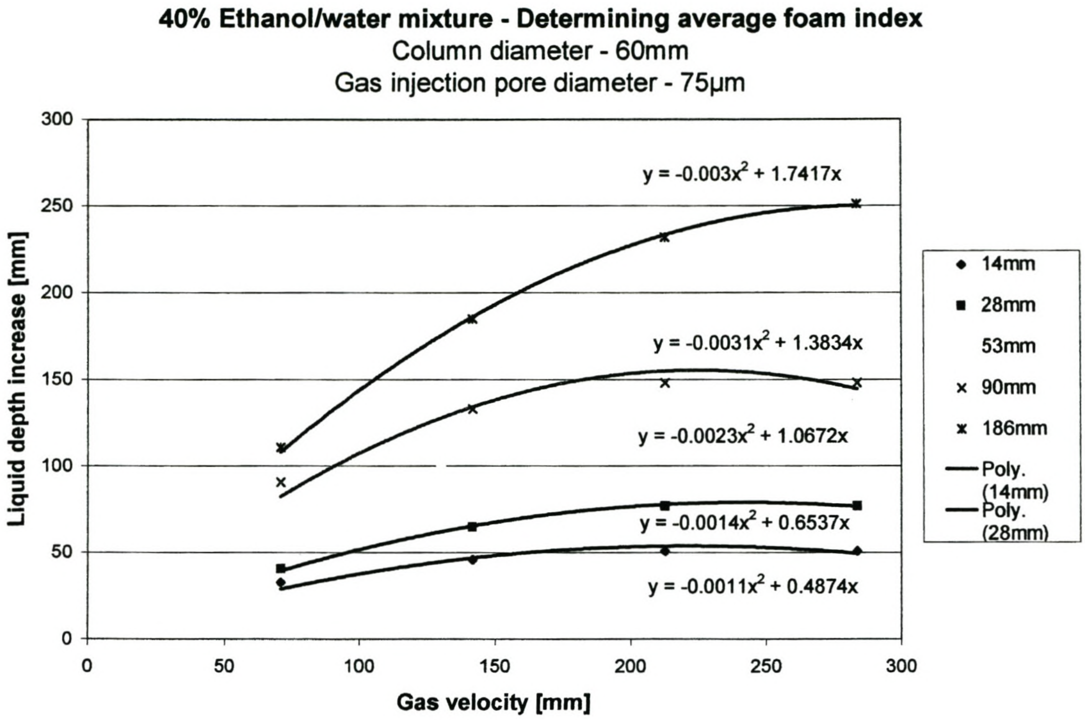


**Appendix B. Figure 7**

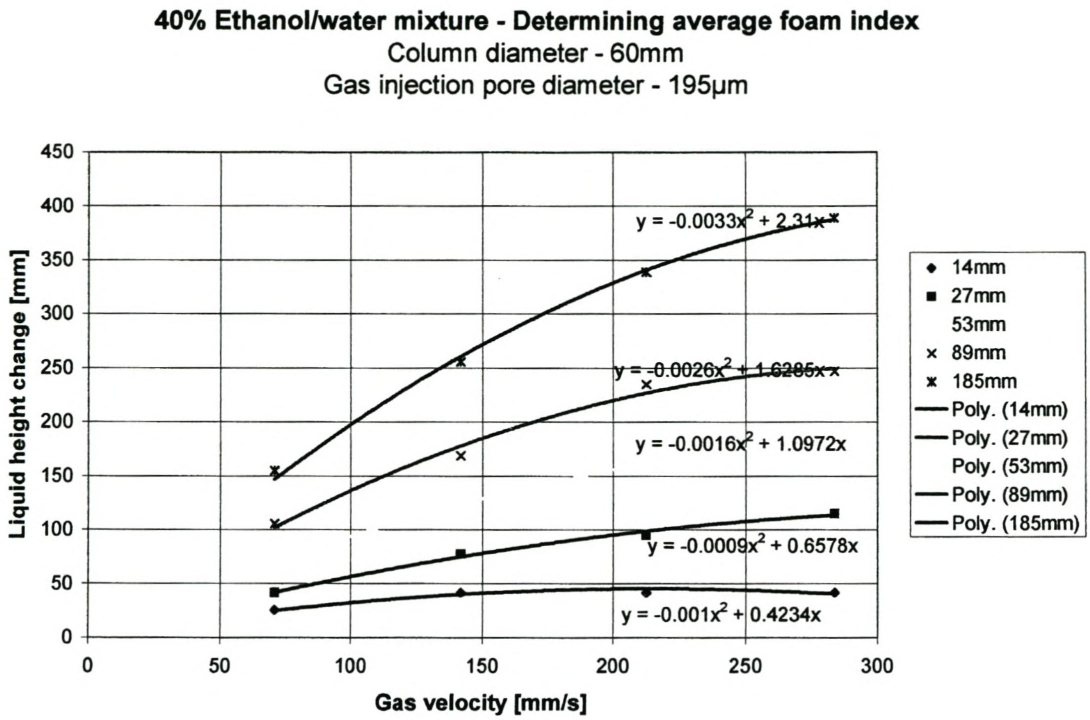


**Appendix B. Figure 8**

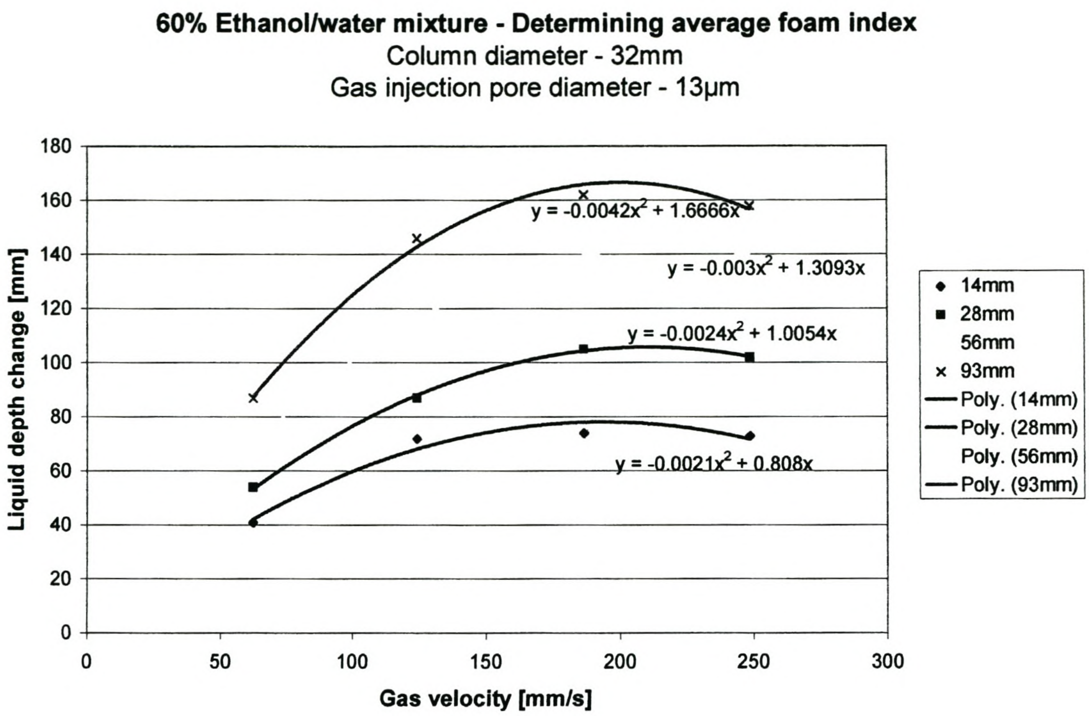


**Appendix B. Figure 9**

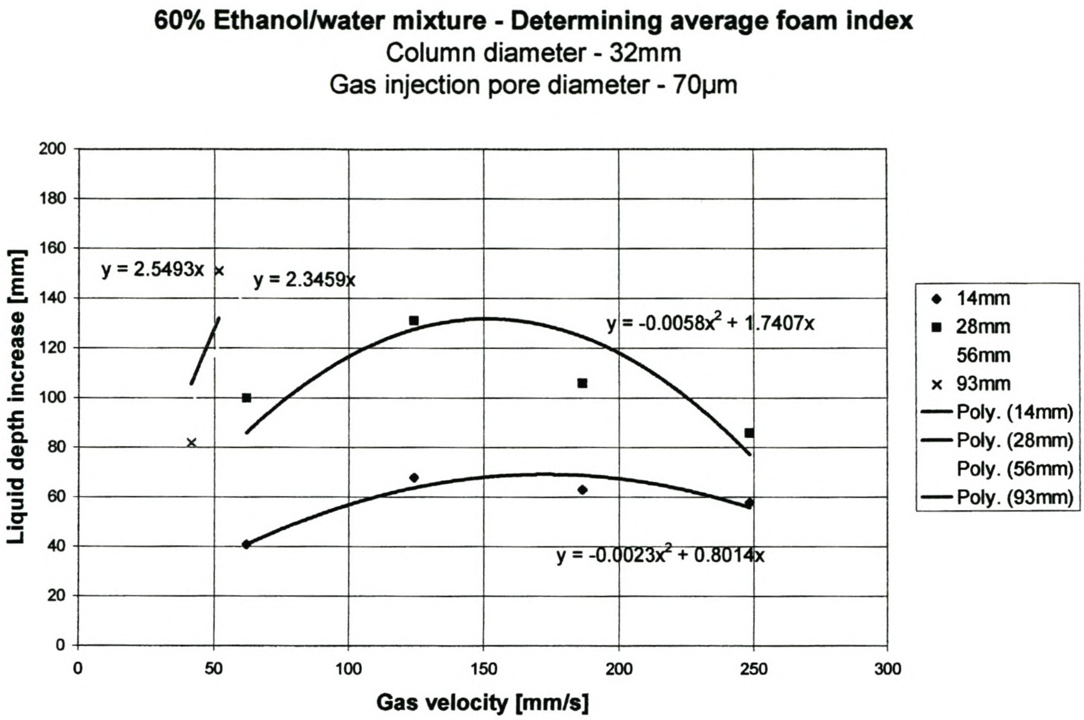


**Appendix B. Figure 10**

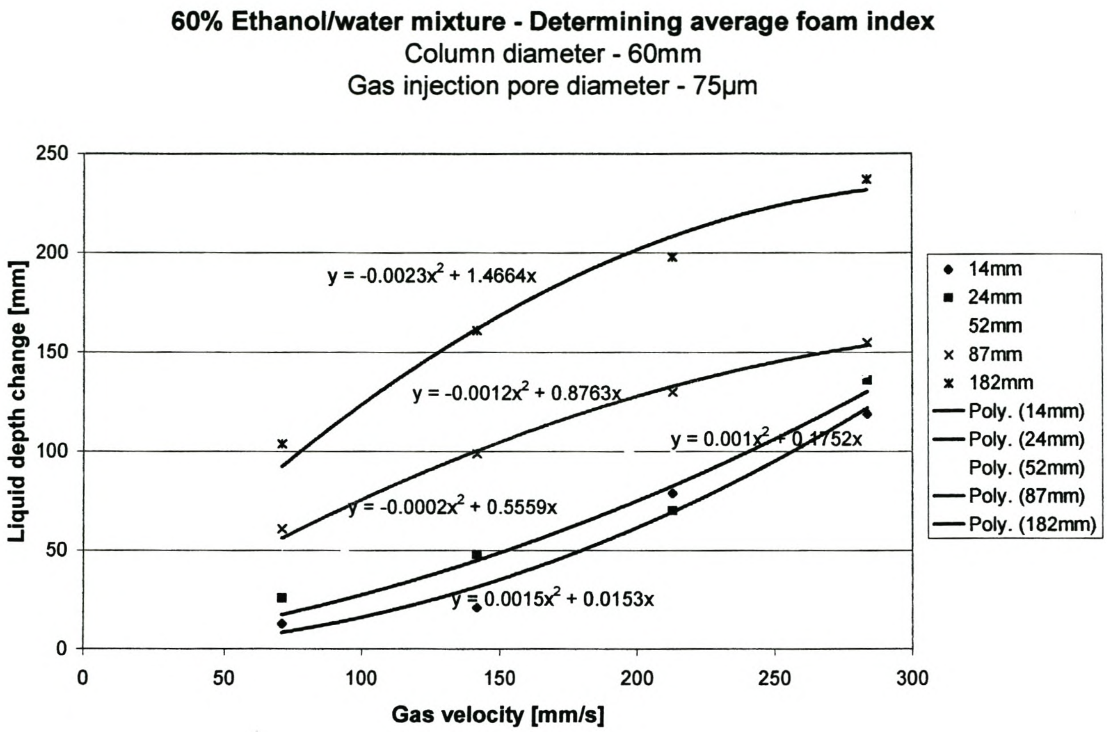


**Appendix B. Figure 11**

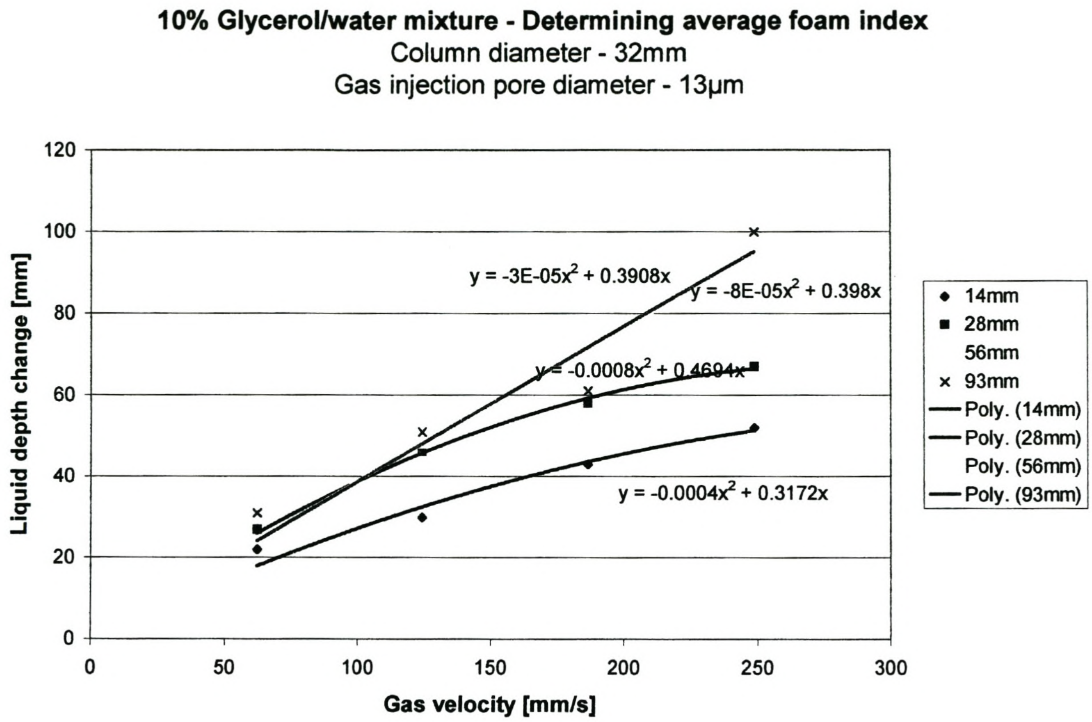


**Appendix B. Figure 12**

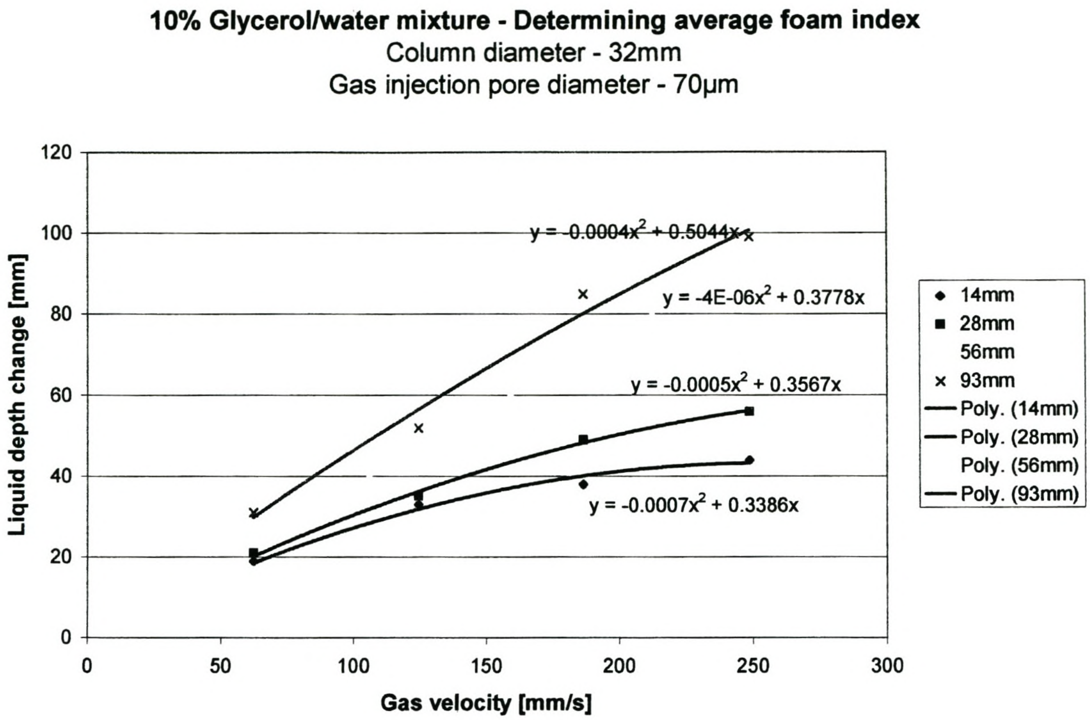


**Appendix B. Figure 13**

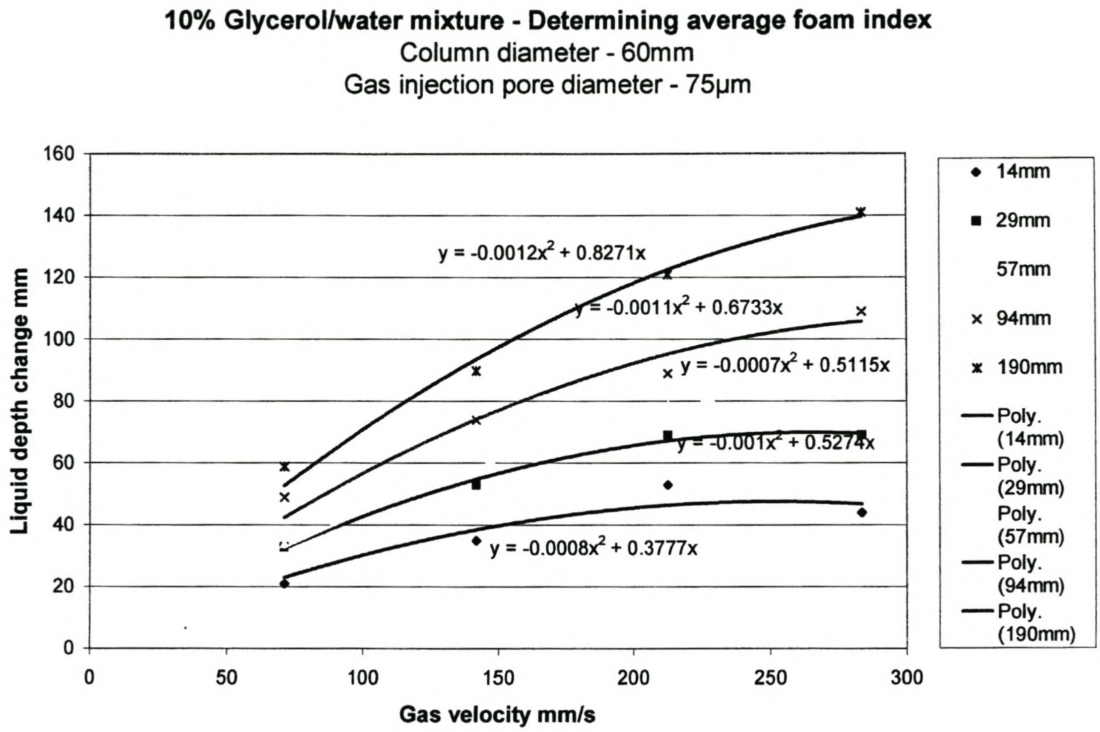


**Appendix B. Figure 14**

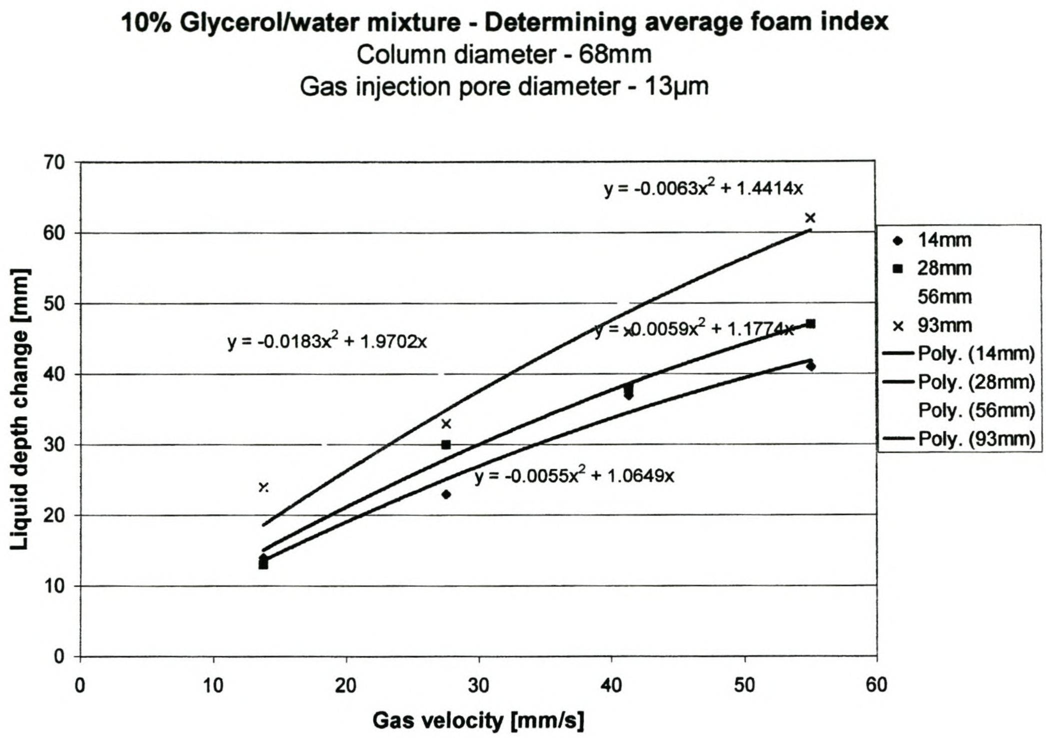


**Appendix B. Figure 15**

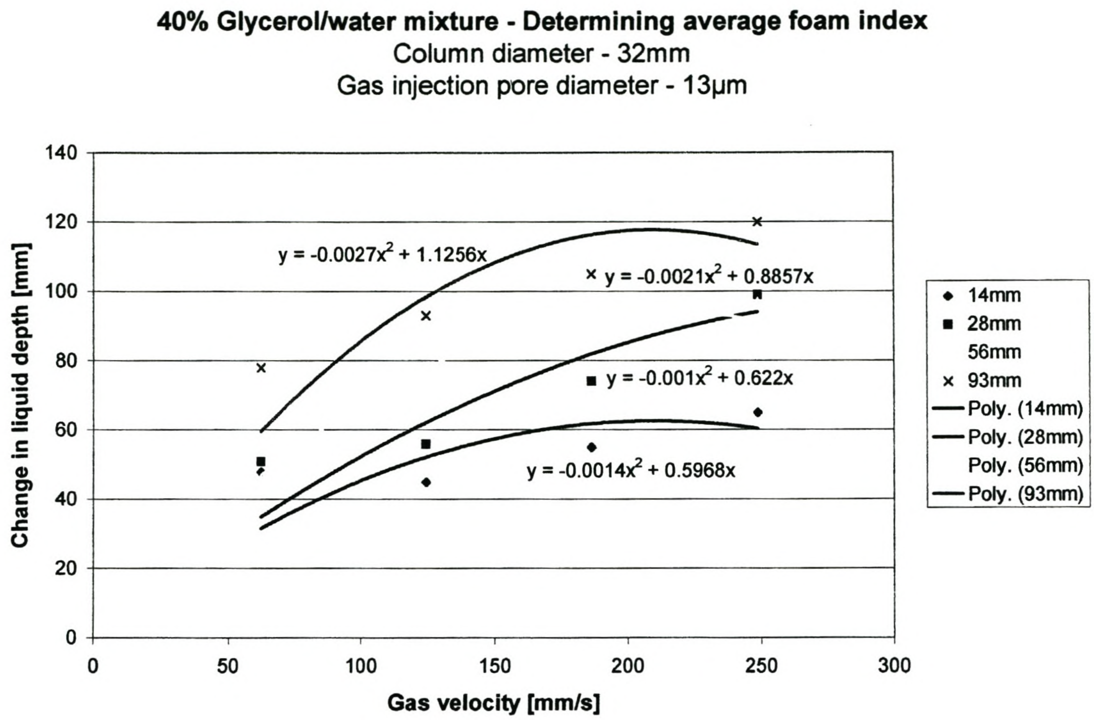


**Appendix B. Figure 16**

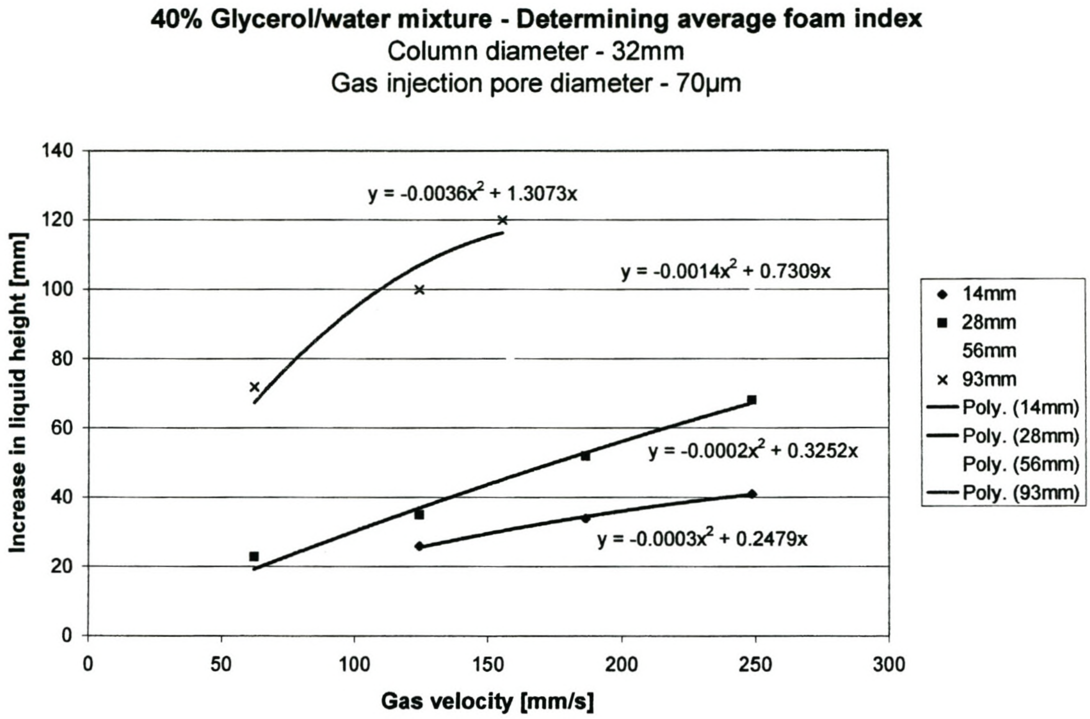


**Appendix B. Figure 17**

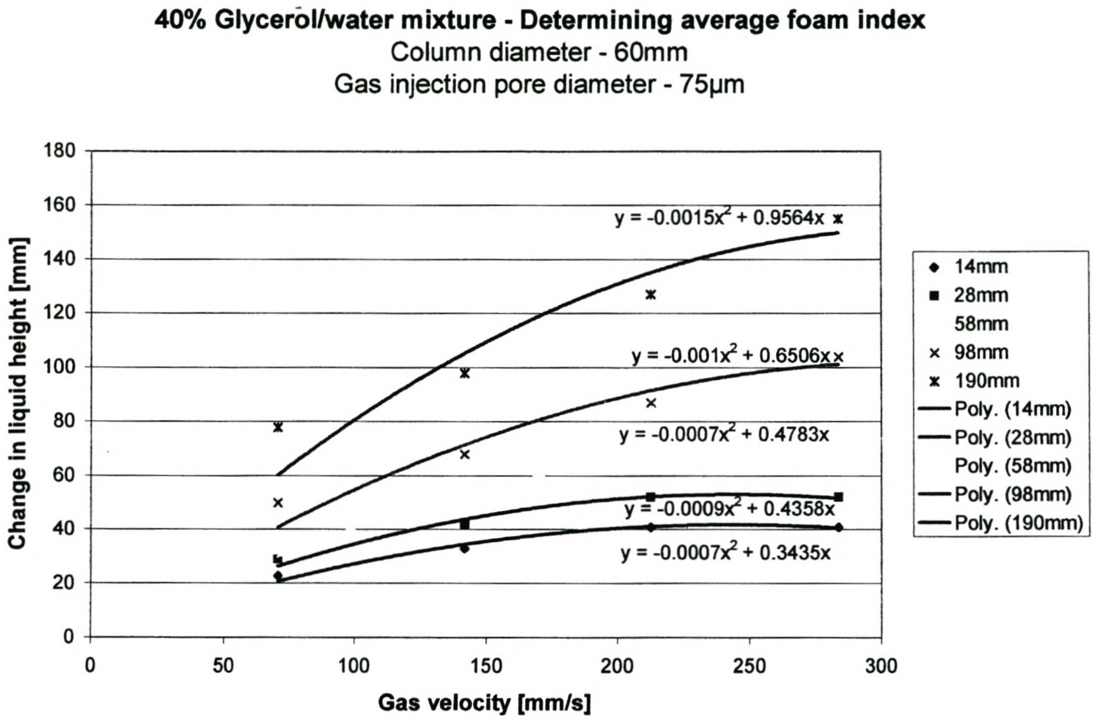


**Appendix B. Figure 18**

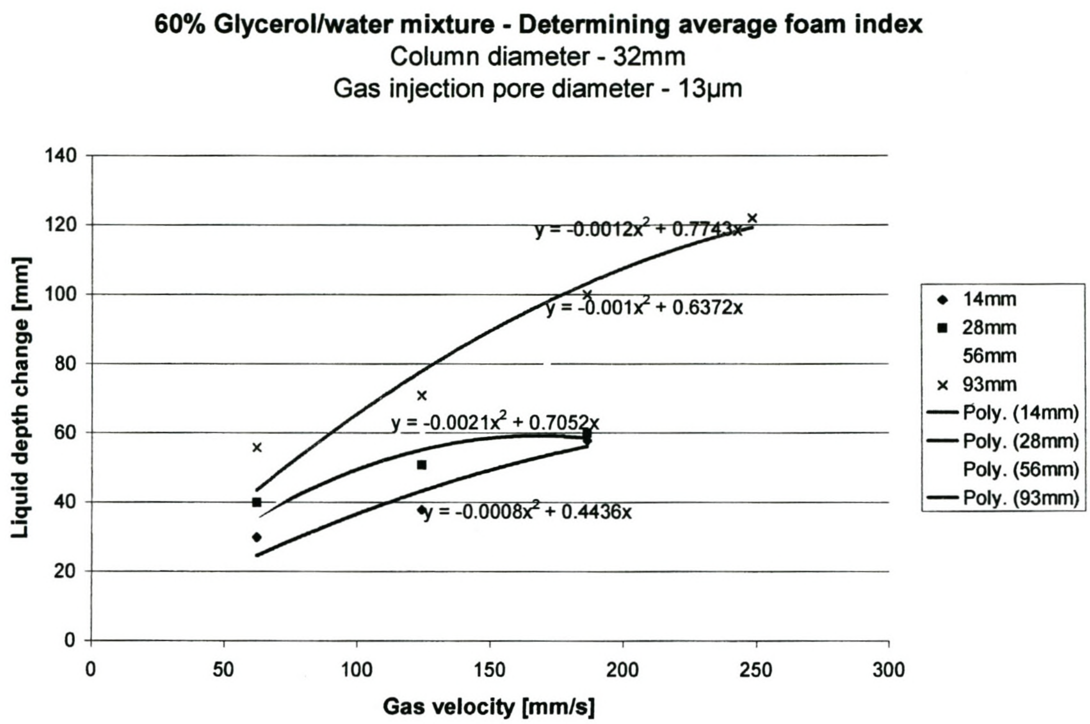


**Appendix B. Figure 19**

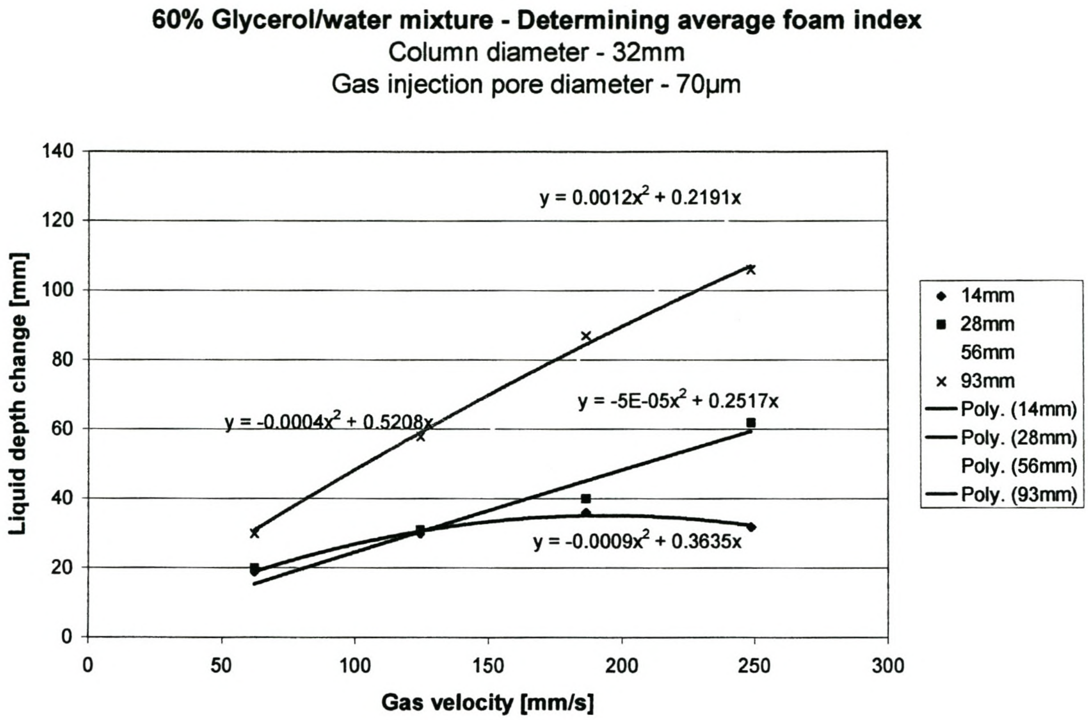


**Appendix B. Figure 20**

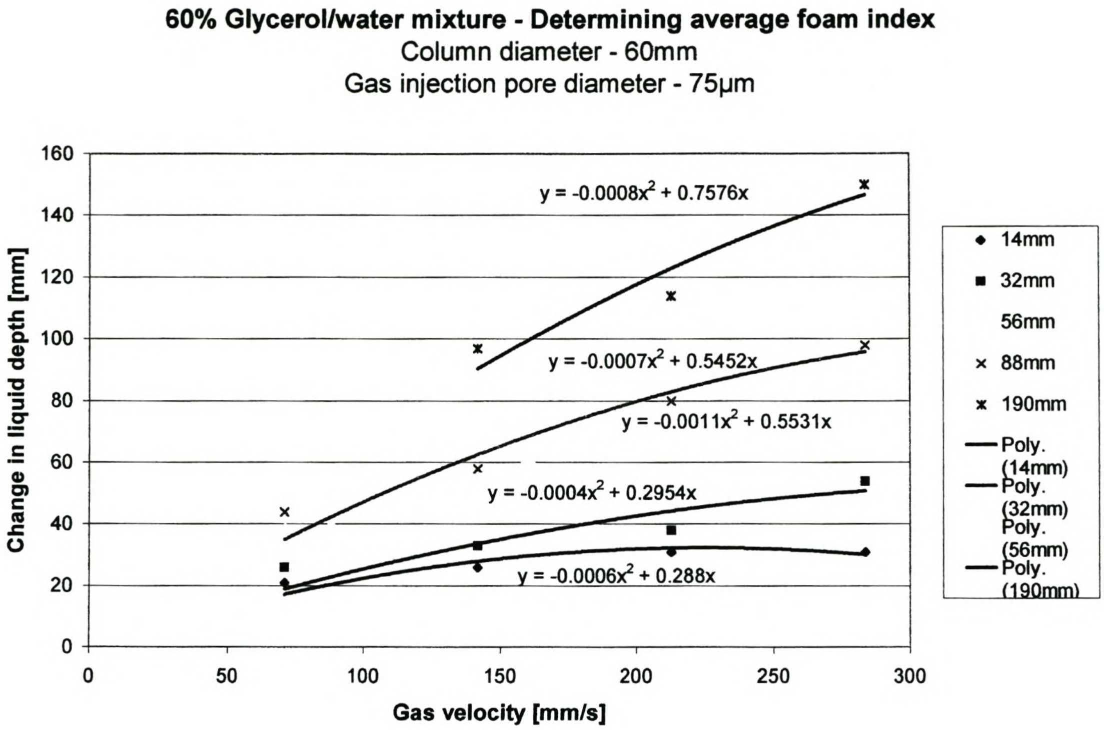


**Appendix B. Figure 21**

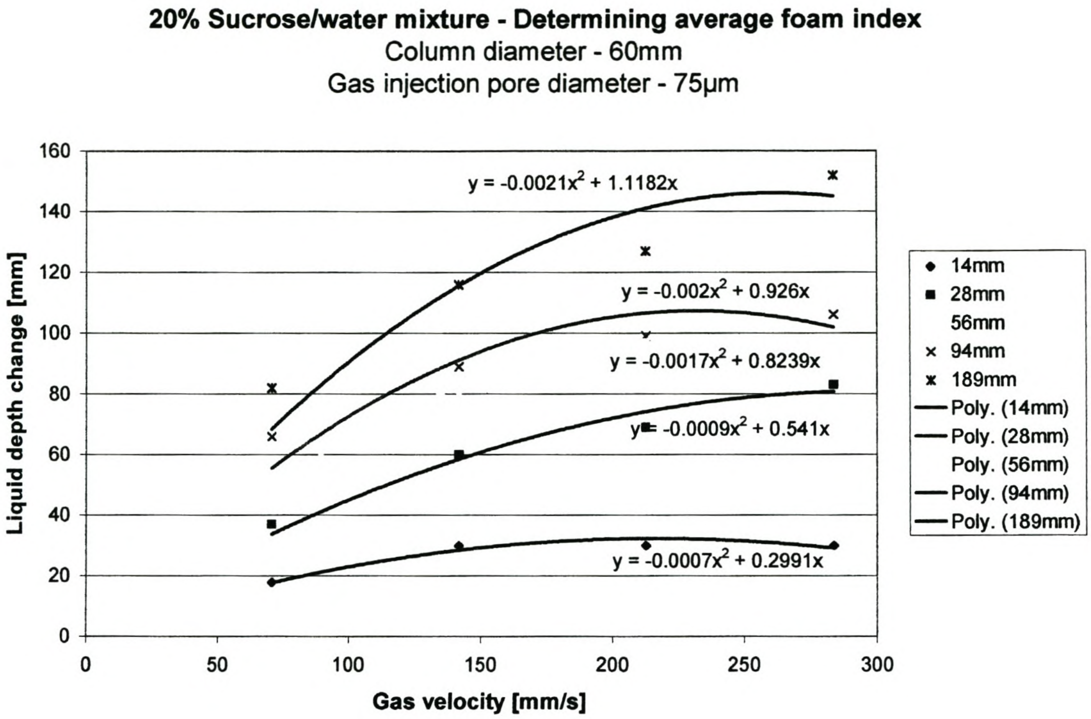


**Appendix B. Figure 22**

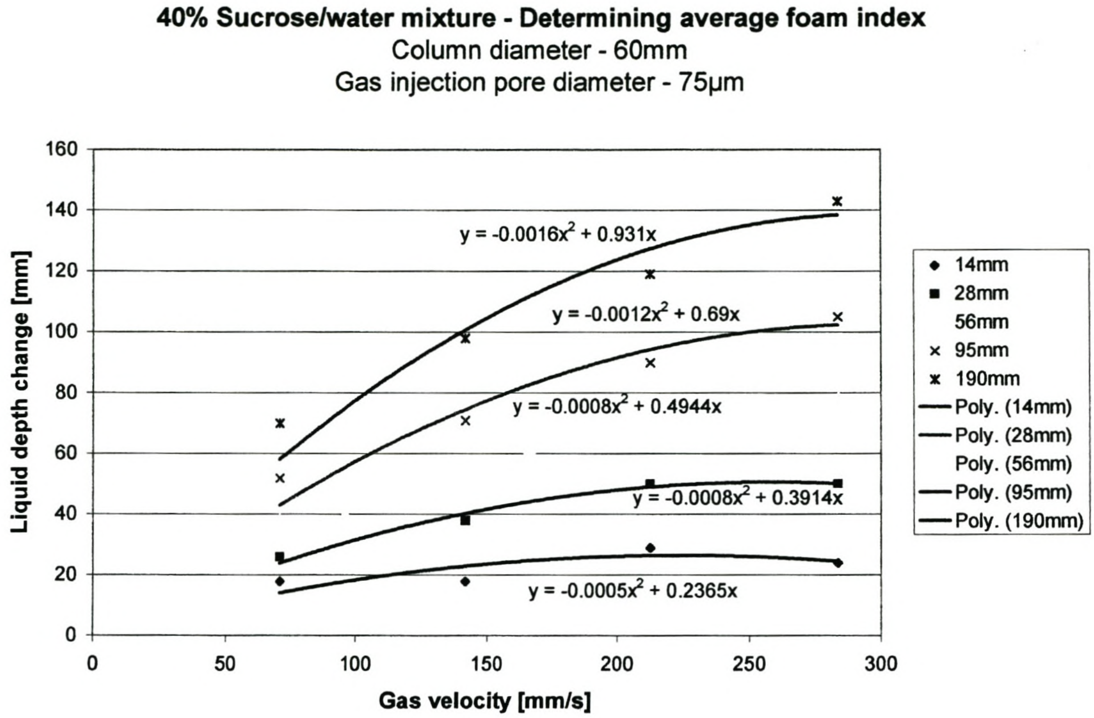


**Appendix B. Figure 23**

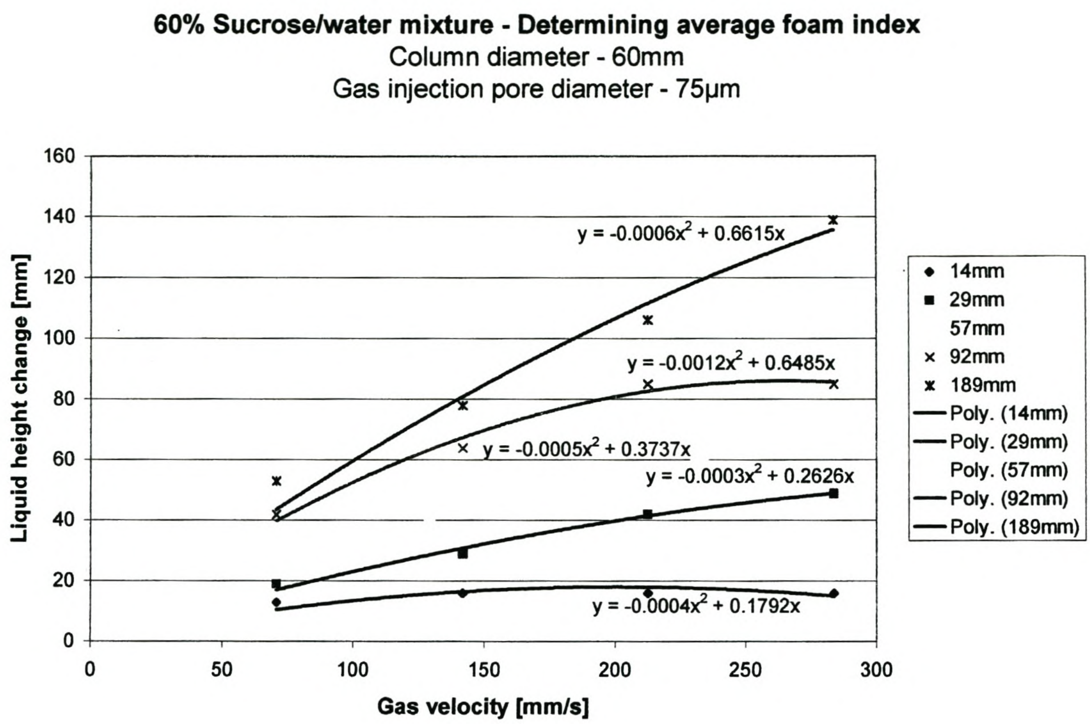


**Appendix B. Figure 24**

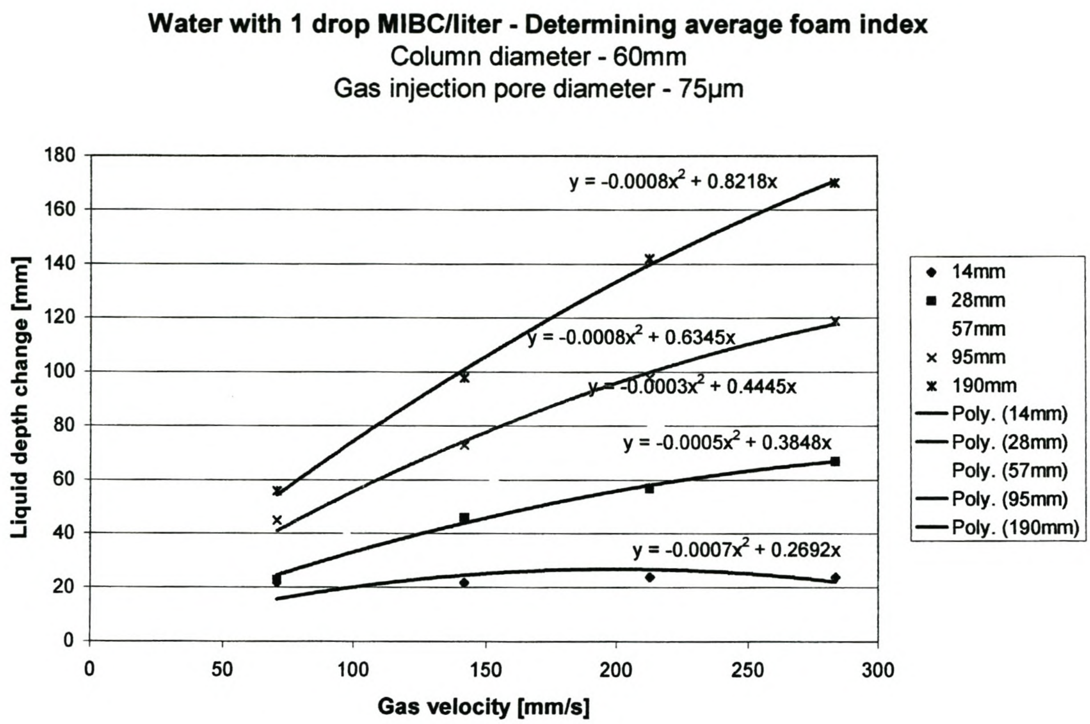


**Appendix B. Figure 25**

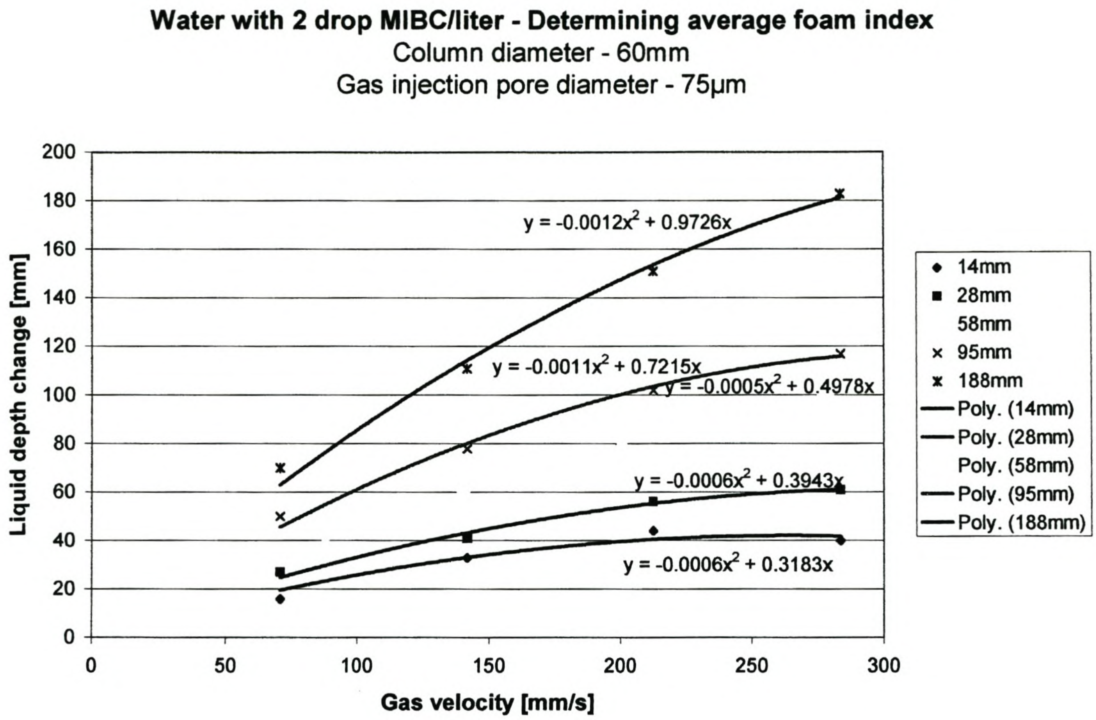


**Appendix B. Figure 26**

## *B.2 40% Glycerol-water mixture – Influence of initial liquid depth on the foam index*

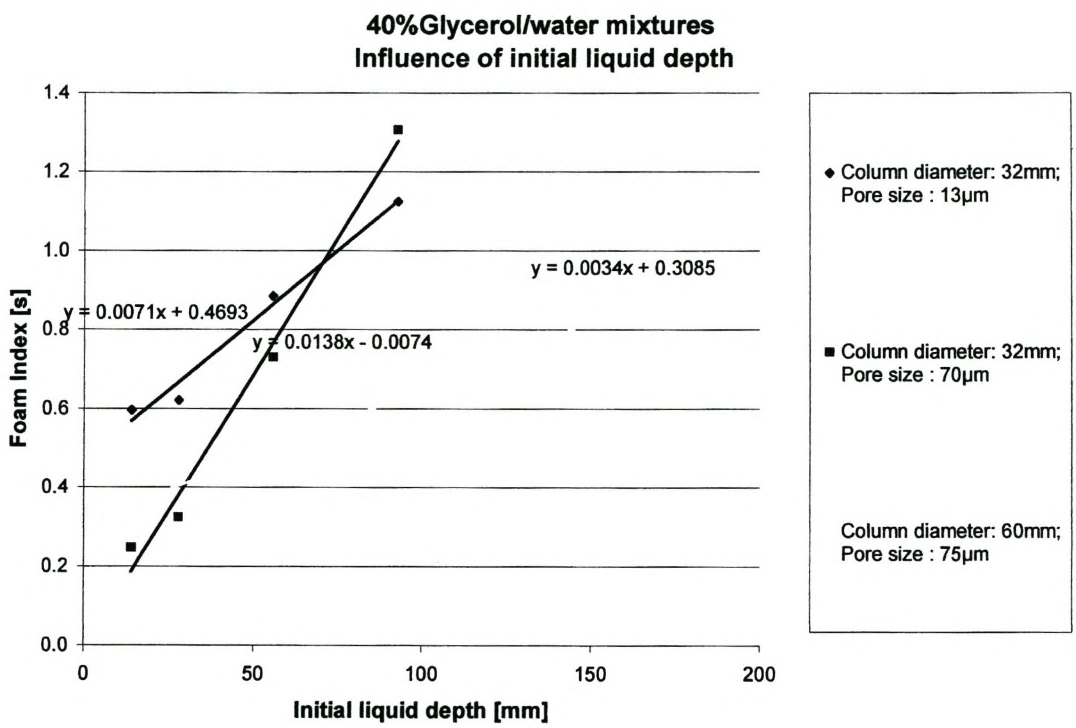


**Appendix B. Figure 27**

## *B.3 Influence of solid particles on foaming behaviour of liquids*

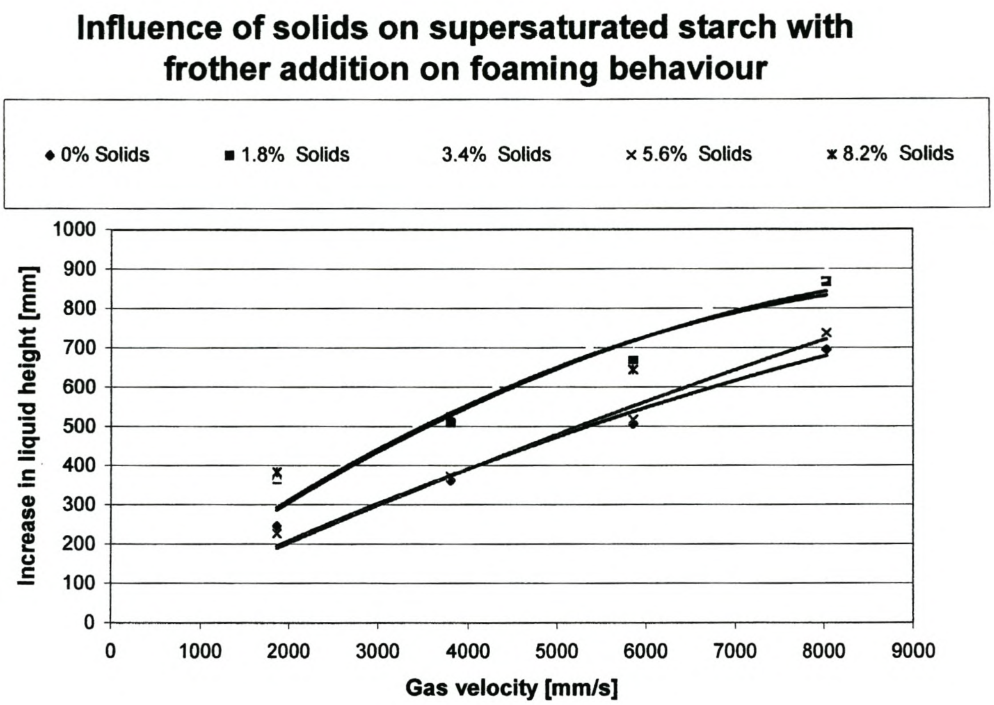


**Appendix B. Figure 28**

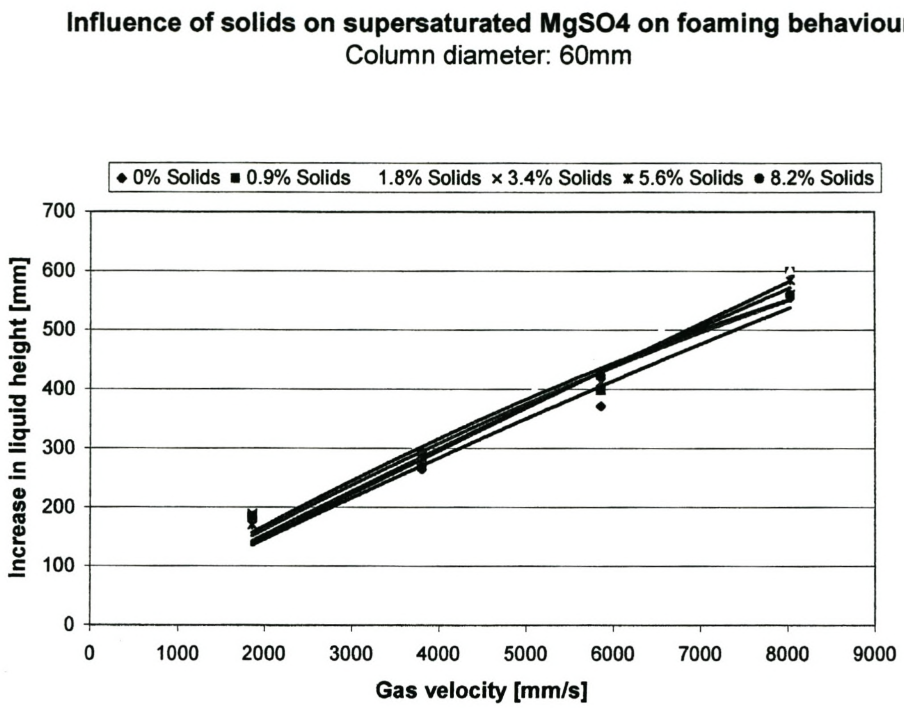


**Appendix B. Figure 29**

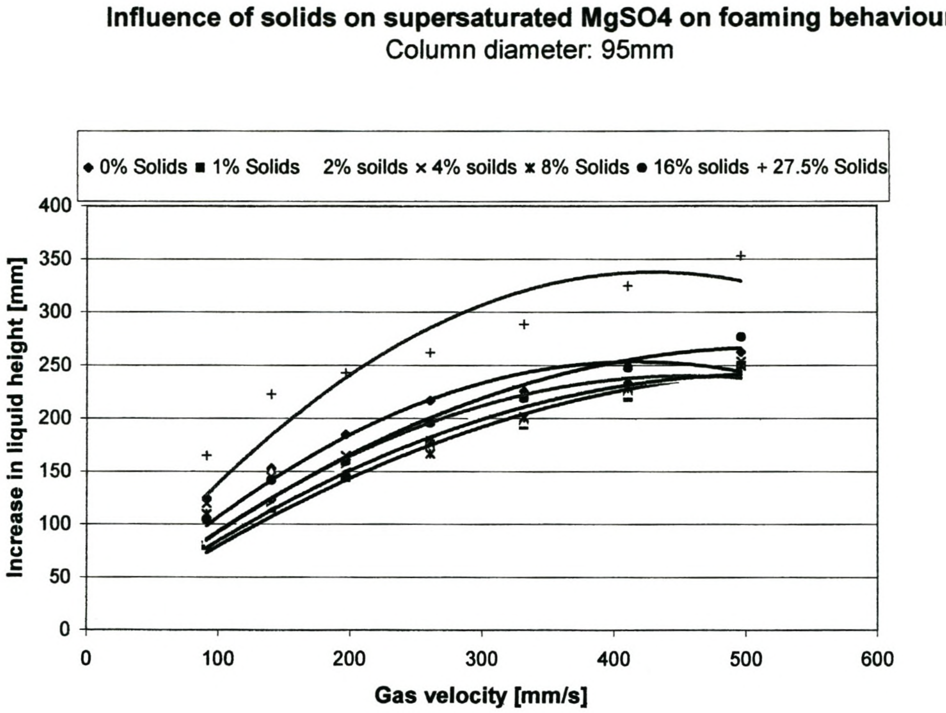


**Appendix B. Figure 30**

## B.4 Dimensionless analysis of foaming data

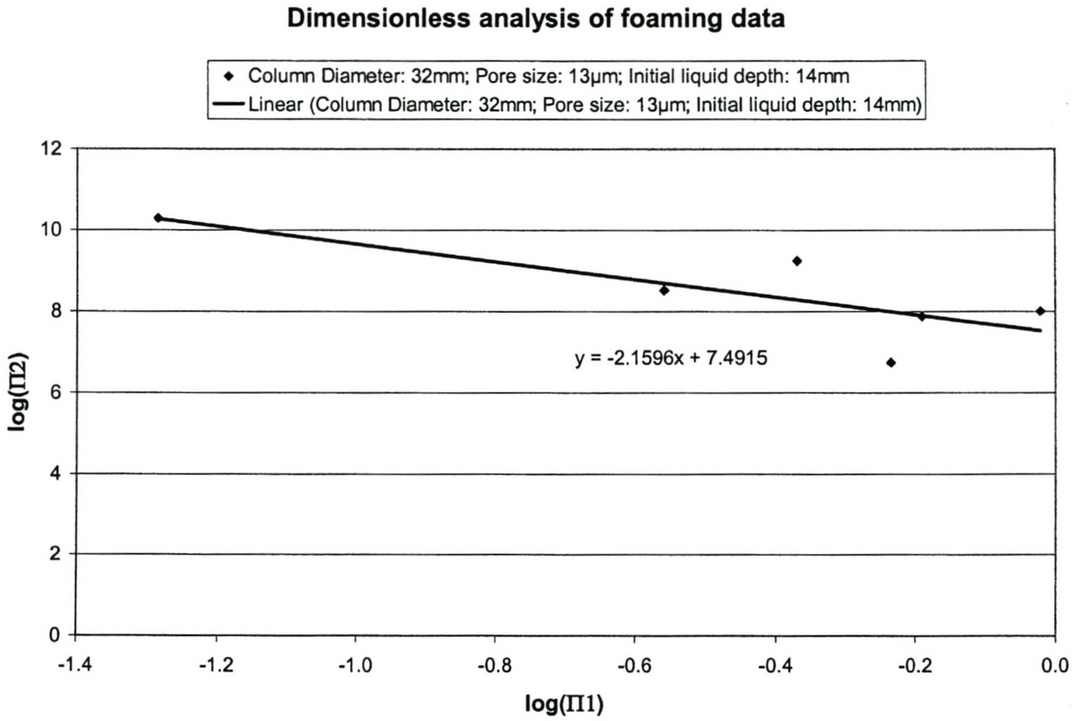


**Appendix B. Figure 31**

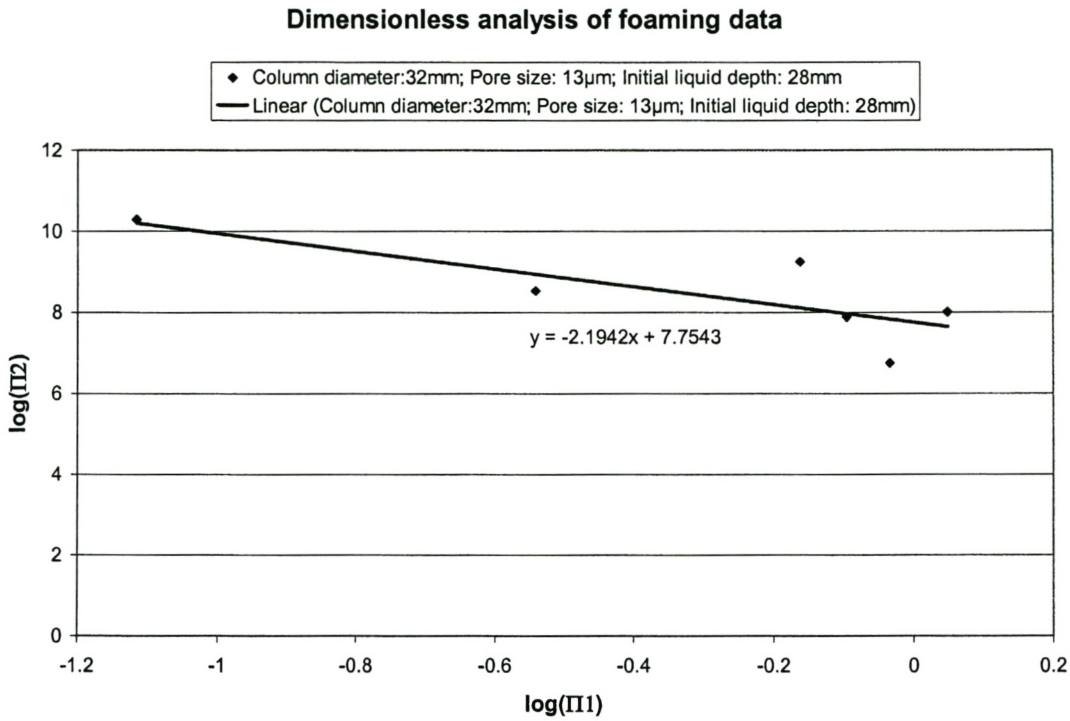


**Appendix B. Figure 32**

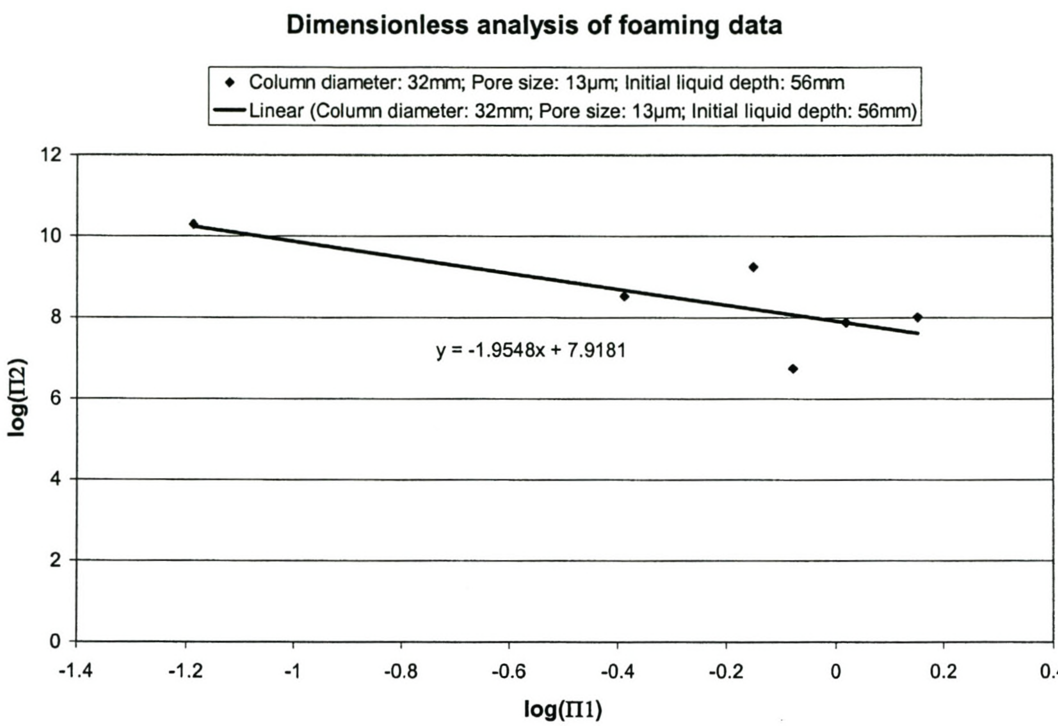


**Appendix B. Figure 33**

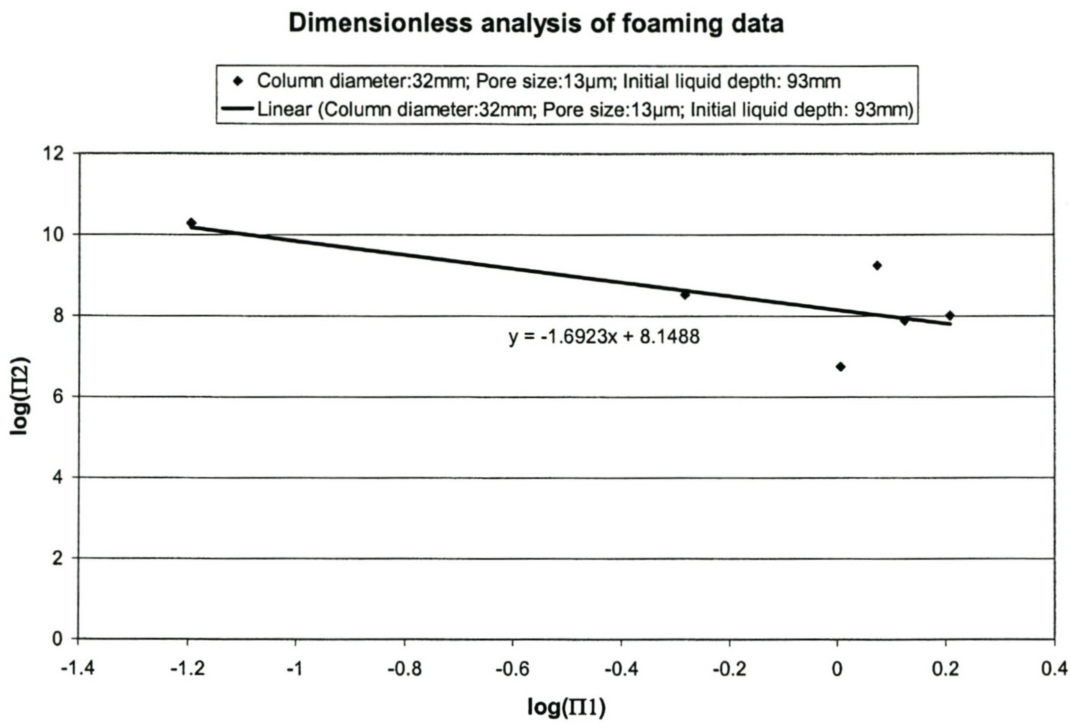


**Appendix B. Figure 34**

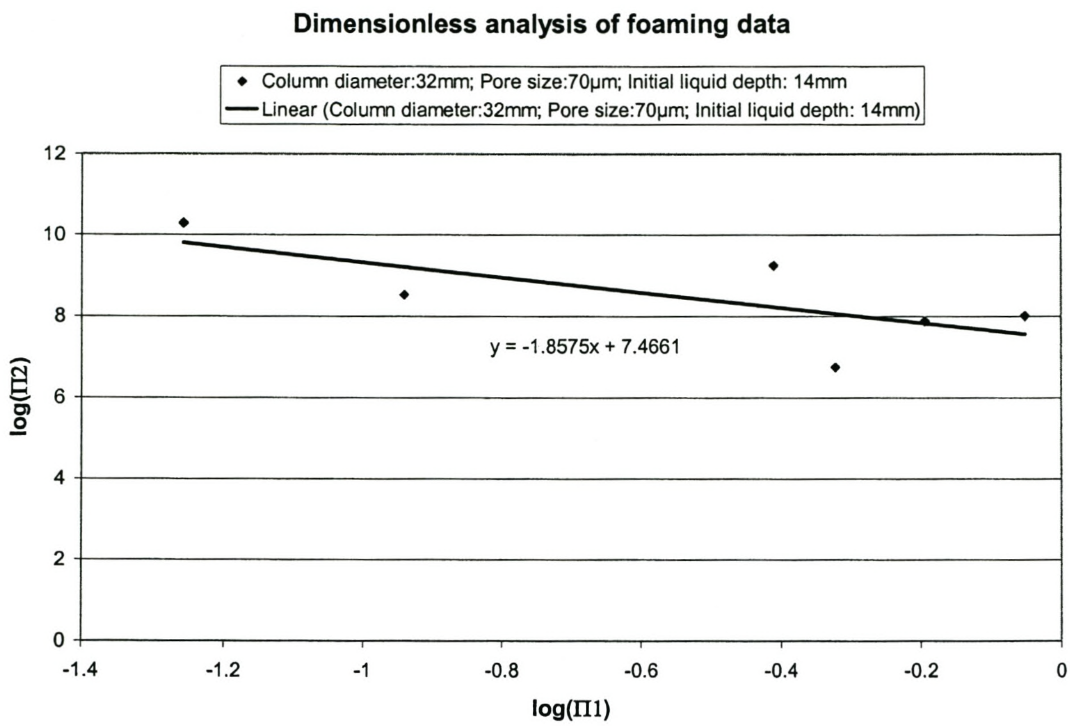


**Appendix B. Figure 35**

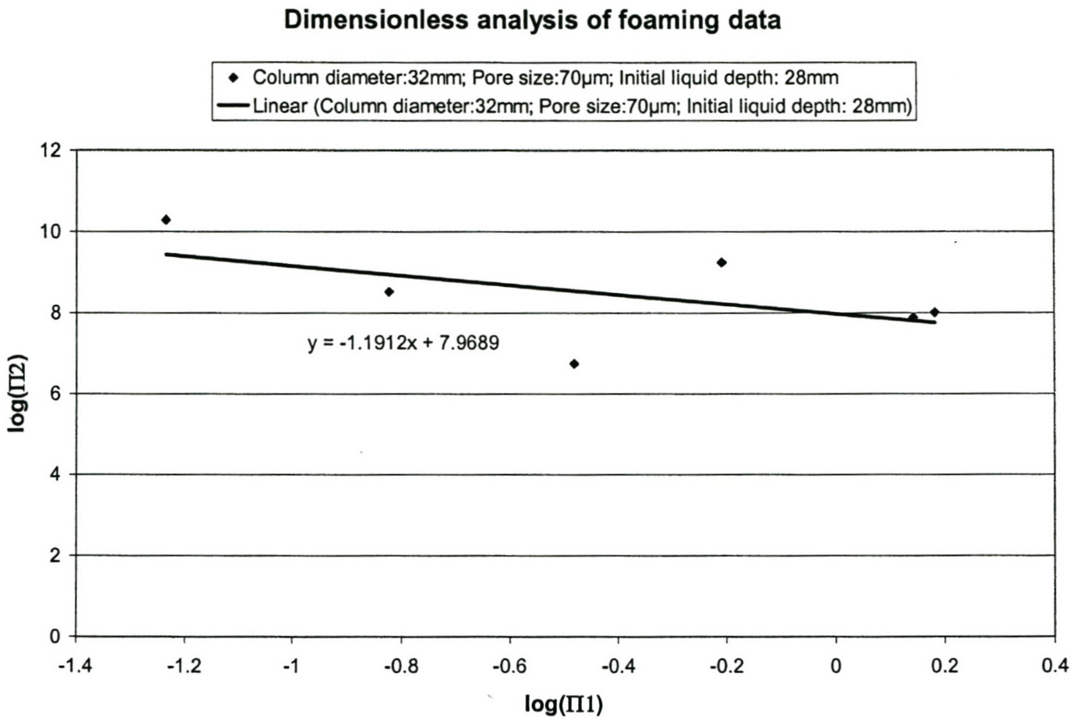


**Appendix B. Figure 36**

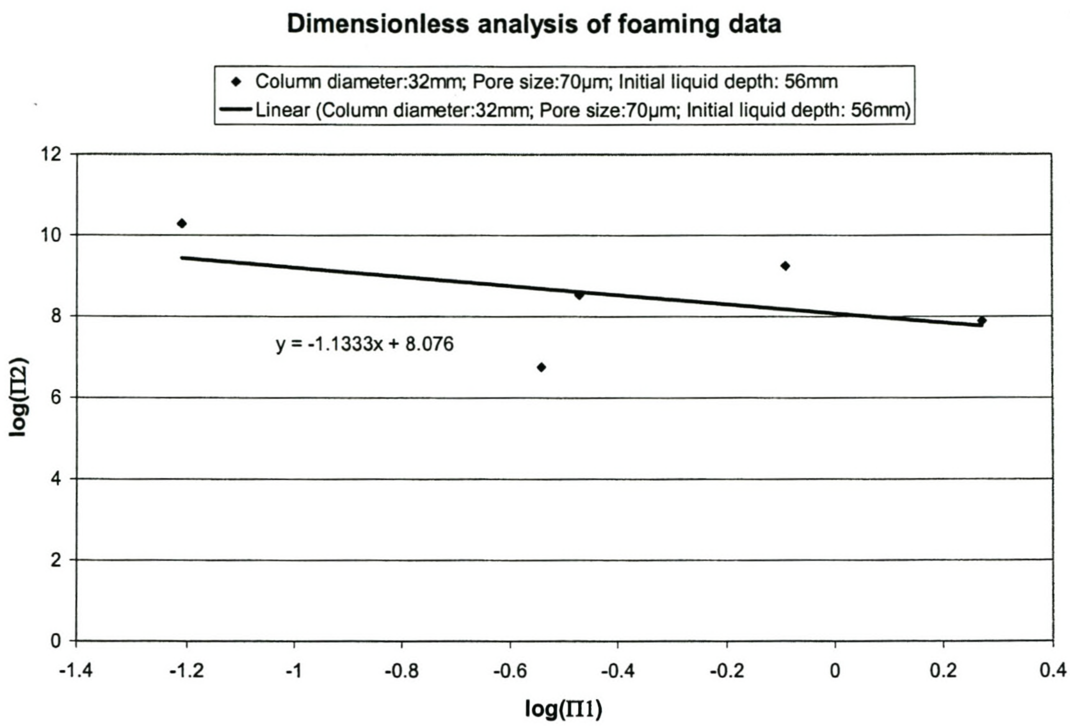


**Appendix B. Figure 37**

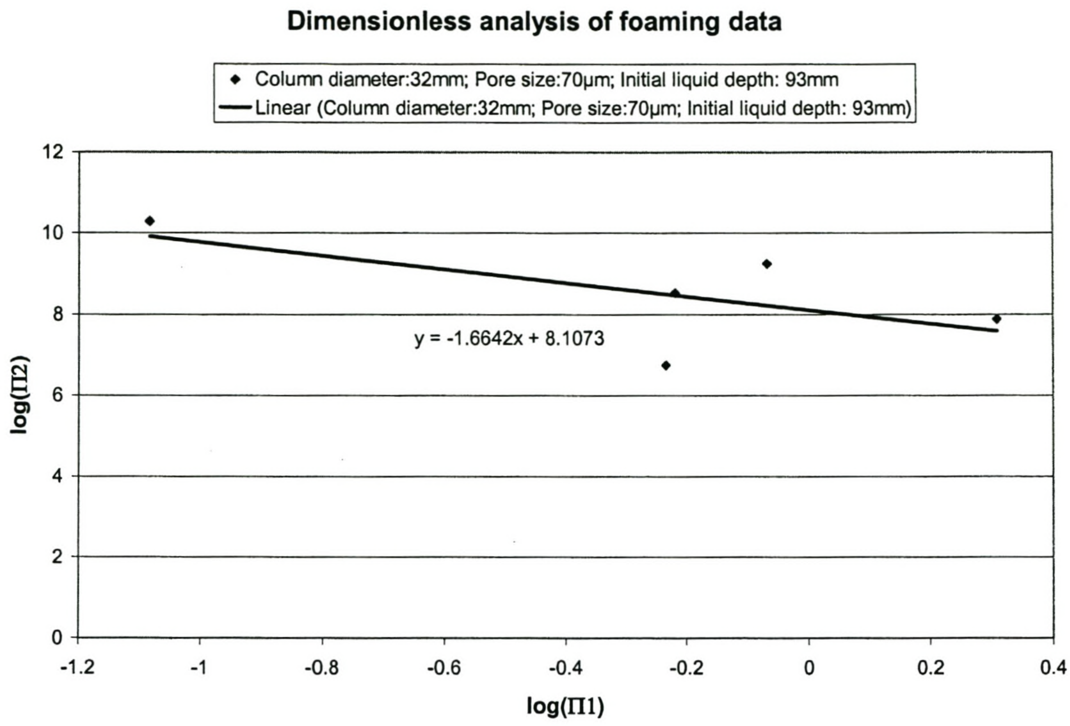


**Appendix B. Figure 38**

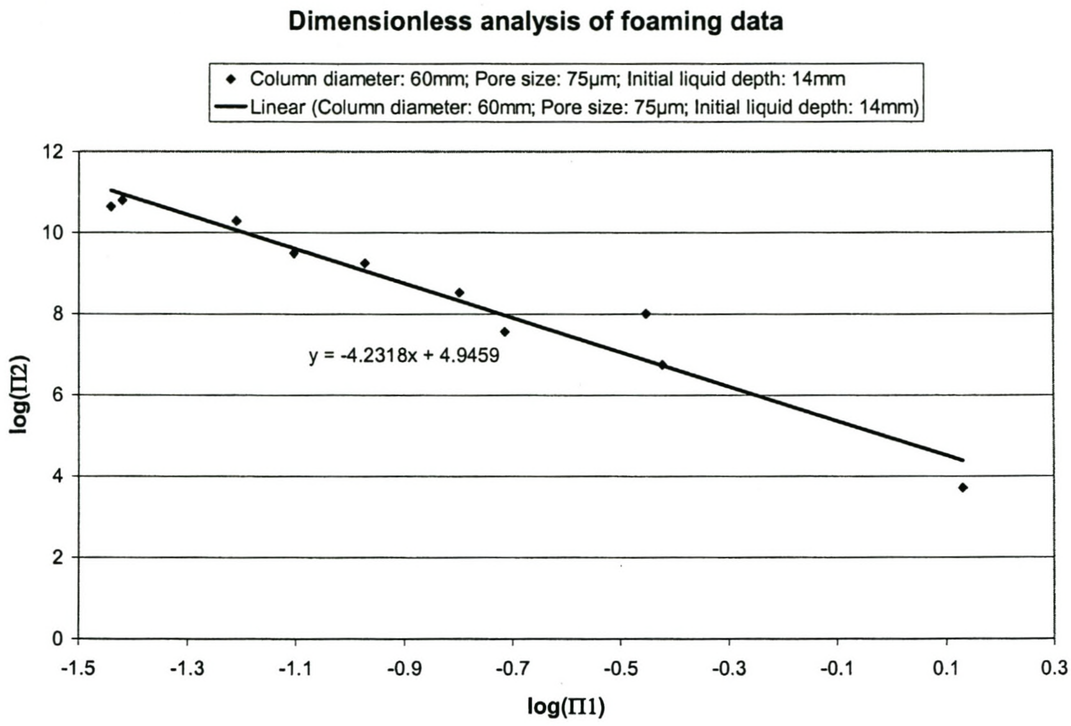


**Appendix B. Figure 39**

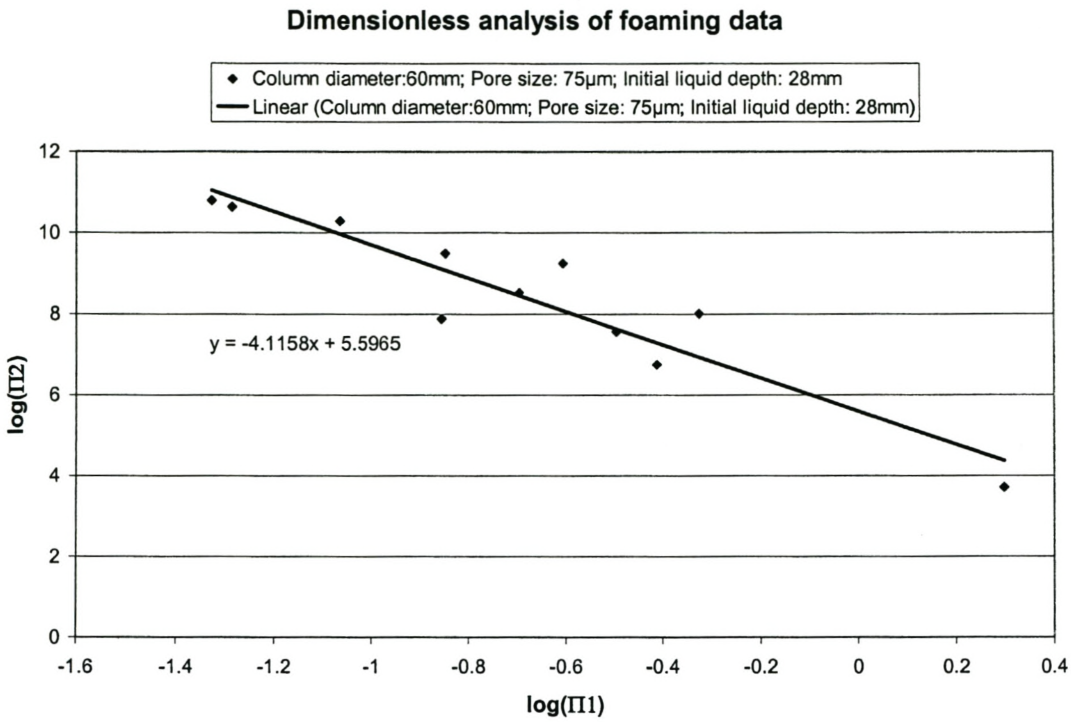


**Appendix B. Figure 40**

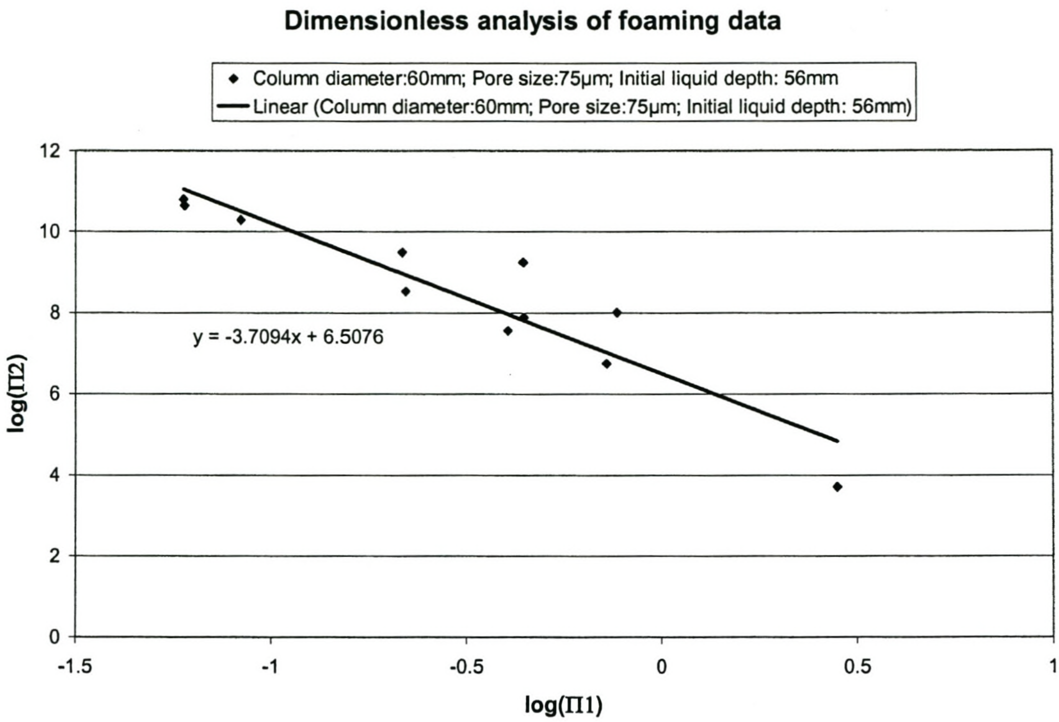


**Appendix B. Figure 41**

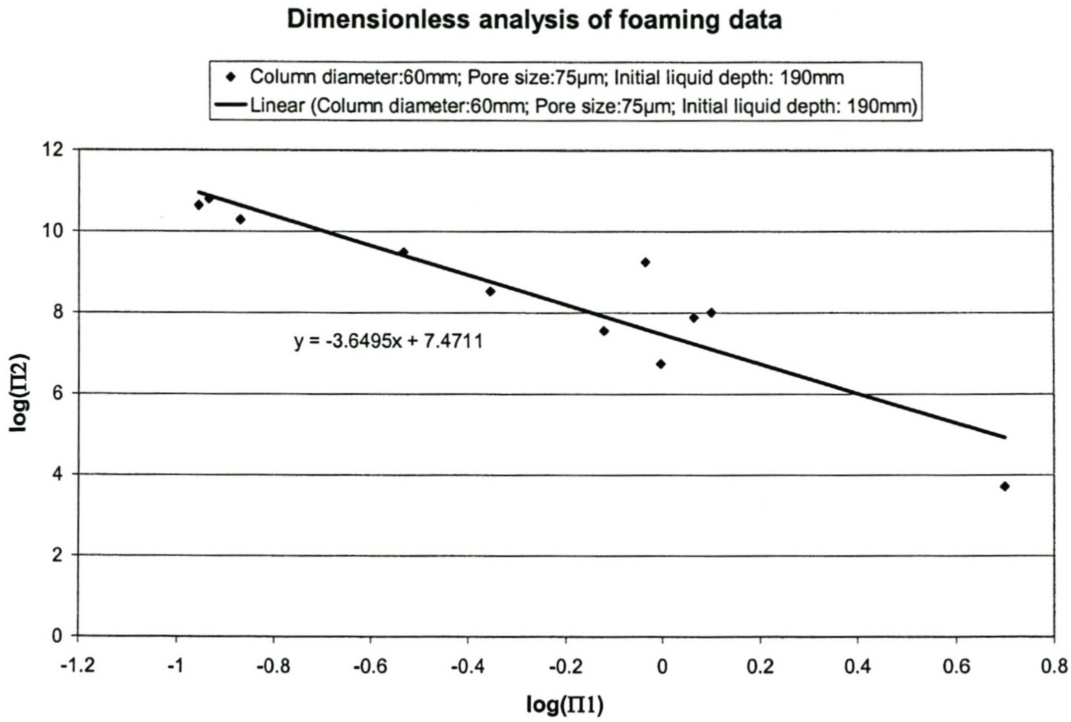


**Appendix B. Figure 42**

# 7 Bibliography

Bafghi, M.S., Kurimoto, H.,Sano, M. (1992). "Effect of slag foaming on the reduction of iron oxide in molten slag by graphite." ISIJ International 32(No. 10): 1084 - 1090.

Bikerman, J.J. (1973). Foams, Springer-Verlag New York Inc.

Ellis, R. (2001). on-line analysis of the stability and other features of froths and foams by use of digital image processing. Chemical Engineering. Stellenbosch, University of Stellenbosch.

Gaskell, D.S.a.D.R. (2000). "The surface tensions and foaming behaviour of melts in the system CaO-FeO-SiO2." Metallurgical and Materials Transactions B 31B(October): 921-925.

Ghag, S.S., Hayes, P.C.,Lee, H.-G. (1998). "Model development of slag foaming." ISIJ International 38(No. 11): 1208 - 1215.

Ghag, S.S., Hayes, P.C.,Lee, H.-G. (1998). "Physical model studies on slag foaming." ISIJ International 38(No. 11): 1201 - 1207.

Gou, H., Irons, G.A.,Lu, W.-K. (1996). "A multiphase fluid mechanics approach to gas holdup in bath smelting processes." Metallurgical and Materials Transactions B 27B(April): 195 - 201.

Gray, T.J. (1971). Oxide Spinels. High Temperature Oxides. Alper, A.M. New York and London, Academic Press. 5-IV: 97.

Gudenau, H.W., Wu, K., Nys, S.,Rosenbaum, H. (1992). "Formation and effect of slag foaming in smelting reduction." Steel research 63(No. 12): 521 - 525.

Happel, J. (1957). "Viscosity of suspensions of uniform spheres." Journal of Applied Physics 28(Number 11): 1288 - 1292.

Hara, S., Kitamura, M.,Ogino, K. (1990). "The surface viscosities and the foaminess of molten oxides." ISIJ International 30(No.9): 714-721.

Hara, S.,Ogino, K. (1986). Foaming of liquid slags containing iron oxide. The Reinhardt Schuhmann International Symposiom on Innovative Technology and Reactor Design in Extraction Metallurgy, Colarado Springs, Colorado, The Metallurgical Society, Inc.

Ito, K.a.F., R.J. (1989). "Study on the foaming of CaO-SiO2-FeO slags." Metallurgical Transactions B 20B.

Jiang, R.,Fruehan, R.J. (1991). "Slag foaming in bath smelting." Metallurgical and Materials Transactions B 22B(August): 481 - 489.

Koch, K.,Ren, J. (1994). "Photoelectric measurement of the foaming process in the reduction of slags containing iron oxide." Steel research 65(No. 1): 3 - 7.

Kondratiev, A. (2001). "Review of Experimental Data and Modelling of the Viscosities of Fully Liquid Slags in the Al2O3-CaO-"FeO"-SiO2 System." Metallurgical and Materials Transactions B 32 B: 1015 - 1025.

Kongoli, F.,A.Yazawa (2001). "Liquidus surface of FeO-Fe2O3-SiO2-CaO slag containing Al2O3, MgO, and Cu2O at intermediate oxygen partial pressures." Metallurgical and Materials Transactions B 22B(August): 583 - 592.

Lin, Z.,Guthrie, R.I.L. (1995). "A model for slag foaming for the in-bath smelting process." ISS Transactions(May): 67 - 73.

Mills, K.C. (1995). Basicity and optical basicities of slags. Slag atlas, Verlag Stahleisen GmbH: 9-19.

Mills, K.C. (1995). Viscosities of molten slags. Slag atlas, Verlag Stahleisen GmbH: 349-401.

Mishra, P., Deo, B.,Chhabra, R.P. (1998). "Dynamic model of slag foaming in oxygen steelmaking converters." ISIJ International 38(No. 11): 1225 - 1232.

Morales, R.D., Lule, R., Lopez, G.F., Camacho, J.,Romero, J.A. (1995). "The slag foaming practice in EAF and its influence on the steelmaking shop productivity." ISIJ International 35(No. 9): 1054 - 1062.

Ogawa, Y., Huin, D., Gaye, H.,Tokumitsu, N. (1993). "Physical model of slag foaming." ISIJ International 33(No. 1): 224 - 232.

Ozturk, B.,Fruehan, R.J. (1995). "Effect of temperature on slag foaming." Metallurgical and Materials Transactions B 26B(October): 1086 - 1088.

Pak, J.J., Min, D.J.,You, B.D. (1996). "Slag foaming phenomena and its suppression techniques in BOF steelmaking process." Steelmaking conference proceedings 79: 763 - 769.

Pathak, D.C., Sardar, M.K., Srivastava, S.K., Sarkar, S.R., Sinha, P.K., Jha, K.N.,Chakraborty, C. (1997). "Foamy slag practise in electric arc furnace steel making." SEAISI Quaterly(October): 94 - 97.

R.K. Paramguru, R.K.G., H.S. Ray (1997). "Influence of slag and foam characteristics on reduction of FeO-containing slags by solid carbon." Metallurgical and Materials Transactions B 28B(October): 805 - 810.

Ren, J., Westholt, M.,Koch, K. (1994). "Influence of MgO, K2O, NaO and gas pressure on slag foaming behaviour under redusing conditions." Steel Research 65(No. 6): 213 - 218.

Roth, R.E., Jiang, R.,Fruehan, R.J. (1993). "Foaming of ladle and BOS-Mn smelting slags." ISS Transactions 14: 95 - 103.

Tucker, J.P. (1994). "An evaluation of a direct method of bubble size distribution measurement in a laboratory batch flotation cell." Minerals Engineering 7(No 5/6): 667-680.

Utigard, T.A.,Zamalloa, M. (1993). "Foam behaviour in liquid FeO-CaO-SiO2 slags." Scandinavian journal of metallurgy(22): 83 - 90.

Worczok, A.,Utigard, T.A. (1994). "Low temperature physical modelling of slag foaming." Canadian Metallurgical Quaterly 33(No. 3): 205 - 215.

Yi, S.-H.,Rhee, C.-H. (1997). "Effects of additives on the foaming behaviour of the FeO-SiO2 based slags." Steel research(No.10): 429 - 433.

Zamalloa, M., Warczok, A.,Utigard (1992). Slag foam formation and stability. The minerals, metals & materials society,1991.

Zhang, Y. (1992). Slag foaming in the bath-smelting process. Department of Materials Science and Engineering. Pittsburgh, Carnegie Mellon University: 164.

Zhang, Y.,Fruehan, R. (1995). "Effect of carbonaceous particles on slag foaming." Metallurgical and Materials Transactions B 26B(August): 813 - 819.

Zhang, Y.,Fruehan, R.J. (1995). "Effect of bubble size and chemical reactions on slag foaming." Metallurgical and Materials Transactions B 26B(August): 803 - 812.

Zhang, Y.,Fruehan, R.J. (1995). "Effect of gas type and pressure on slag foaming." Metallurgical and Materials Transactions B 26B(October): 1088 - 1091.